AN INVESTIGATION OF THE RESONANCE CONE STRUCTURE IN A WARM ANISOTROPIC PLASMA

Thesis by

Keith Howard Burrell

In Partial Fulfillment of the Requirements

for the Degree of

Doctor of Philosophy

California Institute of Technology

Pasadena, California

1974

(Submitted May 28, 1974)

ACKNOWLEDGEMENT

I would like to express my thanks to my thesis advisor, Professor Roy W. Gould, for his advice and guidance throughout the course of this work. His comments on plasma physics, applied both to the present work and to the field in general, have been extremely instructive. I would also like to thank Dr. Robert S. Harp, who functioned as my advisor during Dr. Gould's absence.

I am indebted to Dr. Hans H. Kuehl both for cogently pointing out a possible approach to the asymptotic theory developed here and for suggesting that an afterglow plasma would be most suitable for checking that theory.

To my colleagues, Dr. Charles Moeller, John Wilgen and Bruce Levine, I would like to express my gratitude for their help with aspects of this work: C. Moeller and J. Wilgen for help with the equipment and B. Levine for consultation on mathematics.

This work would not be nearly as legible were it not for Ruth Stratton's skill. She translated awkward revisions into clean copy with ingenious facility and amazing speed.

To my wife, Mary, it is only possible to say thank you for help with data reduction and English style and for other aid, both tangible and intangible, during the course of my studies.

Finally, I gratefully acknowledge the support of the U.S. Atomic Energy Commission in carrying out this work.

ABSTRACT

This work presents a detailed theoretical and experimental investigation of the resonance cone pattern excited by a small antenna in a warm, magnetized plasma.

The warm plasma theory is developed for an infinite, uniform plasma for arbitrary incident frequency $\omega < (\omega_{pe}^2 + \omega_{ce}^2)^{1/2}$ in the limit that $r/\lambda_{de} \gg 1$ and $r/r_{\ell e} \gg 1$. Here, ω_{pe} and ω_{ce} are the electron plasma and cyclotron frequencies, respectively, while λ_{de} is the Debye length, $r_{\ell e}$ is the Larmor radius, and r is the distance from the source to the point of observation. The theory predicts the functional dependence of the angular position of the main resonance cone peak and the angular spacing between interference peaks on the physical parameters. The theory for plasmas with nonuniform density is also developed, but in the cold plasma limit, leading to predictions that the resonance cones can reflect off of density gradients.

Experimental work verifying the theoretical picture is presented. The main cone angle is found to depend on ω, ω_{pe}, ω_{ce}, and r in a manner consistent with the theory, as is the angular interference spacing. The idea of resonance cones reflecting from density gradients can explain features of the data that are otherwise incomprehensible.

From the data, values for ω_{pe} are obtained in two independent ways, and the results are consistent. The data also yield a value for the temperature that is appropriate for the afterglow plasma used in the experiment. Since both density and temperature can be obtained from the same data, resonance cone measurements are a useful diagnostic for plasmas in which antennas can be inserted.

An Märchen

TABLE OF CONTENTS

INTRODUCTION

The electromagnetic fields excited by a small, radio frequency antenna immersed in a plasma in a magnetic field are of interest both to those who work with ionospheric measurements and to those who seek to understand laboratory plasmas. The early work on the fields excited by small antennas was motivated by possible ionospheric applications, but it was almost entirely theoretical. It is only within the last six years that experimental applications in the laboratory have been developed and that theoretical analyses tailored to them have been made.

The present work is concerned with the laboratory applications. From this viewpoint, only the qualitative conclusions of the early theoretical work is of interest; the detailed thrust of their calculations is somewhat tangential to the present effort. However, for completeness, a separate bibliography of the eary work is presented in Appendix F.

Most of the early work considered small dipole antennas in cold, collisionless plasmas. The fundamental conclusion, first enunciated by Kuehl (see Appendix F, 15 and 16), is that the fields produced by an oscillating point dipole should become infinite along a conical surface whose apex is the dipole and whose axis is parallel to the static magnetic field (see Fig. 1). The opening angle of the cone is a function of the plasma density, the incident frequency, and the magnitude of the static magnetic field. The shape of the singularity led to the name resonance cone for this phenomenon.

The presence of this infinity motivated much of the subsequent theoretical work on antennas in magnetized plasmas. The general conclusions were that the singularity was the result of three factors. First, all the theory was done by linearizing the nonlinear plasma equations, which meant that none of the nonlinear saturation effects could limit the amplitude. Second, both collisional and collisionless damping were neglected by considering the plasma to be cold ($T = 0$) and collisionless. Third, the antenna had no dimensions.

The second and third effects can be taken into account without too much trouble; and either collisions, or a nonzero temperature, or an antenna of nonzero dimensions is sufficient to keep the fields finite. (The full nonlinear solution has never been done.) However, even when the fields remain finite, there are still pronounced peaks in the field pattern near the angle where the infinity would have occurred.

Perhaps because much of the early analysis was done in the electromagnetic far-field, the extensive theoretical controversy about the infinity in the field pattern sparked very few experimental investigations of the phenomenon. The first systematic experimental investigation was that by Fisher [1] and Fisher and Gould [2-4]. They verified that there were pronounced peaks in the field pattern excited by a small antenna, and that the angular location of these peaks follows the simple cold plasma predictions. In addition, they found structure in the angular field patterns due to the presence of warm plasma waves.

In order to relate the observed patterns to theoretical predictions, they analyzed the plasma response in the uniaxial limit ($\underline{B}_0 \to \infty$), using the electrostatic approximation and the collisionless Boltzmann equation. Simultaneously, Singh [5] and Singh and Gould [6,7] developed the electromagnetic analysis for the uniaxial plasma. Both calculations predicted that warm plasma waves, whose phase velocity is of the order of the thermal speed, are responsible for the interference structure observed near the resonance cone.

In spite of the fact that the uniaxial approximation was invalid for the plasma in Fisher's experiment, the predictions of that theory which were tested there agreed reasonably well with the experimental results. To remedy this lack of a finite magnetic field theory is one of the goals of the present work.

This work is about equally divided between theoretical derivation and experimental work designed to check that theory. The experimental work is an extension and refinement of the work done by R. K. Fisher. New experimental equipment has been built so that a greater range of experimental parameters is more readily available. The theoretical analysis derives from a suggestion by H. H. Kuehl that an approximate expression for the fields of a small antenna could be obtained by asymptotically expanding the electrostatic Green's function for an oscillating source in a warm, magnetized plasma. Kuehl has also developed such asymptotic expansions himself [8,9]. The analysis given here is somewhat more formal than his, and is capable of more rapid generalization to parameter ranges where the resonance cones do not exist. However, the predictions of each

development which can be tested experimentally are identical.

The first three chapters of this work are devoted to the theoretical development, the next three consider the experimental work, while the last contains the conclusions and suggestions for further work.

In Chapter I, the Green's function for an oscillating source in an infinite, uniform, warm, magnetized plasma is developed. To get some of the physics out of this function before doing the asymptotic expansion, various limiting cases are considered. The cold plasma limit reveals the basic resonance cone, while the uniaxial limit gives some of the properties of the interference structure caused by the warm plasma waves.

Chapter II is devoted entirely to the asymptotic expansion of the Green's function in the limit that the point of observation is far from the source.

Some of the physical predictions of the asymptotic expansion are obtained in the first part of Chapter III. These include the manner in which the plasma parameters influence the angular position of the main resonance cone and the interference structure. In the second part, the Green's function is used to consider how these physical predictions might be modified for an antenna whose length is much greater than its width. The final section is devoted to a simple analysis of some of the effects of a nonuniform plasma density on the resonance cone pattern.

Chapter IV describes the experimental equipment and measurement procedures. Details of the plasma generation, operating

conditions, and magnetic field configuration are given. The construction of the transmitting and receiving probes is shown, and the probe carriage used to position them in the plasma is discussed. The details of the experimental electronics used to detect the received signal are also given.

The measurements of the main resonance cone peak are considered in Chapter V. The changes of cone angle with probe frequency and cyclotron frequency are presented and are shown to agree with the simple cold plasma theory. The slight variations in cone angle caused by warm plasma effects are illustrated, and are seen to agree with the warm plasma theory. The chapter concludes with an experimental demonstration that the resonance cones can reflect off of density gradients, as was discussed in Chapter III.

A detailed investigation of the interference structure is presented in Chapter VI. The angular spacing between peaks is shown to vary with probe separation, probe frequency, cyclotron frequency, and plasma frequency in a manner consistent with the theory. Further, the temperature derived from this spacing using the theory is consistent with the temperature one would expect in the plasma used in the experiment.

Chapter VII provides the final summary, suggestions for further work, and a statement of conclusions.

CHAPTER I

PRELIMINARY THEORETICAL DEVELOPMENT

1.1 The Basic Equations

In this chapter and the following two, we will develop the mathematical model which we will need subsequently for comparison with the experimental results. The basic problem is to calculate the field pattern of a localized, oscillating electrical source immersed in a warm, anisotropic plasma. The source of the anisotropy is an externally imposed, static, uniform magnetic field.

In many laboratory plasmas, and especially in the one used in this experiment, the ratio of plasma dimensions to electromagnetic wavelength is such that the radiation pattern of a small source can be adequately described by solving for the quasi-static, near-field radiation pattern. This quasi-static approximation is identical with the electrostatic approximation often made in warm plasma wave theory, and the complete problem can thus be consistently treated in the electrostatic limit.

Laboratory plasmas are obviously of finite extent, which brings up the troublesome problems of density nonuniformities and boundary conditions at material walls. Some of the effects of finite plasma dimensions will be handled at the end of Chapter III. However, for the moment, we will ignore them and assume an infinite, uniform plasma.

Let the z-axis of a Cartesian coordinate system be oriented along the uniform external magnetic field, so that $\underline{B}_o = B_o \hat{e}_z$. The

motion of the plasma particles will be described using the non-relativistic Boltzmann equation for the phase space distribution function $f(\underline{x},\underline{v},t)$. In principle, one should have one distribution function for the electrons and another for the ions. However, at the frequencies of interest in the experiment ($\gtrsim$ 50 MHz), the motion of the ions can be neglected. They will be treated as a uniform background charge.

The equations that describe the system are the Boltzmann equation for the electrons

$$\frac{\partial f}{\partial t} + \underline{v} \cdot \frac{\partial f}{\partial \underline{x}} + \frac{e}{m} \left(\frac{\partial \phi}{\partial \underline{x}} - \underline{v} \times \underline{B}_o\right) \cdot \frac{\partial f}{\partial \underline{v}} = \left(\frac{\partial f}{\partial t}\right)_{coll} \tag{1}$$

and Poisson's equation for the electrostatic potential

$$\nabla^2 \phi = - \frac{\rho_{ext}}{\varepsilon_o} + e(n - n_o) \tag{2}$$

Here, m is the electron mass, e the magnitude of the electron charge, n_o the ion number density, and n the electron number density, which is given by

$$n(\underline{x},t) = \int d\underline{v}\, f(\underline{x},\underline{v},t) \tag{3}$$

The antenna is the source of the external charge density ρ_{ext}.

Although the frequencies broadcast by the source are sufficiently high that the plasma could be regarded as collisionless, it is extremely useful in the mathematical derivation if a small collision term is retained. The collision term will be modeled as

$$\left(\frac{\partial f}{\partial t}\right)_{coll} = -\nu(f - f^{(o)}) \tag{4}$$

where $f^{(o)}$ is the equilibrium value of f. A collision term of this form applies best to electron collisions with neutrals, but even for these it has some unrealistic features (e.g., particles are not conserved locally). This form does have the great advantage of mathematical simplicity and as long as ν is small, one can expect the results to be qualitatively correct.

Unfortunately, the system of Eqs. (1)-(4) is nonlinear and no general method of solution is known. To obtain a mathematically tractable problem, one can linearize Eq. (1) about an equilibrium distribution by setting $f = f^{(o)} + f^{(1)}$ and keeping only first order terms. (The potential ϕ is considered to be first order as well.) Once a linear system has been obtained, arbitrary antenna configurations can be handled, at least in principle, if the Green's function can be found.

We are thus led to consider the following system of equations

$$\frac{\partial f^{(1)}}{\partial t} + \underline{v} \cdot \frac{\partial f^{(1)}}{\partial \underline{x}} - \frac{e}{m}\,\underline{v} \times \underline{B}_o \cdot \frac{\partial f^{(1)}}{\partial \underline{v}}$$

$$= -\frac{e}{m}\frac{\partial \phi}{\partial \underline{x}} \cdot \frac{\partial f^{(o)}}{\partial \underline{v}} - \nu\, f^{(1)} \tag{5}$$

$$\nabla^2 \phi = -\frac{q}{\varepsilon_o}\,\delta(\underline{x})\, e^{-i\omega t} + \frac{e n_1}{\varepsilon_o} \tag{6}$$

$$n_1 = \int d\underline{v}\, f^{(1)}(\underline{x}, \underline{v}, t) \tag{7}$$

Here, $\delta(x)$ is the Dirac delta function. For the collision model to be reasonable, it is necessary that $\nu/\omega << 1$.

Equations very similar to this set have been studied reasonably thoroughly in recent years [10,11]. The solution can be effected most easily by using Fourier transforms. The details are carried out in Appendix A. Assuming that $f^{(o)}$ is an isotropic Maxwellian and then utilizing the cylindrical symmetry about $\underline{B}_o$, the solution for the potential can be written as

$$\phi(\rho,z,t) = \frac{qe^{-i\omega t}}{4\pi^2\varepsilon_o}\int_{-\infty}^{\infty} dk_{\parallel}\, e^{ik_{\parallel}z}\int_0^{\infty} dk_{\perp}\, \frac{k_{\perp}J_o(k_{\perp}\rho)}{D(k_{\perp},k_{\parallel})} \tag{8}$$

where $\rho = (x^2+y^2)^{1/2}$ is the cylindrical coordinate in the direction perpendicular to $\underline{B}_o$, $D(k_{\perp},k_{\parallel})$ is the electrostatic dispersion function given by [10,12]

$$D(k_{\perp},k_{\parallel}) = k_{\perp}^2 + k_{\parallel}^2 + k_{de}^2(1+i\nu/\omega)\left(1 + i(\omega+i\nu)\int_0^{\infty} dt\, \exp\left\{i(\omega+i\nu)t - \frac{k_{\perp}^2 v_{th}^2}{\omega_{ce}^2}\sin^2\frac{\omega_{ce}t}{2} - \frac{1}{4}k_{\parallel}^2 v_{th}^2 t^2\right\}\right) \tag{9}$$

and where

$$k_{de}^2 = \frac{n_o e^2}{\varepsilon_o \kappa T_e} \qquad v_{th}^2 = \frac{2\kappa T_e}{m}$$

Here T_e is the electron temperature and the cyclotron frequency is defined by $\omega_{ce} = eB_o/m$.

In Eq. (8) we have the electrostatic Green's function for a warm, magnetized plasma. It is sufficiently complicated in its present

form that it is almost impossible to interpret. To do so, one must either resort to numerical procedures or make further approximations. Both courses will be followed in the remainder of this chapter.

1.2 The Cold Plasma Approximation

There is one limit in which the integrals in Eq. (8) can be done explicitly. If we let $T_e \to 0$, then the dispersion function reduces to

$$D(k_\perp, k_\parallel) = K_\perp k_\perp^2 + K_\parallel k_\parallel^2 \tag{10}$$

where

$$K_\perp = 1 - \frac{\omega_{pe}^2(1 + i\nu/\omega)}{(\omega+i\nu)^2 - \omega_{ce}^2}$$

$$K_\parallel = 1 - \frac{\omega_{pe}^2}{\omega(\omega+i\nu)}$$

Here, the plasma frequency has been defined by $\omega_{pe} = (n_o e^2/\varepsilon_o m)^{1/2}$. (Reducing Eq. (9) to this form is one of the places where a nonzero collision frequency is very useful.)

The integrals in Eq. (8) are now standard forms [13]; hence

$$\phi(\rho,z,t) = \frac{qe^{-i\omega t}}{4\pi\varepsilon_o(K_\perp^2 K_\parallel)^{1/2}} \left[\frac{\rho^2}{K_\perp} + \frac{z^2}{K_\parallel}\right]^{-1/2} \tag{11}$$

This answer is intuitively very satisfying. In the zero temperature limit, the plasma is just an anisotropic dielectric, and $K_\perp$ and $K_\parallel$ are the diagonal components of the dielectric tensor. The potential we have obtained is the usual point source solution,

but the coordinates parallel and perpendicular to the magnetic field are scaled with the appropriate dielectric tensor components.

As a dielectric, the cold plasma has one unusual property: the real part of $K_\perp$ or $K_\parallel$ can have either algebraic sign. Since $\nu/\omega \ll 1$, this means that it is possible for the square root in Eq. (11) to be quite small, and for the potential to be very large. If $\nu = 0$, the potential is infinite when

$$\cot^2\theta = \frac{z^2}{\rho^2} = -\frac{K_\parallel}{K_\perp}$$

This points up the most basic fact about the waves excited by a source in a magnetized plasma. Whenever $\text{Re } K_\parallel / \text{Re } K_\perp < 0$, there are directions in space along which the potential created by a small antenna can be quite large. Geometrically, the location of these maxima of $|\phi(\rho,z,t)|$ form conical surfaces in space with the source at the apex of the cone, as is shown in Fig. 1.

The reason for the large amplitude is that a resonant collective particle mode is excited by the antenna. Unlike more familiar resonant systems, it is the collective behavior of a group of particles with many degrees of freedom that gives this resonance its unique geometrical character. Like all resonant systems, if dissipation is left out (i.e., $\nu = 0$), the amplitude at resonance is infinite. Both collisions and, as we will see later, the effects of finite temperature will act to limit the amplitude in any actual system.

Since $K_\perp$ and $K_\parallel$ are functions of frequency, the resonance cones will exist only in certain frequency ranges. These ranges are

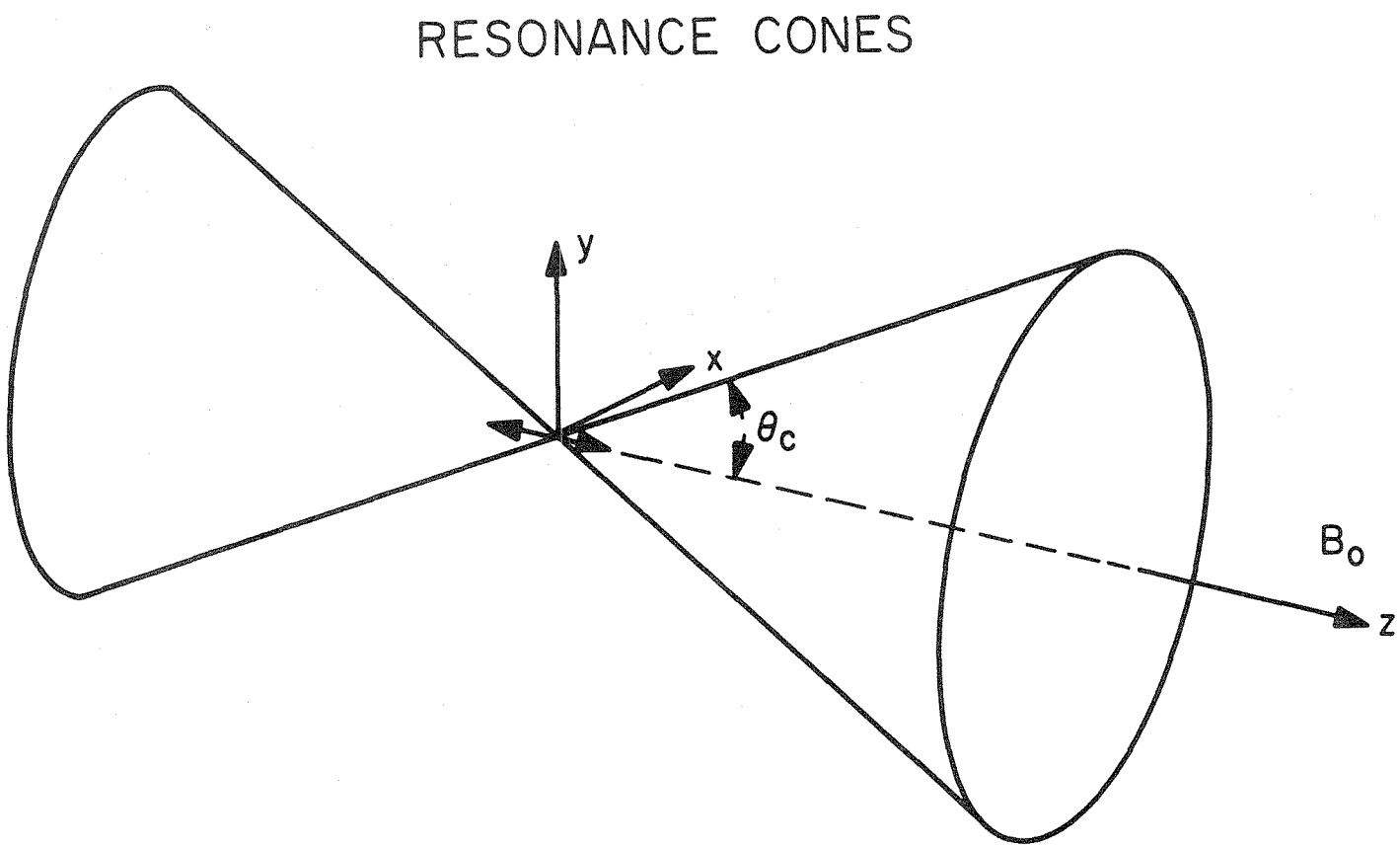

Fig. 1 Diagram showing resonance cones for a small antenna located at the origin. The antenna is at the apex of the cones and their axes are parallel to the magnetic field(after Fisher[1]).

shown in Fig. 2 for the case $\nu = 0$. As long as $\nu/\omega << 1$, the boundaries shown will be appropriate for the collisional case as well.

As can be seen from Fig. 2, the resonance cones exist for two frequency regions: 1) $0 \leq \omega \leq \min(\omega_{pe},\omega_{ce})$, usually called the lower branch, and 2) $\max(\omega_{pe},\omega_{ce}) \leq \omega \leq (\omega_{pe}^2 + \omega_{ce}^2)^{1/2}$, called the upper branch. The low frequency end of the lower branch should be shown dotted, since the motion of the ions becomes important at these low frequencies.

For future reference, the place where the potential given in Eq. (11) has its maximum magnitude will be called the cold plasma resonance cone angle θ_c. If we consider $|\phi(\rho,z,t)|$ as a function of the spherical coordinates (r,θ) with $\rho = r \sin\theta$ and $z = r\cos\theta$, then one can easily show that $\partial|\phi|/\partial\theta = 0$ when

$$\cot^2\theta = \cot^2\theta_c = -\frac{\text{Re } K_{\parallel}\,(K_{\parallel}^* - K_{\perp}^*)}{\text{Re } K_{\perp}(K_{\parallel}^* - K_{\perp}^*)} \tag{12}$$

If $\nu = 0$, this simplifies to

$$\cot^2\theta_c = -\frac{K_{\parallel}}{K_{\perp}} \tag{13}$$

In the following sections, we will often need to evaluate expressions like $(i\cot\theta_c \pm (K_{\parallel}/K_{\perp})^{1/2})$ in the limit $\nu \to 0$. To know what value to give this, make the following definition: In the collisionless limit

$$\cot\theta_c = \lim_{\nu \to 0} e^{-i\pi/2}\left(\frac{K_{\parallel}}{K_{\perp}}\right)^{1/2} \tag{14}$$

The square root has positive real part and θ_c is in the range

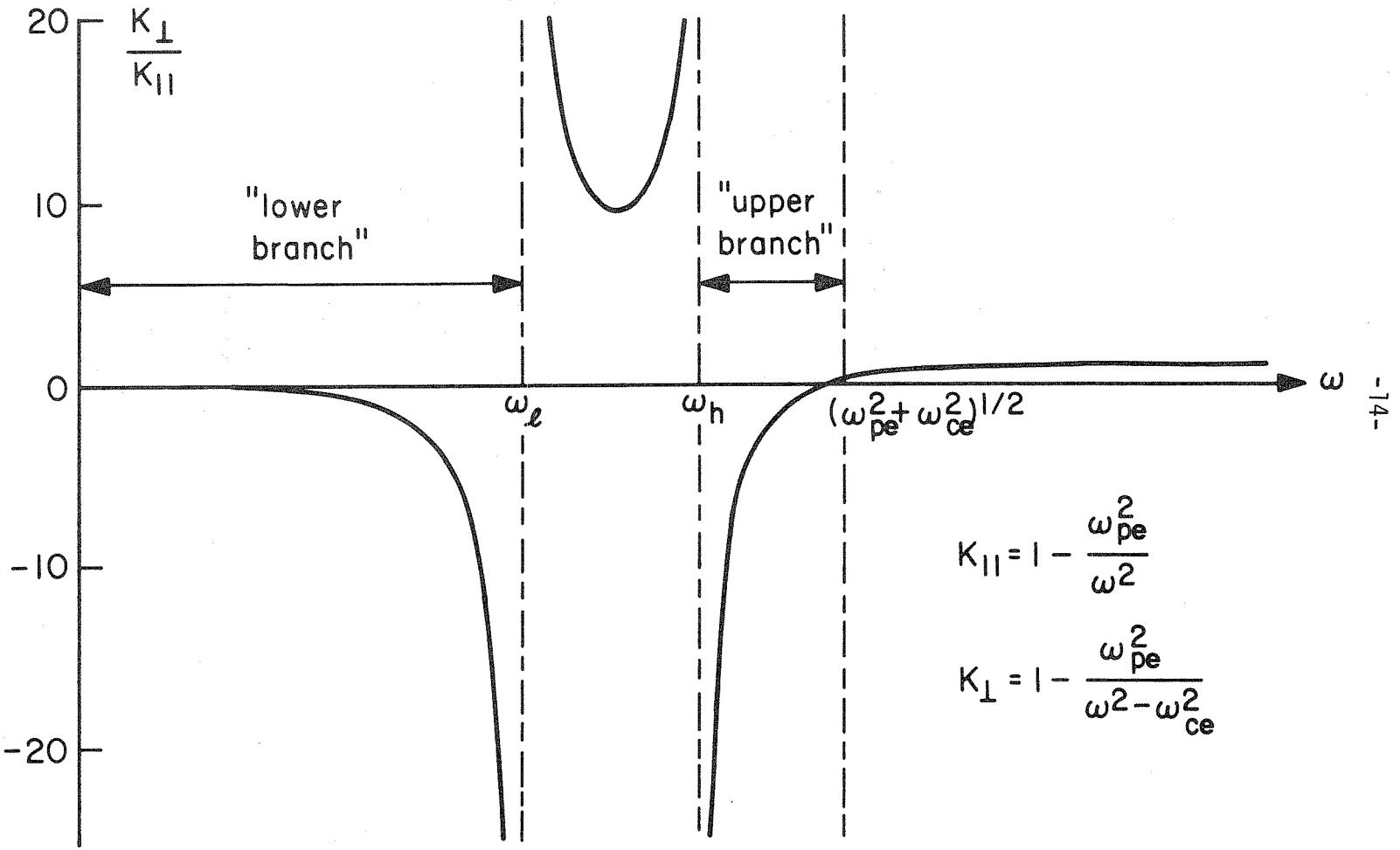

Fig. 2 $K_\perp/K_{||}$ as a function of the frequency ω for a collisionless plasma. Resonance cones exist in the regions where $K_\perp/K_{||} \leq 0$: the lower branch $0 \leq \omega \leq \omega_\ell = \min(\omega_{pe},\omega_{ce})$ and the upper branch $\omega_h = \max(\omega_{pe},\omega_{ce}) \leq \omega \leq (\omega_{pe}^2 + \omega_{ce}^2)^{1/2}$ (after Fisher[1]).

$0 \leq \theta_c \leq \pi$. This means that, for $\nu \to 0$

$$i \cot \theta_c - \left(\frac{K_{\parallel}}{K_{\perp}}\right)^{1/2} = 0$$

Notice that both $\theta = \theta_c$ and $\theta = \pi - \theta_c$ satisfy Eq. (12). (Including a nonzero collision frequency in the problem has made these definitions much easier than they would have been if we had taken $\nu = 0$ from the start.)

1.3 The Warm Uniaxial Plasma

In order to see how the resonance cones are modified by a nonzero electron temperature, it is easiest to make the uniaxial approximation $B_0 \to \infty$. This means that the electrons can move only along the magnetic field lines, and the effects that would occur because of electron thermal motion transverse to $\underline{B}_0$ are left out. Further, as long as ω remains finite, only the lower branch resonance cones are accessible. Since $\omega_{ce} \to \infty$, the dispersion function becomes

$$D(k_{\perp}, k_{\parallel}) = k_{\perp}^2 + k_{\parallel}^2 + k_{de}^2 (1+i\nu/\omega)\left(1 + i(\omega+i\nu)\int_0^{\infty} dt \exp\left\{i(\omega+i\nu)t - \frac{1}{4} k_{\parallel}^2 v_{th}^2 t^2\right\}\right)$$

The $k_{\perp}$ integral in Eq. (8) can now be done explicitly [14], and the potential can be expressed as

$$\phi(\rho,z,t) = \frac{qe^{-i\omega t}}{2\pi^2 \varepsilon_0} \int_0^{\infty} dk_{\parallel} \cos k_{\parallel} z \; K_0(\rho P(k_{\parallel})) \qquad (15)$$

with

$$P(k_{\parallel}) = \{k_{\parallel}^2 - \tfrac{1}{2} k_{de}^2 (1+i\nu/\omega)\, Z'((\omega+i\nu)/k_{\parallel} v_{th})\}^{1/2}$$

where the square root is defined with $\mathrm{Re}\, P(k_{\parallel}) \geq 0$. The symmetry of $D(k_{\perp}, k_{\parallel})$ has been used here to reduce the range of integration to the positive real axis. After this is done, the integrand in Eq. (15) can be expressed in terms of Z' , which is the derivative of the plasma dispersion function [15]. Since Z' is not an even function of its argument, we may only use it for $\mathrm{Re}\, k_{\parallel} \geq 0$.

Equation (15) can be put in a more succinct form by introducing the normalized variables $\tilde{\rho} = k_{de}\rho/\sqrt{2}$, $\tilde{z} = k_{de} z/\sqrt{2}$, $\tilde{r} = k_{de} r/\sqrt{2} = k_{de}(\rho^2 + z^2)^{1/2}/\sqrt{2}$, $\tilde{k} = k_{\parallel}\sqrt{2}/k_{de}$, and $\Phi = 4\pi\varepsilon_o r\, \phi(\rho,z,t)\, e^{i\omega t}/q$. Using these,

$$\Phi(\tilde{\rho},\tilde{z}) = \frac{2\tilde{r}}{\pi} \int_0^{\infty} d\tilde{k} \cos \tilde{k}\tilde{z}\, K_o(\tilde{\rho}\tilde{P}(\tilde{k})) \qquad (16)$$

where

$$\tilde{P}(\tilde{k}) = \{\tilde{k}^2 - (1+i\nu/\omega)\, Z'((\omega+i\nu)/\tilde{k}\omega_{pe})\}^{1/2}$$

The integral in Eq. (16) can be evaluated numerically without too much difficulty. The method of integration used is quite standard, but the efficient evaluation of the Bessel function in the integrand required the development of new algorithms [16]. The details are given in Appendix B.

In the cold plasma limit, if the resonance cones exist at all, they exist at the same value of ρ/z , no matter how big ρ or z are. To compare this behavior with the present case, let $\tilde{\rho} = \tilde{r} \sin\theta$

and $\tilde{z} = \tilde{r} \cos\theta$ and consider $\Phi(\tilde{\rho},\tilde{z})$ as a function of θ for fixed $\tilde{r}$. Since $\Phi(\tilde{\rho},\tilde{z})$ is an even function of $\tilde{z}$, we need only consider $0 \leq \theta \leq \pi/2$.

Figure 3 shows the magnitude and phase of $\Phi(\tilde{\rho},\tilde{z})$ for one set of parameter values. Also shown are the corresponding graphs for the function

$$\Phi_c = (K_{\parallel} \sin^2\theta + \cos^2\theta)^{-1/2}$$

which is the equivalent form of the cold plasma result in the normalized notation.

There are several important differences between Φ and Φ_c. First, even though $\nu = 0$, $|\Phi|$ is finite for all θ, which shows that a nonzero temperature limits the amplitude of the resonance. Second, the largest maximum of $|\Phi|$ occurs at an angle slightly smaller than the cold plasma resonance cone angle

$$\cot^2\theta_c = -K_{\parallel}$$

Third, there is a series of subsidiary maxima that occur inside the resonance cone. These are due to the presence of electrostatic waves propagating in the plasma. In a warm magnetized plasma, the wavelength of an electrostatic wave depends on its direction of propagation relative to the magnetic field [17]. The subsidiary peaks represent an interference between the quasi-static electromagnetic field and the electrostatic waves.

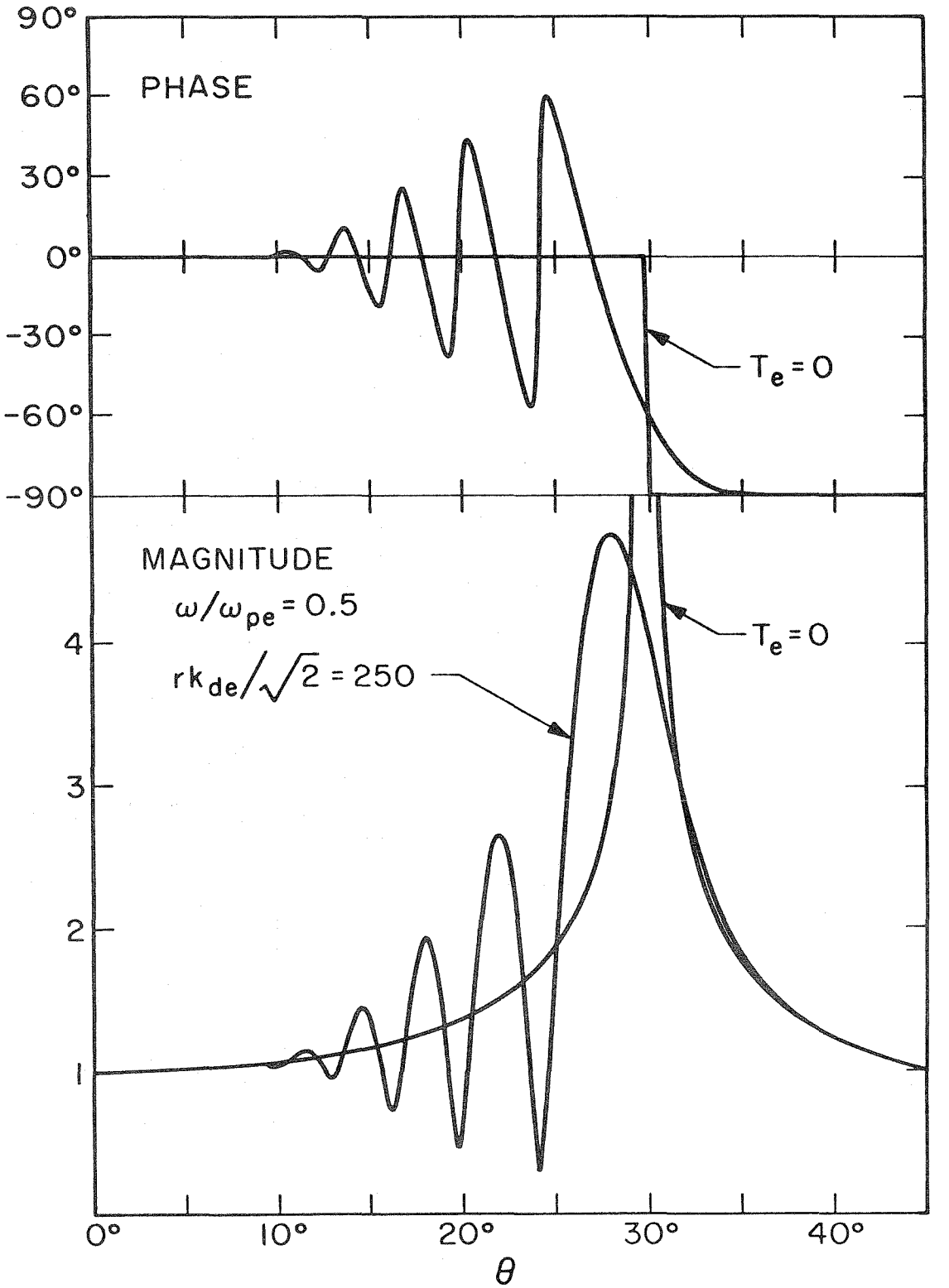

Fig. 3 Angular dependence of the magnitude and phase of the normalized potentials Φ and Φ_c for a warm and a cold uniaxial plasma, respectively.

This numerical example has revealed most of the qualitative modifications that occur when the temperature is nonzero. However, we need more than just a qualitative understanding. One would like to be able to make quantitative predictions of how $\phi(\rho,z,t)$ changes when the plasma parameters change. One could try to do this in a brute force fashion by grinding out a multitude of numerical examples, but even if one had the time and money to do it, it is difficult to get functional relations out of computer solutions. The asymptotic expansion developed in the next chapter overcomes these problems.

CHAPTER II

ASYMPTOTIC EXPANSION OF THE ELECTROSTATIC GREEN'S FUNCTION

Even though the integral in Eq. (8) cannot be done analytically, if we let $\rho = r \sin\theta$ and $z = r\cos\theta$, then we can get explicit asymptotic approximations for $\phi(\rho,z,t)$ in the limit $r \to \infty$. It is the goal of this chapter to develop these expansions. Physically, this means that we will be able to compute $\phi(\rho,z,t)$ if there are many wavelengths of the warm plasma waves between our point of observation and the source.

A number of authors have worked on the asymptotic expansion of multidimensional Fourier integrals [18,19,20]. Unfortunately, their results are only of marginal use here, since they are not uniformly valid for angles near the cold plasma resonance cone angle. One is thus forced to develop asymptotic expansions from first principles.

Consider the integral over $k_\perp$ in Eq. (8). By using the identities [21]

$$J_0(z) = \frac{1}{2}\left[H_0^{(1)}(z) + H_0^{(2)}(z)\right]$$

$$H_0^{(2)}(z) = -H_0^{(1)}(ze^{i\pi})$$

and the fact that $D(k_\perp, k_\parallel)$ is an even function of $k_\perp$, we may write

$$\int_0^\infty \frac{J_0(k_\perp\rho)k_\perp\, dk_\perp}{D(k_\perp,k_\parallel)} = \frac{1}{2}\int_{-\infty}^{+\infty} \frac{H_0^{(1)}(k_\perp\rho)k_\perp\, dk_\perp}{D(k_\perp,k_\parallel)}$$

This latter integral can be done, at least formally, by using the residue theorem. Hence, if $\rho \neq 0$,

$$\int_0^\infty \frac{J_0(k_\perp \rho) k_\perp \, dk_\perp}{D(k_\perp, k_\parallel)} = \sum_{n=0}^{\infty} \frac{K_0(\rho P_n(k_\parallel))}{R_n(k_\parallel)} \tag{17}$$

Here $k_\perp = iP_n(k_\parallel)$ is one of the solutions to $D(k_\perp, k_\parallel) = 0$ and

$$R_n(k_\parallel) = \left. \frac{\partial D}{\partial (k_\perp^2)} \right|_{k_\perp^2 = -P_n^2}$$

The quantity $P_n(k_\parallel)$ is chosen so that $\mathrm{Re}\, P_n(k_\parallel) \geq 0$.

In obtaining Eq. (17) we have assumed that all the zeros of the dispersion relation for which $k_\perp \neq 0$ are simple. This is mathematically equivalent to saying that $R_n(k_\parallel) \neq 0$. It is not obvious that this is always the case. It will be shown in Appendix C that for the $k_\parallel$'s involved in the asymptotic expansion, $R_n(k_\parallel) \neq 0$.

We may now write the Green's function as

$$\phi(\rho, z) = \frac{q e^{-i\omega t}}{4\pi^2 \varepsilon_0} \sum_{n=0}^{\infty} \mathscr{I}_n(\rho, z) \tag{18}$$

where the $\mathscr{I}_n$ are the remaining integrals

$$\mathscr{I}_n(\rho, z) = \int_{-\infty}^{+\infty} dk \, e^{ikz} \frac{K_0(\rho P_n(k))}{R_n(k)} \tag{19}$$

In Eq. (19), the subscript on $k_\parallel$ has been dropped; from now on, it will be left off, except in cases where ambiguity would result.

If the integrand in Eq. (19) could be put in the proper form, the method of steepest descents [22] could be used to asymptotically expand the integral. If $P_n(k)$ were never zero and if $\sin\theta \neq 0$, then as $r \to \infty$, one could use the asymptotic form of the Bessel function

$$K_o(z) \sim \sqrt{\frac{\pi}{2z}}\, e^{-z}$$

which would give an integrand of the right type.

We thus need to investigate whether $P_n(k)$ can ever be zero for real k. If one considers the dispersion function, Eq. (9), then $D(k_\perp, k_\parallel) = 0$ and $P_n(k_\parallel) = 0$ imply that

$$k_\parallel^2 + k_{de}^2(1 + i\nu/\omega)\left(1 + i(\omega+i\nu)\int_0^\infty dt \exp\left\{i(\omega+i\nu)t - \frac{1}{4}k_\parallel^2 v_{th}^2 t^2\right\}\right) = 0 \qquad (20)$$

This is the well known electrostatic plasma wave dispersion relation first obtained by Landau [23] for the case $\nu = 0$. Landau showed that for all real $k_\parallel \neq 0$, the only solutions to this equation demand ω complex and $\mathrm{Im}\,\omega < 0$. Since $\nu \neq 0$ just adds more damping, there are still no solutions with real ω and $k_\parallel \neq 0$. Clearly, $k_\parallel = 0$ is a solution to Eq. (20). Accordingly, we have $P_n(k_\parallel) = 0$ for real $k_\parallel$ if and only if $k_\parallel = 0$.

Let us now investigate $D(k_\perp, k_\parallel) = 0$ under the condition $k_\parallel = 0$. We then obtain

$$k_\perp^2 + k_{de}^2(1+i\nu/\omega)\left(1 + i(\omega+i\nu)\int_0^\infty dt\, \exp\{i(\omega+i\nu)t - \frac{k_\perp^2 v_{th}^2}{\omega_{ce}^2}\sin^2\tfrac{1}{2}\omega_{ce}t\}\right) = 0 \qquad (21)$$

This is the cyclotron harmonic wave dispersion relation, first obtained by Bernstein [10], again for the case $\nu = 0$. Obviously, $k_\perp = 0$ is a a solution to Eq. (21), no matter what the value of the plasma parameters. Consequently, there is at least one $P_n(k_\parallel)$ that approaches zero as $k_\parallel \to 0$. Since $D(k_\perp, k_\parallel)$ is an even function of $k_\perp$, there will be more than one P_n with this property if $\partial^2 D/\partial k_\perp^2 = 0$ when $k_\perp$ and $k_\parallel$ are both zero. From Eq. (9),

$$\left.\frac{\partial^2 D}{\partial k_\perp^2}\right|_0 = 2K_\perp$$

Thus, as long as $K_\perp \neq 0$, there is only one $P_n(k_\parallel)$ that is zero for $k_\parallel$ real.

It is possible to have $K_\perp = 0$ only if $\nu = 0$ and $\omega = \omega_{UH}$, where ω_{UH} is the upper hybrid frequency, defined by $\omega_{UH}^2 = \omega_{pe}^2 + \omega_{ce}^2$. In the case $\nu = 0$, there are also solutions with $k_\perp = 0$ when $\omega = m\omega_{ce}$ $(m=2,3,4,\cdots)$ [24]. However, as shown by Shkarofsky and Johnston [25], both the nonrelativistic Boltzmann equation, Eq. (1), and the electrostatic approximation are not valid near the cyclotron harmonics. Consequently, we will limit our investigation to frequencies $\omega \neq m\omega_{ce}$ $(m=1,2,3,\cdots)$.

The P_n's will be ordered so that $P_o(0) = 0$, while $P_1(0) = 0$ only when $\nu = 0$ and $\omega = \omega_{UH}$. For simplicity, we will confine our attention to frequencies $\omega < \omega_{UH}$. This simplifies the mathematics, but is still sufficiently general for our later applications.

Accordingly, for all $n \geq 1$ we have

$$\mathscr{I}_n(\rho,z) \sim \sqrt{\frac{\pi}{2\rho}} \int_{-\infty}^{+\infty} dk \, \frac{\exp\{ikz - \rho P_n(k)\}}{R_n(k)\, P_n^{1/2}(k)} \tag{22}$$

By using the method of steepest descents, one can show that, as $r \to \infty$

$$\mathscr{I}_n(\rho,z) \sim \frac{\pi}{r} \sum_j \frac{\exp\{r[ik_{nj}\cos\theta - \sin\theta\, P_n(k_{nj})]\}}{R_n(k_{nj})[\cos^2\theta + \mathscr{D}_n'(k_{nj})\sin^2\theta]^{1/2}} \tag{23}$$

Here, the k_{nj} are the solutions of the stationary point condition

$$P_n'(k_{nj}) = i\cot\theta \tag{24}$$

and we have allowed for the possibility that there may be more than one k which will solve Eq. (24) for a given n. The function $\mathscr{D}_n'(k_{nj})$ is the derivative of

$$\mathscr{D}_n(k) = \frac{1}{2}\frac{d}{dk} P_n^2(k)$$

Also, we have used the identity $P_n''(k_{nj})P_n(k_{nj}) = \cot^2\theta + \mathscr{D}_n'(k_{nj})$.

In making this expansion, we have implicitly assumed that $R_n(k_{nj}) \neq 0$ and that $P_n''(k_{nj}) \neq 0$. This latter statement is equivalent to saying that $\cos^2\theta + \mathscr{D}_n'(k_{nj})\sin^2\theta \neq 0$, or to saying that each stationary point is isolated.

The stationary point condition, Eq. (24), has a very useful geometrical interpretation [26]. Since $k_\perp = iP_n(k_{||})$ is one root of

the dispersion relation, Eq. (24) may be restated as

$$\frac{\partial k_\perp}{\partial k_\parallel} = -\cot\theta \tag{25}$$

Differentiating the dispersion relation $D(k_\perp, k_\parallel) = 0$, we obtain

$$\frac{\partial D/\partial k_\parallel}{\partial D/\partial k_\perp} = \cot\theta \tag{26}$$

If we define the group velocity of a wave as $\partial\omega/\partial\underline{k}$, then the angle that the group velocity makes with the magnetic field is

$$\tan\psi = \frac{\partial D/\partial k_\perp}{\partial D/\partial k_\parallel}$$

Hence, $\psi = \theta$, and the stationary point condition tells us that the group velocity is directed from the source to the point of observation.

Having this seemingly infinite number of $\mathscr{I}_n$'s, each of which may have several terms, appears to be extremely unwieldy. However, almost all the $\mathscr{I}_n$'s are so strongly damped that their contributions to the potential are negligible for $r \to \infty$. Electrostatic waves in a warm, magnetized plasma are damped, even when $\nu = 0$, whenever a solution to the dispersion relation exists with $k_\parallel \neq 0$ [11,17]. We can use this fact in investigating the assumptions made in obtaining Eq. (23).

In going from Eq. (22) to Eq. (23), we assumed that $R_n(k_{nj}) \neq 0$ and $P_n''(k_{nj}) \neq 0$. If either of these were not true, the form of the asymptotic expansion would have to be modified. Such changes would be important only if they occurred in one of the $\mathscr{I}_n$'s that is

lightly damped. These terms with $n \geq 1$ do not enter into our applications of the asymptotic expansion in later chapters; however, they are of theoretical interest, so we discuss whether any changes need to be made in Appendix C.

Let us now turn to the most difficult term, $n = 0$. For this case, the Bessel function in Eq. (19) may not be automatically replaced with its asymptotic form because $P_0(0) = 0$. To cope with this, we need to investigate how $P_0(k_{\parallel})$ behaves when $k_{\parallel}$ is small. Expanding the dispersion function, Eq. (9), for small $k_\perp$ and $k_{\parallel}$, one obtains

$$D(k_\perp, k_{\parallel}) = K_\perp k_\perp^2 + K_{\parallel} k_{\parallel}^2 + \cdots \tag{27}$$

which is the same as the cold plasma result. Hence, for small $k_{\parallel}$

$$P_0(k_{\parallel}) \cong \sqrt{k_{\parallel}^2 K_{\parallel} / K_\perp} \tag{28}$$

where the square root has positive real part. Equation (27) also shows that $R_0(0) = K_\perp$.

These limiting forms suggest one way to take care of the fact that $P_0(0) = 0$: add and subtract the cold plasma result in Eq. (19)

$$\mathcal{J}_0(\rho, z) = \frac{\pi}{(K_\perp^2 K_{\parallel})^{1/2}} \left(\frac{\rho^2}{K_\perp} + \frac{z^2}{K_{\parallel}}\right)^{-1/2}$$

$$+ \int_{-\infty}^{+\infty} dk\, e^{ikz} \left\{ \frac{K_0(\rho P_0(k))}{R_0(k)} - \frac{K_0(\rho |k| \sqrt{K_{\parallel} / K_\perp})}{K_\perp} \right\} \tag{29}$$

The remaining integrand is zero at $k = 0$; thus, as $r \to \infty$, the integral is asymptotic to

$$\left(\frac{\pi}{2\rho}\right)^{1/2} \int_{-\infty}^{+\infty} dk\, e^{ikz} \left\{ \frac{\exp(\rho P_0(k))}{R_0(k) P_0^{1/2}(k)} - \frac{\exp(\rho |k| \sqrt{K_{\parallel} / K_\perp})}{K_\perp (|k| \sqrt{K_{\parallel} / K_\perp})^{1/2}} \right\}$$

If we now split the above integral into two, consideration of their forms shows that each is a convergent integral, one of which can be done exactly. Accordingly,

$$\mathcal{J}_0(\rho,z) \sim \frac{\pi}{K_\perp}\left\{\left(z^2+\rho^2\frac{K_\parallel}{K_\perp}\right)^{-1/2} - \left(2\rho\sqrt{\frac{K_\parallel}{K_\perp}}\right)^{-1/2}\left[\left(\rho\sqrt{\frac{K_\parallel}{K_\perp}}+iz\right)^{-1/2} + \left(\rho\sqrt{\frac{K_\parallel}{K_\perp}}-iz\right)^{-1/2}\right]\right\}$$

$$+ \left(\frac{\pi}{2\rho}\right)^{1/2}\int_{-\infty}^{+\infty} dk\,\frac{\exp[ikz - \rho P_0(k)]}{R_0(k)\,P_0^{1/2}(k)} \qquad (30)$$

The term in braces in Eq. (30) is finite and $O(1/r)$ for all ρ and z, even if $\nu = 0$. Thus, the procedure used to obtain Eq. (30) has not introduced any singularity at the cold plasma resonance cone angle.

The final term in Eq. (30) has most of the interesting physics in it. Defining it to be a new quantity $H(\rho,z)$, it can be rewritten in the form

$$H(\rho,z) = \left(\frac{\pi}{2\rho}\right)^{1/2}\int_0^{\infty} dk\,\left\{\frac{\exp[ikz - \rho P_0(k)]}{R_0(k)\,P_0^{1/2}(k)} + \frac{\exp[-ikz - \rho P_0(k)]}{R_0(k)\,P_0^{1/2}(k)}\right\} \qquad (31)$$

Here we have used the fact that $P_0(k)$, like all the P_n, is an even function of k. By restricting k to $\mathrm{Re}\,k \geq 0$, we no longer have to worry about the fact that $P_0'(k)$ is discontinuous at $k = 0$ (see Eq. (28)).

When asymptotically expanding integrals with finite limits of integration, one must consider in addition to the contribution from

the stationary points, the contributions from the end points [27]. If $P_o(k)$ were finite at $k = 0$ and if it had a continuous first derivative there, then the end point contributions from the two terms in Eq. (31) would cancel each other. However, $P_o(0) = 0$ and Eq. (28) shows that

$$\lim_{k \to 0-} P_o'(k) = - \lim_{k \to 0+} P_o'(k) \neq 0$$

To handle this manifestation of the fact that $P_o(0) = 0$, change variables to $\eta^2 = k$. This yields

$$H(\rho,z) = \left(\frac{2\pi}{\rho}\right)^{1/2} \left\{ \int_0^\infty d\eta \, \frac{\eta}{R_o(\eta^2) P_o^{1/2}(\eta^2)} \exp[i\eta^2 z - \rho P_o(\eta^2)] \right.$$
$$\left. + \int_0^\infty d\eta \, \frac{\eta}{R_o(\eta^2) P_o^{1/2}(\eta^2)} \exp[- i\eta^2 z - \rho P_o(\eta^2)] \right\} \qquad (32)$$

The factor multiplying the exponential in each integral in Eq. (32) is now finite for all η.

When we asymptotically expand the integrals in Eq. (32), the stationary point condition becomes

$$\eta[i\sigma \cos\theta - \sin\theta \, P_o'(\eta^2)] = 0$$

where $\sigma = +1$ for the first integral in Eq. (32) and $\sigma = -1$ for the second. One set of solutions to this is

$$P_o'(\eta^2) = i\sigma \cot\theta \qquad \mathrm{Re}\, \eta^2 \geq 0 \qquad (33)$$

which is just what Eq. (24) becomes under the change of variable. The

other solution is $\eta = 0$, which is a new stationary point located at the lower limit of integration. If all the solutions of Eq. (33) also satisfy $\eta^2 P_o''(\eta^2) \neq 0$, then

$$H(\rho,z) \sim \frac{\pi}{K_\perp}\left(2\rho\sqrt{\frac{K_\parallel}{K_\perp}}\right)^{-1/2}\left[\left(\rho\sqrt{\frac{K_\parallel}{K_\perp}} + iz\right)^{-1/2} + \left(\rho\sqrt{\frac{K_\parallel}{K_\perp}} - iz\right)^{-1/2}\right] + \frac{\pi}{r}\sum_j \frac{\exp\{r[i\sigma\eta_j^2\cos\theta - \sin\theta\, P_o(\eta_j^2)]\}}{R_o(\eta_j^2)[\cos^2\theta + \mathscr{D}_o'(\eta_j^2)\sin^2\theta]^{1/2}} \quad (34)$$

The quantities η_j^2 are the solutions to Eq. (33).

At first glance, we seem to have reacquired singularities at the cold plasma resonance cone angle when $\nu = 0$. Equation (34), however, is not valid for $\cot^2\theta = \cot^2\theta_c$. To see this, consider the fact that $P_o^2(k)$ is an even function of k and is proportional to k^2 for small k (see Eq. (28)). Thus, near $k = 0$, we must have

$$P_o^2(k) = \frac{K_\parallel}{K_\perp} k^2 + \alpha k^4 + \ldots$$

Consequently, for $\mathrm{Re}\, k \geq 0$

$$P_o(k) = k\sqrt{\frac{K_\parallel}{K_\perp}}\left(1 + \frac{K_\perp \alpha}{2K_\parallel} k^2 + \ldots\right)$$

This means that $P_o''(0) = 0$. Further, from the form of $P_o(k)$, $k = 0$ (i.e., $\eta^2 = 0$) is a solution to Eq. (33) when $\cot^2\theta = \cot^2\theta_c$ and $\nu = 0$. Hence, Eq. (34) is valid only for angles sufficiently far from the cold plasma resonance cone angle.

Mathematically, the problem is that one of the η_j approaches the stationary point at $\eta = 0$ as $\cot^2\theta \to \cot^2\theta_c$. Accordingly, we

need a method of asymptotic expansion which can handle integrals with coalescing stationary points. One such method has been worked out by Chester, Friedman and Ursell [28]. It consists of changing variables in the integral in question to obtain more analytically tractable forms while preserving the nature of the stationary points.

In general, for $\sigma = +1$ there is one η_j^2 that approaches zero as $\theta \to \theta_c$, while for $\sigma = -1$ another η_j^2 approaches zero in the same manner when $\theta \to \pi - \theta_c$. Consequently, the contribution due to the first two stationary points in each integral in Eq. (32) will have to be modified for certain angles. The contributions of all other stationary points are still given by the sum in Eq. (34).

We are thus led to consider the large r expansion of integrals of the form

$$G_{\pm}(r,\theta) = \left(\frac{2\pi}{r \sin\theta}\right)^{1/2} \int_0^{M_{\pm}} d\eta \, \frac{\eta}{R_o(\eta^2) P_o^{1/2}(\eta^2)} \exp[\pm i r \eta^2 \cos\theta - r \sin\theta \, P_o(\eta^2)] \qquad (35)$$

where $M_{\pm} = M_{\pm}(\theta)$ is chosen so that only the first nonzero stationary points of the exponent are included in each range of integration. Let us name these two stationary points $\eta_{\pm}^2$. In Eq. (34), we already have the asymptotic expansions of $G_{\pm}(r,\theta)$ when $\eta_{\pm}^2$ are not near $\eta = 0$. Consequently, we only need consider the cases where one of them is small.

The form of the change of variable is suggested by the small η expansion of the exponents in Eq. (35), but its validity is not

dependent on having η small. Let

$$\pm i\eta^2 \cos\theta - \sin\theta\, P_o(\eta^2) = \frac{1}{6}u^6 - \zeta_\pm(\theta)\, S(u^2)\, u^2 \tag{36}$$

where

$$S(z) = \begin{cases} +1 & \text{Re } z > 0 \\ -1 & \text{Re } z < 0 \end{cases}$$

With the inclusion of $S(u^2)$, both the right and left hand sides of Eq. (36) have two stationary points for $|\eta| \leq M_\pm$.

For the change of variable to be one to one, we require $d\eta/du$ to be finite and nonzero in the range of interest. Since

$$2\eta[\pm i \cos\theta - \sin\theta\, P_o'(\eta^2)]\frac{d\eta}{du} = u[u^4 - 2\zeta_\pm(\theta)\, S(u^2)]$$

this means that the points $u = 0$ and $u^2 = (2\zeta_\pm)^{1/2}$ must correspond to $\eta = 0$ and $\eta^2 = \eta_\pm^2(\theta)$. Consequently,

$$\zeta_\pm(\theta) = -\frac{1}{2}\{3\sin\theta[\pm\cot\theta\,\eta_\pm^2 + iP_o(\eta_\pm^2)]\}^{2/3} \tag{37}$$

Notice that the $\zeta_\pm$ go to zero when $\eta_\pm^2 \to 0$.

We can now write Eq. (35) as

$$G_\pm(r,\theta) = \left(\frac{2\pi}{r\sin\theta}\right)^{1/2} \int_0^{\infty e^{i\pi/6}} du\, \frac{d\eta}{du} \frac{\eta}{R_o(\eta^2)P_o^{1/2}(\eta^2)} \times \exp[r(\frac{1}{6}u^6 - \zeta_\pm u^2)]$$

Here we have replaced the finite upper limit of the integral in Eq. (35) by infinity. This produces a negligible error in the asymptotic

limit. The factor $e^{i\pi/6}$ insures that the path of steepest descent is taken as $u \to \infty$.

We are concerned with $\cot^2\theta$ near $\cot^2\theta_c$; thus, the two stationary points are close together. Accordingly, in the asymptotic limit, the factor in front of the exponential can be evaluated at $u = 0$ and taken out of the integral. Consequently,

$$G_{\pm}(r,\theta) \sim \frac{(2\pi)^{1/2}}{r^{2/3}\sin\theta} \left(\frac{K_{\parallel}}{K_{\perp}}\right)^{-1/4} \left[\frac{-\zeta_{\pm}(\theta)}{\pm i\cot\theta - (K_{\parallel}/K_{\perp})^{1/2}}\right]^{1/2} \times F(2^{-1/3} r^{2/3}\zeta_{\pm}) \qquad (38)$$

where

$$F(x) = e^{i\pi/6} \int_0^{\infty} d\lambda \exp(-\frac{1}{6}\lambda^6 - x2^{1/3} e^{i\pi/3}\lambda^2)$$

It is easy to show that

$$F'''(x) - 4xF'(x) - 2F(x) = 0$$

This is the differential equation satisfied by the product of Airy functions [29]; hence, its three linearly independent solutions are $Ai^2(x)$, $Ai(x)Bi(x)$, and $Bi^2(x)$. By considering the values of $F(0)$, $F'(0)$, and $F''(0)$, one may show after a bit of algebra that

$$F(x) = \frac{\pi^{3/2}}{2^{1/6}} Ai(x)[Bi(x) + iAi(x)] \qquad (39)$$

It is this function which will control the primary contribution to the asymptotic expansion near the resonance cone. As long as

$F(2^{-1/3}r^{2/3}\zeta_{\pm})$ is $O(1)$, then $G_{\pm}(r,\theta)$ are $O(r^{-2/3})$. Contrast this with all the other terms in the expansion, which are at most $O(r^{-1})$. In Fig. 4, we show the magnitude and phase of $Ai(x)[Bi(x) + iAi(x)]$ for real values of x. Note that the magnitude plot has qualitative features similar to those shown by the magnitude plot in Fig. 3. This combination of Airy functions will give us the mathematical description of the interference structure in the asymptotic limit.

The Airy functions do not give the whole story, of course. The complete expansion will never have points where the magnitude of the potential is zero. Near the points where $|F(x)| = 0$, the $O(r^{-1})$ terms in the expansion give important contributions. This fact will also affect the phase. However, the location of the maxima in the interference structure will be given by the maxima of $|F(2^{-1/3}r^{2/3}\zeta_{\pm})|$. Furthermore, in the complete expansion, $\zeta_{\pm}(\theta)$ will generally be complex, due to Landau damping. Only near $\zeta_{\pm} = 0$ will they be predominantly real.

The asymptotic expansion is now complete; however, the results are scattered over the last ten pages and involve a host of intermediate functions. By simple manipulations, everything can be related back to the dispersion function. The result is

$$\phi(\rho,z,t) \sim \frac{qe^{-i\omega t}}{4\pi^2\varepsilon_o}\left(\frac{\pi}{K_\perp r}\left\{\left(\cos^2\theta + \frac{K_\parallel}{K_\perp}\sin^2\theta\right)^{-1/2}\right.\right.$$

$$\left.\left. - \frac{1}{\sqrt{2}\sin\theta}\left(\frac{K_\parallel}{K_\perp}\right)^{-1/4}\left[\left(\sqrt{\frac{K_\parallel}{K_\perp}} + i\cot\theta\right)^{-1/2} + \left(\sqrt{\frac{K_\parallel}{K_\perp}} - i\cot\theta\right)^{-1/2}\right]\right\}$$

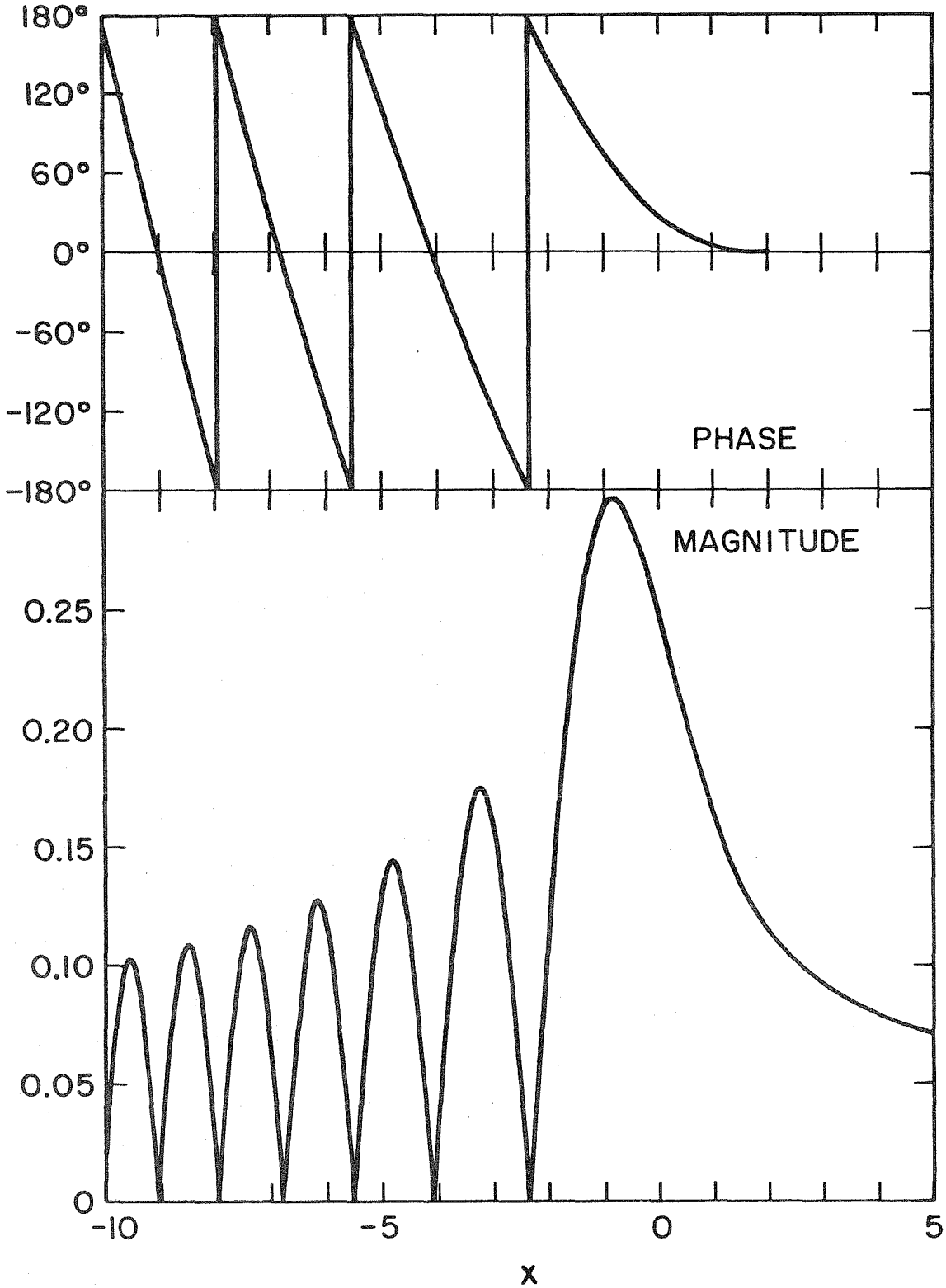

Fig. 4 Magnitude and phase of Ai(x)[Bi(x) + iAi(x)].

$$+ G_+(r,\theta) + G_-(r,\theta) + \frac{\pi}{r} \sum_n \frac{\exp[ir(k_{\parallel n}\cos\theta + k_{\perp n}\sin\theta)]}{Q(k_{\perp n}, k_{\parallel n})} \Bigg) \tag{40}$$

where

$$Q(k_\perp, k_\parallel) = \left[\frac{1}{2k_\perp}\frac{\partial D}{\partial k_\perp}\left(\cos^2\theta\,\frac{\partial^2 D}{\partial k_\perp^2} - 2\sin\theta\cos\theta\,\frac{\partial^2 D}{\partial k_\perp \partial k_\parallel} + \sin^2\theta\,\frac{\partial^2 D}{\partial k_\parallel^2}\right)\right]^{\frac{1}{2}}$$

and where the $(k_{\perp n}, k_{\parallel n})$ are almost all the solutions to

$$D(k_\perp, k_\parallel) = 0 \qquad \text{Im } k_\perp \geq 0 \tag{41}$$

$$\frac{\partial D/\partial k_\parallel}{\partial D/\partial k_\perp} = \cot\theta \tag{42}$$

The solutions to Eqs. (40) and (41) which are not included in $(k_{\perp n}, k_{\parallel n})$ are the one that approaches (0,0) as $\theta \to \theta_c$, which will be called $(k_{\perp +}, k_{\parallel +})$, and the one that approaches (0,0) as $\theta \to \pi - \theta_c$, which will be called $(k_{\perp -}, k_{\parallel -})$. Notice that $k_{\perp +}(\theta) = k_{\perp -}(\pi-\theta)$ and $k_{\parallel +}(\theta) = -k_{\parallel -}(\pi-\theta)$.

If θ is not near θ_c (for +), or $\pi-\theta_c$ (for -)

$$G_\pm(r,\theta) \sim \frac{\pi}{K_\perp r\sqrt{2}\sin\theta}\left(\frac{K_\parallel}{K_\perp}\right)^{-1/4}\left(\sqrt{\frac{K_\parallel}{K_\perp}} \mp i\cot\theta\right)^{-1/2}$$

$$+ \frac{\pi}{r}\,\frac{\exp[ir(k_{\parallel\pm}\cos\theta + k_{\perp\pm}\sin\theta)]}{Q(k_{\perp\pm}, k_{\parallel\pm})} \tag{43}$$

If θ is near θ_c (for +), or near $\pi-\theta_c$ (for -)

$$G_\pm(r,\theta) \sim \frac{2^{1/3}\pi^2}{r^{2/3}\sin\theta}\left(\frac{K_\parallel}{K_\perp}\right)^{-1/4}\left[\frac{\zeta_\pm(\theta)}{(K_\parallel/K_\perp)^{1/2} \mp i\cot\theta}\right]^{1/2}$$

$$\times \text{Ai}(X_\pm)[\text{Bi}(X_\pm) + i\text{Ai}(X_\pm)] \tag{44}$$

where

$$X_{\pm}(\theta) = 2^{-1/3} r^{2/3} \zeta_{\pm}(\theta) = - \left(\frac{3r}{4}\right)^{2/3} (\cos\theta\, k_{\parallel\pm} + \sin\theta\, k_{\perp\pm})^{2/3}$$

The asymptotic expansion was derived under the assumption that $\sin\theta \neq 0$ and $\omega < \omega_{UH}$. However, the result is finite as $\sin\theta \to 0$. The terms in the braces in Eq. (40) which appear to give an infinite result are exactly canceled by two corresponding terms in $G_{\pm}(r,\theta)$. One can show that as long as $K_{\perp} \neq 0$, the expansion in Eq. (40) is also correct as $\sin\theta \to 0$. This proof requires the results in Appendix C, and so will be done in Appendix D.

In Eqs. (40)-(43) we have the asymptotic expansion for the electrostatic Green's function for frequencies $\omega < \omega_{UH}$. (See Appendix C for a discussion of some restrictions on the region of validity of the terms in the sum in Eq. (40).) The frequency range could be extended to $\omega \leq \omega_{UH}$ by handling the $n = 1$ term in Eq. (18) in a manner similar to that used for the $n = 0$ term. However, that would have made the expansion needlessly complex. The present expansion is sufficient for our purposes.

CHAPTER III

FURTHER THEORETICAL CONSIDERATIONS

3.1 Physical Predictions from the Asymptotic Expansion

The results in Eqs. (40)-(44) are still of a rather formal nature. To get the physics out of them, we need more explicit information on the solutions to Eqs. (41) and (42). If one needed all the solutions to these equations, he would have to resort to numerical procedures; the dispersion function is much too complicated to be handled in general by analytic means. Special cases, however, can be done by explicit analysis.

One quantitative result can be obtained immediately. In an anisotropic medium, the phase and group velocities of a wave do not have to be parallel; in general, there can be an arbitrary angle between the two vectors. By considering the form of $(k_{\perp +}, k_{\parallel +})$ for θ near θ_c, one can show that the phase and group velocities of this mode are actually orthogonal at $\theta = \theta_c$ when $\nu = 0$.

For θ near θ_c, both $k_{\perp +}$ and $k_{\parallel +}$ are small; hence the dispersion relation becomes

$$K_\perp k_{\perp +}^2 + K_\parallel k_{\parallel +}^2 \tilde{=} 0$$

At $\theta = \theta_c$, the angle between the phase velocity and the magnetic field is

$$\cot^2 \lambda_c = \lim_{\theta \to \theta_c} \frac{k_{\parallel +}^2}{k_{\perp +}^2} = - \frac{K_\perp}{K_\parallel} \tag{45}$$

We have shown in Chapter II that θ is the angle between the group

velocity and the magnetic field. Since $\cot^2\theta_c = -K_{\parallel}/K_{\perp}$ when $\nu = 0$, λ_c and θ_c are complementary angles; thus, the group and phase velocity are orthogonal on the resonance cone. (A similar proof can be carried out to show that the same conclusions hold at $\theta = \pi - \theta_c$).

One qualitative prediction can also be made rather easily. Due to Landau damping, only solutions to Eqs. (41) and (42) with small $k_{\parallel}$ will contribute significantly to the potential in the asymptotic limit. Consider $k_{\parallel} = 0$ in order to find what terms in Eq. (40) might be significant in the lower and upper branches. In the lower branch ($\omega \leq \min(\omega_{pe},\omega_{ce})$), the only solutions to the dispersion relation that have $k_{\perp}$ real when $k_{\parallel} = 0$ are $(k_{\perp+},k_{\parallel+})$ at $\theta = \theta_c$ and $(k_{\perp-},k_{\parallel-})$ at $\theta = \pi - \theta_c$ [30]. Consequently, none of the terms in the sum in Eq. (40) is significant. In the upper branch ($\max(\omega_{pe},\omega_{ce}) \leq \omega \leq \omega_{UH}$), in addition to the previous solution, the Bernstein mode solution exists. Since this has $k_{\perp}$ real and nonzero for $k_{\parallel} = 0$, at least one of the terms in the sum in Eq. (40) can contribute appreciably to the potential.

More detailed predictions take further analysis. To make these, it would be useful to have approximate forms for $\zeta_{\pm}$ when they are small; this would allow detailed computations of parts of the resonance cone structure.

Returning to the original definition in Eq. (37), we see that we need to know $\eta_{\pm}^2$ to find $\zeta_{\pm}(\theta)$. For small η^2

$$P_o(\eta^2) \cong \left(\frac{K_{\parallel}}{K_{\perp}}\right)^{1/2} \eta^2 + \frac{1}{6} P_o'''(0)\, \eta^6 + \ldots \qquad (46)$$

Thus, when each $\eta_\pm^2$ is small, the solution to the stationary point condition, Eq. (33), yields

$$\eta_\pm^4 = \frac{2}{P_o'''(0)}\left[\pm i \cot\theta - \left(\frac{K_\parallel}{K_\perp}\right)^{1/2}\right] \tag{47}$$

Using these approximations,

$$\zeta_\pm(\theta) = -\left[\frac{i \sin^2\theta}{P_o'''(0)}\right]^{1/3}\left[\pm\cot\theta + i\left(\frac{K_\parallel}{K_\perp}\right)^{1/2}\right] \tag{48}$$

Since $k_\perp = iP_o(k_\parallel)$ is one of the solutions to the dispersion relation, one can show by differentiating three times that

$$P_o'''(0) = i \lim_{\substack{k_\parallel \to 0 \\ k_\perp \to 0}} k_\perp\left(\frac{\partial D}{\partial k_\perp}\right)^{-1}\left\{\frac{1}{k_\perp}\frac{\partial^3 D}{\partial k_\perp^3}\left(\frac{\partial k_\perp}{\partial k_\parallel}\right)^3 + \frac{3}{k_\perp}\frac{\partial^3 D}{\partial k_\perp^2 \partial k_\parallel}\left(\frac{\partial k_\perp}{\partial k_\parallel}\right)^2\right.$$

$$\left. + \frac{3}{k_\perp}\frac{\partial^3 D}{\partial k_\parallel^2 \partial k_\perp}\frac{\partial k_\perp}{\partial k_\parallel} + \frac{1}{k_\perp}\frac{\partial^3 D}{\partial k_\parallel^3} + \frac{3}{k_\perp}\frac{\partial^2 D}{\partial k_\perp^2}\frac{\partial k_\perp}{\partial k_\parallel}\frac{\partial^2 k_\perp}{\partial k_\parallel^2} + \frac{3}{k_\perp}\frac{\partial^2 D}{\partial k_\perp \partial k_\parallel}\frac{\partial^2 k_\perp}{\partial k_\parallel^2}\right\}$$

The evaluation of this expression is straightforward but laborious. First, one must relate $\partial^2 k_\perp/\partial k_\parallel^2$ and $\partial k_\perp/\partial k_\parallel$ to derivatives of the dispersion function $D(k_\perp, k_\parallel)$. Once this is done, Eq. (9) can be used to compute explicitly the derivatives of $D(k_\perp, k_\parallel)$. Fortunately, all the resultant integrals can be done analytically in the limit that $k_\parallel \to 0$ and $k_\perp \to 0$. The result is

$$P_o'''(0) = -\frac{1}{K_\perp}\left(\frac{K_\parallel}{K_\perp}\right)^{-1/2}\frac{9\omega_{pe}^2(1+i\nu/\omega)v_{th}^2}{2\omega^4}\Delta \tag{49}$$

where

$$\Delta = 1 - \frac{(\omega+i\nu)^2}{3[(\omega+i\nu)^2 - \omega_{ce}^2]} \left\{ \frac{6(\omega+i\nu)^4 - 3(\omega+i\nu)^2\omega_{ce}^2 + \omega_{ce}^4}{[(\omega+i\nu)^2 - \omega_{ce}^2]^2} \frac{K_{\parallel}}{K_{\perp}} - \frac{3(\omega+i\nu)^2}{(\omega+i\nu)^2 - 4\omega_{ce}^2} \left(\frac{K_{\parallel}}{K_{\perp}}\right)^2 \right\}$$

The combination $K_{\perp}(K_{\parallel}/K_{\perp})^{1/2}$ has been left in this form so that the proper sign can be obtained in the $\nu \to 0$ limit.

Using Eq. (49), we have

$$X_{\pm} \equiv 2^{-1/3} r^{2/3} \zeta_{\pm}(\theta) = \left[i \sin^2\theta \, K_{\perp} \left(\frac{K_{\parallel}}{K_{\perp}}\right)^{1/2} \frac{r^2\omega^4}{9\omega_{pe}^2(1+i\nu/\omega)v_{th}^2\Delta} \right]^{1/3} \times \left[\pm \cot\theta + i\left(\frac{K_{\parallel}}{K_{\perp}}\right)^{1/2} \right] \tag{50}$$

For each sign, this result is only valid when $|\zeta_{\pm}(\theta)| \ll 1$ for that sign.

Having Eq. (50), we can predict where the local maxima in $|\phi(\rho,z,t)|$ will occur. These maxima are controlled solely by one or the other of the $G_{\pm}(r,\theta)$ terms in the asymptotic expansion; thus, the maxima occur wherever $|Ai(X_{\pm})(Bi(X_{\pm}) + iAi(X_{\pm}))|$ have relative maxima. For $\nu = 0$, the values of $X_{\pm}$ that give the maxima are real. Their values, computed by methods given in Appendix B, are given in Table 1.

By differentiating the potential, one can get the electric field components. For future reference, the values of $X_{\pm}$ that give the maxima in the magnitude in the electric field components are also listed in Table 1, again with $\nu = 0$.

Table 1

Location of the Maxima of $|F(x)|$ and $|F'(x)|$ where $F(x) = Ai(x)(Bi(x) + iAi(x))$

n	$-x_n$	$-x_n'$
1	0.78543	1.63257
2	3.22483	3.65280
3	4.80934	5.16230
4	6.15677	6.46978
5	7.36759	7.65439
6	8.48502	8.75271
7	9.53270	9.78552

Notice from the table (or from Fig. 4) that all the maxima occur for $X_\pm < 0$. Since $X_\pm = 0$ on the cold plasma resonance cone, it is more useful to discuss the location of the peaks relative to the cold cone. Define $\Delta\theta_n = \theta_c - \theta_n$, where θ_n is the angular position of the n^{th} maximum; the maximum closest to θ_c is numbered $n = 1$. Consequently, as $r \to \infty$, we have, when $\nu = 0$,

$$\Delta\theta_n = -x_n \left[\frac{9\omega_{pe}^2 v_{th}^2 \sin^4\theta_c \Delta}{r^2\omega^4 \text{sign}(K_\perp)(-K_\parallel K_\perp)^{1/2}} \right]^{1/3} \tag{51}$$

where the x_n are given in Table 1. The original definition of $\Delta\theta_n$ is appropriate to X_+; for X_- the analogous definition would be $\Delta\theta_n = (\pi - \theta_c) - \theta_n$ and these $\Delta\theta_n$ are just the negative of the ones given in Eq. (51).

Equation (51) will be used quite extensively in Chapter VI, so it is worth discussing in some detail. First, notice that each of the $\Delta\theta_n$ has the same dependence on the plasma parameters. All the $\Delta\theta_n$ just differ by a scale factor. This leads to an interesting prediction: the ratio $\Delta\theta_n/\Delta\theta_m$ should be a constant, independent of the plasma conditions, whose value depends only on m and n. Second, the dependence on temperature and radius is particularly simple: $\Delta\theta_n$ is proportional to $T_e^{1/3}$ and to $r^{-2/3}$. The dependence on ω, ω_{pe}, and ω_{ce} is a good deal more complicated.

To study the dependence on the frequency parameters, define

$$\Lambda(\omega,\omega_{pe},\omega_{ce}) = \left[\frac{9\omega_{pe}^2\omega_{ce}^2 \sin^4\theta_c \Delta}{\omega^4 \text{sign}(K_\perp)(-K_\perp K_\parallel)^{1/2}}\right]^{1/3} \tag{52}$$

Using this,

$$\Delta\theta_n = -x_n\left(\frac{v_{th}}{r\omega_{ce}}\right)^{2/3} \Lambda$$

Considering the definitions of θ_c and Δ, it is easy to show that Λ depends only on the dimensionless ratios ω/ω_{ce} and ω_{pe}/ω_{ce}. To show the functional form of Λ, it has been plotted in Figs. 5 and 6 for the case $\nu = 0$. In Fig. 5, we have Λ vs ω/ω_{ce} for various values of ω_{pe}/ω_{ce}, while in Fig. 6 we see Λ vs ω_{pe}/ω_{ce} for $\omega/\omega_{ce} < 1$. Figure 5 is very similar to a plot given by Kuehl [8]. In the upper branch region in Fig. 5, the plot has been stopped at $\Lambda = 0$. One can show that $\Lambda \to \infty$ as $\omega \to \omega_{UH}$. The asymptotic expansion is not valid, however, for frequencies too near the

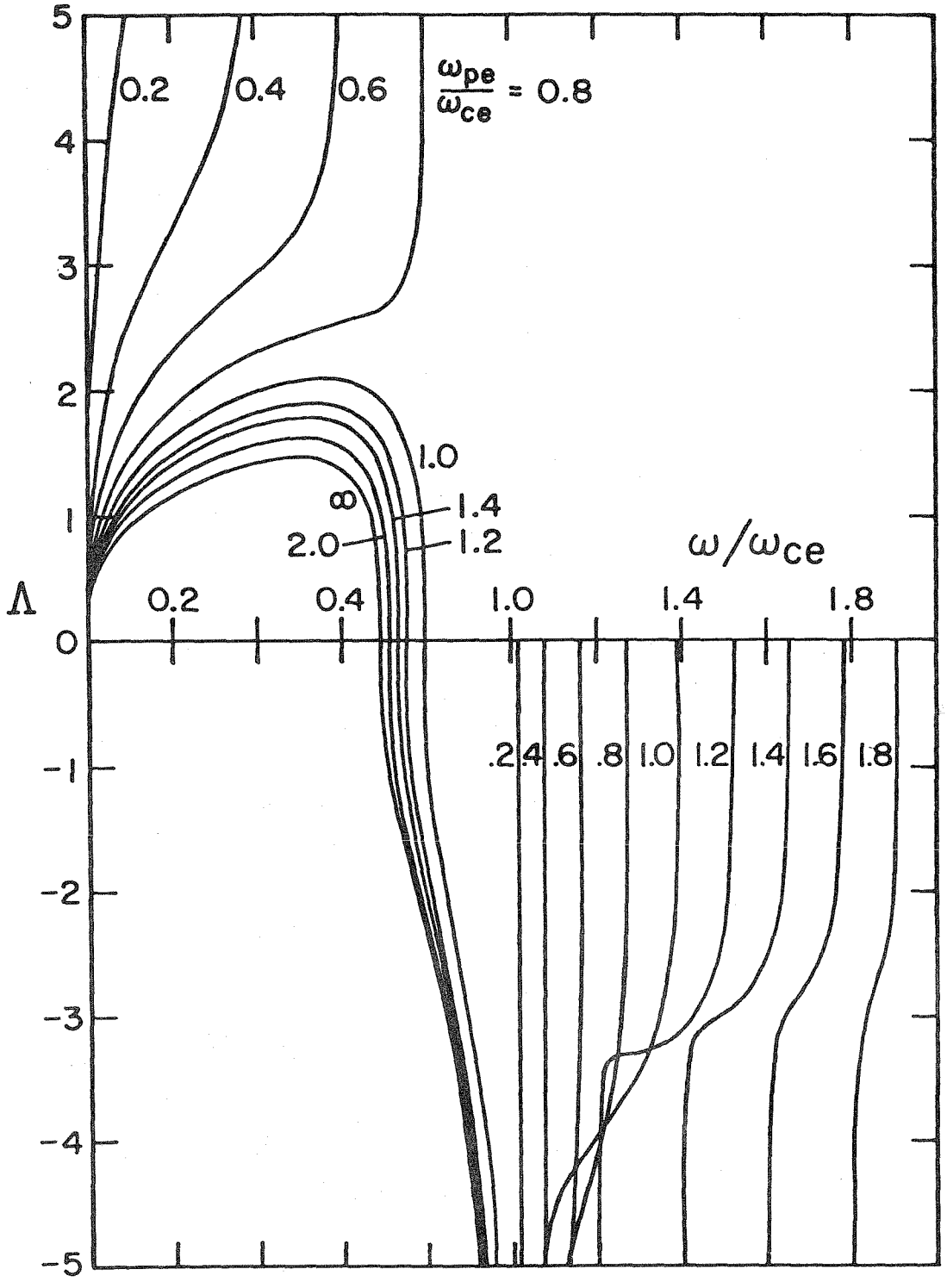

Fig. 5 Dependence of Λ on ω/ω_{ce} with ω_{pe}/ω_{ce} as a parameter for the case $\nu = 0$.

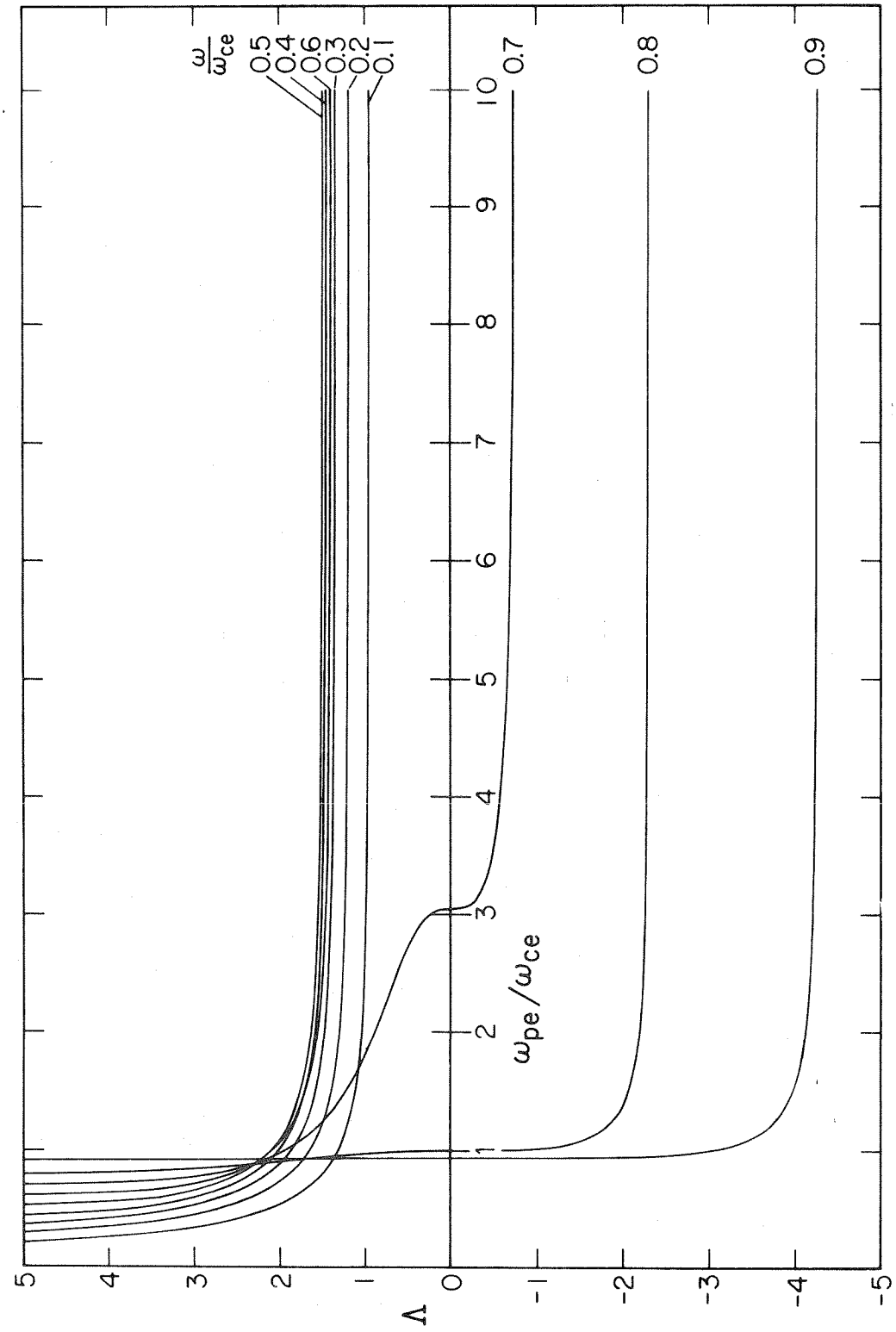

Fig. 6 Dependence of Λ on ω_{pe}/ω_{ce} with ω/ω_{ce} as a parameter for the case $\nu = 0$.

upper hybrid. Since $\Lambda = 0$ at a frequency just a bit below ω_{UH}, it is a convenient place to stop.

From Fig. 5, it is obvious that Λ can have either sign. Hence, the interference structure can appear either inside the cold plasma cone angle ($\Lambda > 0$) or outside it ($\Lambda < 0$). Also, as is apparent from Fig. 5, and obvious from Fig. 6, Λ is independent of ω_{pe}/ω_{ce} for frequencies in the lower branch when ω_{pe}/ω_{ce} is large enough. Except for ω/ω_{ce} near 0.7, ω_{pe}/ω_{ce} is large enough when $\omega_{pe}/\omega_{ce} \geq 2$.

We now have the predictions which we must have to compare with the experimental investigations discussed in the last three chapters of this work. There is much more that we could investigate about this asymptotic expansion. For example, it would be interesting to compare the complete asymptotic expansion in the upper branch with Kuehl's numerical results [8]. However, since we have what we need, we will have to forego the pleasure of further investigation.

3.2 The Line Source Antenna

In any experimental investigation, the actual antenna is, of course, not a point source. One can regard it as such only if the antenna dimensions are much smaller than the wavelength radiated. The antennas used in the present experimental work are long, thin wires, 0.25 mm in diameter and 3.5 or 7.5 cm in length. The wavelengths involved are usually greater than 1 mm, so the antennas can be suitably modeled as a finite length line source. Unfortunately, the easiest line source to handle mathematically is one that is infinitely long.

However, this model will not give too inaccurate a comparison with the experimental data as long as those data are taken close to the actual antenna.

Model the antenna as an oscillating line source of charge density $\sigma\delta(x)\delta(z)e^{-i\omega t}$. Just as in the case of a line source in electrostatics, the potential in this case will not approach zero as $r \to \infty$. This leads to Fourier integrals which are defined only as generalized functions, and these are difficult to expand asymptotically. However, the integrals for the electric fields are well defined in the classical sense, and we will work with them rather than with the potential.

Using the representation in Eqs. (18) and (19) for the electrostatic Green's function, we can find the electric fields by first differentiating with respect to x or z, and then integrating over the new charge distribution. The results are

$$E_x(x,z,t) = \frac{\sigma e^{-i\omega t}}{4\pi\varepsilon_o} \sum_{n=0}^{\infty} \int_{-\infty}^{\infty} dk \, \frac{\exp[ikz - xP_n(k)]}{R_n(k)} \tag{53}$$

$$E_z(x,z,t) = \frac{\sigma e^{-i\omega t}}{4\pi\varepsilon_o} \sum_{n=0}^{\infty} \int_{-\infty}^{\infty} dk \left[\frac{-ik}{P_n(k)}\right] \frac{\exp[ikz - xP_n(k)]}{R_n(k)} \tag{54}$$

Each integrand in Eq. (54) differs from the one in Eq. (53) by the factor $-ik/P_n(k)$. Since this is well behaved for all k, we may asymptotically expand the integrals in Eq. (53) and then obtain Eq. (54) simply by multiplying each term by the appropriate factor.

In doing the asymptotic expansion, we learned that the interesting physics comes out of the $n = 0$ term. The expansion of all the other terms can be done by standard methods, so we will concentrate on that term.

From our previous work, we know that $P_0'(k)$ is discontinuous at $k = 0$; hence, it is worth defining the analog of $H(\rho,z)$ as

$$H(x,z) = \int_0^\infty dk \frac{\exp[ikz - xP_0(k)]}{R_n(k)} + \int_0^\infty dk \frac{\exp[-ikz - xP_0(k)]}{R_n(k)} \qquad (55)$$

If we now define $z = r \cos\theta$ and $x = r \sin\theta$, we can attempt to expand $H(x,z)$ as $r \to \infty$.

Just as in the former case, we attempt to do the asymptotic expansion using the method of steepest descent. However, we know from our previous work that for θ near the resonance cone, one of the stationary point conditions $P_0'(k) = \pm i \cot\theta$ will have a solution with k small. Accordingly, $P_0''(k)$ will also be quite small, and the usual steepest descents formula will no longer apply. Unlike the earlier case, we do not have two stationary points which approach each other as $\cot^2\theta \to \cot^2\theta_c$; we simply have an exponent that violates one of the usual assumptions made in the method of steepest descents.

Scorer [31] has developed a method to handle exponents of the type that occur here. His arguments are based on the stationary phase approach, but this method and the more exact steepest descents procedure always agree on the first term in the asymptotic expansion [22]. Adapting his results to our notation, we obtain

$$\int_0^\infty dk \, \frac{\exp[r(\pm i \cos\theta - \sin\theta P_o(k))]}{R_o(k)}$$

$$\sim \frac{\pi}{R_o(k_\pm)} \left[\frac{-2i}{r \sin\theta P_o'''(k_\pm)}\right]^{1/3} e^{\beta_\pm} [Ai(X_\pm) + iGi(X_\pm)] \qquad (56)$$

Here, $k_\pm$ are the solutions to $P_o'(k_\pm) = \pm i \cot\theta$, $Gi(X)$ is a relative of the Airy function [29], and

$$\beta_\pm = r\left\{\pm ik \cos\theta - \sin\theta\left[P_o(k_\pm) - \frac{1}{3}\frac{(P_o''(k_\pm))^3}{(P_o'''(k_\pm))^2}\right]\right\}$$

$$X_\pm = \left(\frac{r \sin\theta}{2}\right)^{2/3} \frac{(P_o''(k_\pm))^2}{(iP_o'''(k_\pm))^{4/3}}$$

The expansion in Eq. (56) is valid for all θ. One can show, although it is a bit laborious, that if $P_o''(k_\pm)$ is sufficiently large that $|X_\pm| \gg 1$, then this expansion reduces to the one given by the standard steepest descents methods.

If we are interested in angles θ near θ_c (for +) or near $\pi-\theta_c$ (for -), then the right hand side of Eq. (56) can be simplified to

$$\frac{\pi}{K_\perp} \left[\frac{-2i}{r \sin\theta P_o'''(0)}\right]^{1/3} [\, Ai(X_\pm) + i\, Gi(X_\pm)\,] \qquad (57)$$

where

$$X_\pm = -\left[\frac{2ir^2\sin^2\theta}{P_o'''(0)}\right]^{1/3} \left[\pm \cot\theta + i\left(\frac{K_{\|}}{K_\perp}\right)^{1/2}\right] \qquad (58)$$

The quantities $X_{\pm}$ that were defined in the earlier asymptotic expansion have exactly the same functional form as the ones given in Eq. (58), but the previous ones are smaller by a factor of $2^{2/3}$. Since the functional form is the same; all of the discussion in Section 3.1 on how $X_{\pm}$ depend on the physical parameters holds here, too.

To show what the interference structure looks like in this case, in Fig. 7 we have plotted the magnitude and phase of $Ai(x) + i\ Gi(x)$ for real x. The qualitative features are much the same as before; specifically, the interference structure still occurs only on one side of the cold plasma resonance cone angle.

To relate the angular interference spacing to the physical parameters, we can again define $\Delta\theta_n$ to be the spacing between the cold plasma cone angle and the n^{th} interference peak. In terms of our previously defined functions, as $r \to \infty$

$$\Delta\theta_n = -y_n \left(\frac{v_{th}}{r\omega_{ce}}\right)^{2/3} \Lambda \tag{59}$$

where $y_n = 2^{-2/3} x_n$, and where x_n are the values of x at which $|Ai(x) + i\ Gi(x)|$ has a maximum. In Table 2, we give x_n and y_n as computed by the numerical methods given in Appendix B.

If one wishes to compare the line source results with the previous point source prediction, the y_n in Table 2 should be contrasted with the x_n' in Table 1. (To compare the y_n with the x_n in Table 1 is to compare the incommensurable, since there is no reason to believe that the potential has its maximum modulus at the same point where the

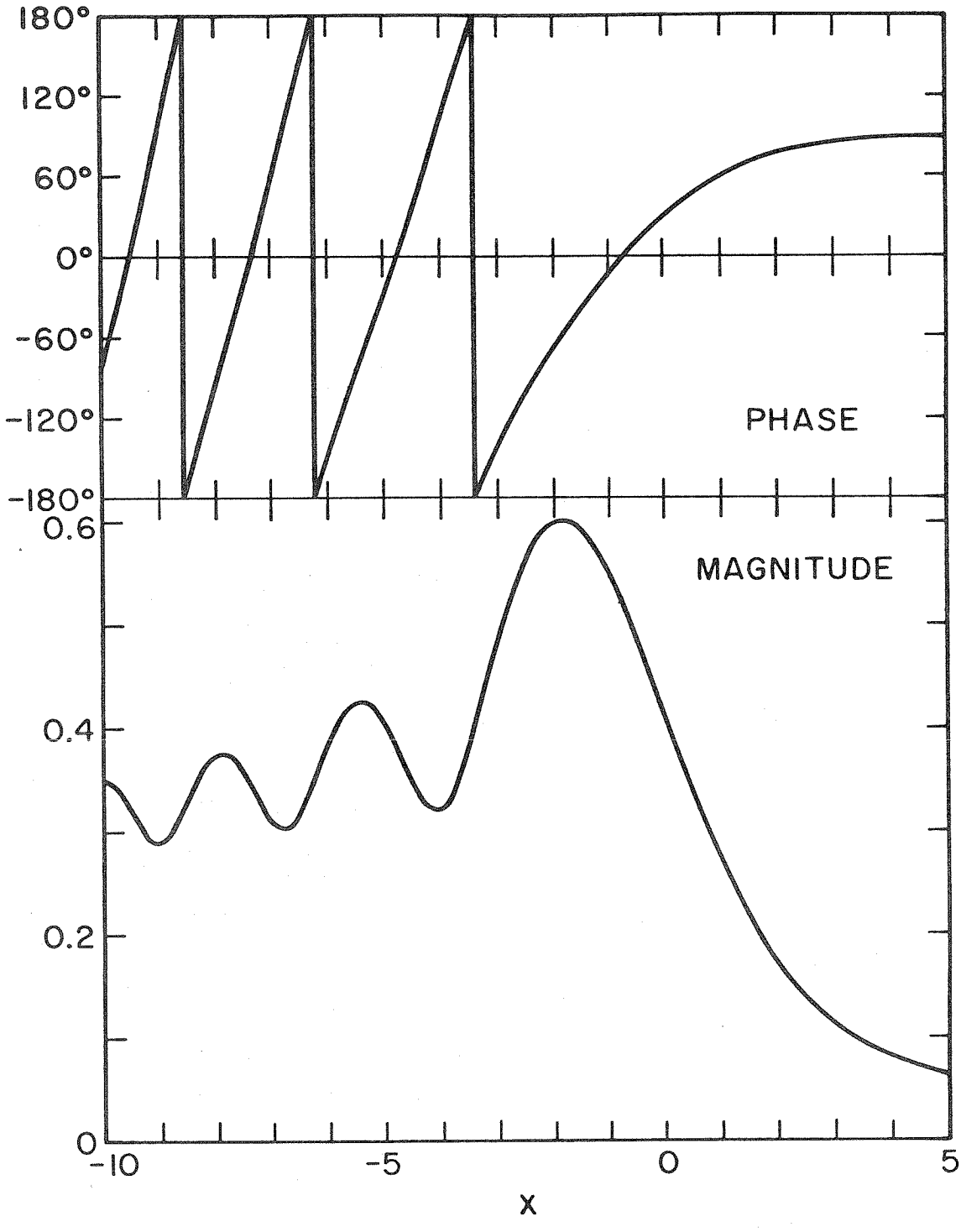

Fig. 7 Magnitude and phase of Ai(x) + iGi(x).

TABLE 2

LOCATION OF THE MAXIMA OF $|Ai(x) + iGi(x)|$

n	$-x_n$	$-y_n = -2^{-2/3}x_n$
1	1.84481	1.16216
2	5.42096	3.41499
3	7.88888	4.96969
4	10.0018	6.30074
5	11.9065	7.50062
6	13.6675	8.61000
7	15.3204	9.65127

electric fields do.) Except for the first element in each list, the y_n and x'_n are approximately equal. More importantly, the first differences of the elements agree within 1%, again excepting the ones involving the first elements. These differences also agree with those taken among the x_n of Table 1. Since the interpretation of the experimental measurements will depend on these differences, it is good to know that these numbers agree so closely.

In summary, consideration of a line source, rather than a point source, has not modified any of the qualitative features of the resonance cone structure, nor has it affected the way these features depend on the plasma parameters. Only a few of the numerical details have changed somewhat.

3.3 The Influence of Density Gradients

Up to this point, we have confined our attention to infinite, uniform plasmas. Wave propagation in plasmas with density gradients is a vast subject, and if the plasma in a given situation is uniform enough, it is a subject that one usually ignores in the first analysis. In this experiment, however, certain major features seen in some of the data could only be explained by considering some of the effects of the density gradient that exists in any laboratory plasma.

We are interested in the effect that a density gradient has on the location of the resonance cone. As a first attempt (which turns out to be good enough), let us try the simplest model possible. To make the geometry as simple as possible, consider a line source $\sigma\delta(x)\delta(z)e^{-i\omega t}$ in a plasma that is infinite, uniform in the y and z directions, and that has a density gradient in the x direction. To simplify the plasma dynamics, let the plasma be cold.

Under these conditions, the plasma is an anisotropic dielectric with a dielectric tensor that is now a function of position. The electrostatic potential is governed by

$$\frac{\partial}{\partial x}\left(K_{\perp}(x)\,\frac{\partial\phi}{\partial x}\right) + K_{\parallel}(x)\,\frac{\partial^2\phi}{\partial z^2} = -\frac{\sigma}{\varepsilon_o}\,\delta(x-x_o)\delta(z)e^{-i\omega t} \qquad (60)$$

where

$$K_{\perp}(x) = 1 - \frac{\omega_{pe}^2(x)\,(1 + i\nu/\omega)}{(\omega+i\nu)^2 - \omega_{ce}^2}$$

$$K_{\parallel}(x) = 1 - \frac{\omega_{pe}^2(x)}{\omega(\omega+i\nu)}$$

In the source function we have inserted the parameter x_o, so that the source can be located at an arbitrary point relative to the density gradient. From now on, the time harmonic factor $e^{-i\omega t}$ will be suppressed.

Notice that in the collisionless case, in frequency ranges where the resonance cones could exist, we have $K_{\parallel}(x)/K_{\perp}(x) < 0$. This means that, in the collisionless limit, Eq. (60) is not an elliptic differential equation, but rather a hyperbolic one.

Since the plasma is uniform in the z-direction, and since Eq. (60) is even in the z-coordinate, the solution can be effected by a Fourier cosine transform

$$\phi(x,k) = 2 \int_0^\infty dz \cos kz \; \phi(x,z)$$

$$\phi(x,z) = \frac{1}{\pi} \int_0^\infty dk \cos kz \; \phi(x,k)$$

Using this, Eq. (60) becomes

$$\frac{\partial}{\partial x} \left(K_{\perp}(x) \frac{\partial}{\partial x} \phi(x,k) \right) - k^2 K_{\parallel}(x) \; \phi(x,k) = - \frac{\sigma}{\varepsilon_o} \delta(x-x_o) \qquad (61)$$

In general, Eq. (61) cannot be solved unless we know the functional form of $\omega_{pe}^2(x)$. If the density gradients are gentle, however, and if we stay away from points where $K_{\perp}(x) \; K_{\parallel}(x) = 0$, then we can get an approximate solution using the JWKB method. First, we need to make the standard transformation into JWKB form [32], and then the method can be applied. The solution is

$$\phi(x,k) = \frac{\sigma}{2\varepsilon_0} [K_\perp(x_>)\, K_\perp(x_<)]^{-1/2} [F(x_>,k)\, F(x_<,k)]^{-1/4}$$

$$\times \exp\left\{ - \int_{x_<}^{x_>} [F(\xi,k)]^{1/2}\, d\xi \right\} \qquad (62)$$

where

$$F(x,k) = \frac{1}{2} \frac{K_\perp''(x)}{K_\perp(x)} - \frac{1}{4}\left(\frac{K_\perp'(x)}{K_\perp(x)}\right)^2 + k^2 \frac{K_\parallel(x)}{K_\perp(x)}$$

and where $x_> = \max(x,x_0)$ and $x_< = \min(x,x_0)$.

The functional form of $F(x,k)$ is such that the inverse Fourier transform to obtain $\phi(x,z)$ cannot be done in general. However, in the collisionless case, it is easy to see where the resonance cones lie.

Consider the large k behavior of the integrand in the inverse Fourier transform; it is proportional to

$$\frac{\cos kz}{k} \left\{ \exp\ -k \int_{x_<}^{x_>} \left[\frac{K_\parallel(\xi)}{K_\perp(\xi)}\right]^{1/2} d\xi \right\}$$

Since $K_\parallel(x)/K_\perp(x) < 0$, both the cosine and the exponential are oscillatory functions. If they oscillate in phase, the k^{-1} factor is not enough to make the integral converge. Consequently, the resonance cones are located along the lines

$$z = \pm i \int_{x_<}^{x_>} \left[\frac{K_\parallel(\xi)}{K_\perp(\xi)}\right]^{1/2} d\xi$$

This can be rewritten as a differential equation for the cone location.

$$\frac{dx}{dz} = \pm i \left[\frac{K_\perp(x)}{K_{||}(x)}\right]^{1/2} \tag{63}$$

Equation (63) is very suggestive. It says that the resonance cones in an inhomogeneous, collisionless plasma propagate along the characteristics of the hyperbolic differential equation, Eq. (60). One might have expected such a result solely on the basis of the theory of such differential equations. It is well known [33] that singularities in the solution of hyperbolic differential equations propagate along the characteristics. We have confirmed this fact for Eq. (60) in the JWKB limit. However, the argument from the theory of differential equations indicates that the resonance cones should follow characteristics even when the JWKB solution is not appropriate, e.g., even when $K_\perp(x)K_{||}(x)$ is near zero.

To see what can happen near the point $K_\perp(x)K_{||}(x) = 0$, take the simplest case possible. Let $\nu = 0$, $\omega_{ce} \to \infty$ and let the density be a linear function of x. Accordingly, Eq. (61) becomes

$$\frac{\partial^2\phi}{\partial x^2} - k^2(K_{||}(0) + \frac{x}{\lambda})\phi = -\frac{\sigma}{\varepsilon_o}\delta(x) \tag{64}$$

Here, $K_{||}(0)$ is the value of $K_{||}$ at $x = 0$, and we have taken $x_o = 0$. There is no loss of generality in this choice of x_o, because we can change the density at the antenna by changing $K_{||}(0)$.

In taking the $\nu = 0$ limit, we have made it difficult to uniquely determine the solution to Eq. (64). (When $\nu \neq 0$, in addition to the damped solutions, there can be solutions to the differential equation which grow without bound; one naturally picks the damped

solutions.) Let us agree that the solution we want is the one that, as $\lambda \to \infty$, agrees with the $\nu \to 0$ limit of the solution of Eq. (60) for a homogeneous, collisional plasma.

We can put Eq. (64) in a more succinct form by the substitution $\xi = K_{\parallel}(0) + x/\lambda$. Hence,

$$\frac{\partial^2 \phi}{\partial \xi^2} - k^2\lambda^2 \xi \phi = - \frac{\sigma L}{\varepsilon_o} \delta(\xi - K_{\parallel}(0))$$

The method for solving this is the standard method for obtaining the Green's function for an ordinary differential equation. Using it, and then writing the inverse Fourier transform, we have

$$\phi(x,z) = \frac{\sigma\lambda^{1/3}}{\varepsilon_o} \int_0^\infty dk \, \frac{\cos kz}{k^{2/3}} \, Ai((k\lambda)^{2/3}\xi_>)[Bi((k\lambda)^{2/3}\xi_<) - iAi((k\lambda)^{2/3}\xi_<)] \qquad (65)$$

where Ai and Bi are the Airy functions [21], $\xi_> = \max(\xi, K_{\parallel}(0))$ and $\xi_< = \min(\xi, K_{\parallel}(0))$.

As with the JWKB solution, we again have a Fourier integral that is difficult to do in general. The resonance cone location can again be found by considering the large k behavior of the integrand, and looking for the parameter combinations that make the integral diverge.

If we are in the region where the resonance cones can exist ($K_{\parallel}(x) < 0$), then both $\xi_>$ and $\xi_<$ are negative. Consequently, as $k \to \infty$

$$\mathrm{Ai}((k\lambda)^{2/3}\xi_>)[\mathrm{Bi}((k\lambda)^{2/3}\xi_<) - i\mathrm{Ai}((k\lambda)^{2/3}\xi_<)]$$

$$\sim -\frac{i}{2\pi}(k\lambda)^{-1/3}(\xi_<\xi_>)^{-1/4}\{\exp[\tfrac{2i}{3}k\lambda((-\xi_>)^{3/2} - (-\xi_<)^{3/2})]$$

$$- \exp[-\tfrac{2i}{3}k\lambda((-\xi_>)^{3/2} + (-\xi_<)^{3/2})]\}$$

When this is multiplied by $k^{-2/3}\cos kz$, we obtain an integrand that can be expressed as the sum of four complex exponentials, multiplied by k^{-1}. If the argument of any one of these is zero, the integral in Eq. (65) is divergent. The loci of points where this happens is

$$(-\xi)^{3/2} = \pm(K_{\parallel}(0))^{3/2} \pm \frac{3z}{2\lambda} \tag{66}$$

Equation (66) is actually four equations; all possible sign combinations that yield $\xi < 0$ are to be taken.

The loci described by Eq. (66) are graphed in Fig. 8. As is clear from the figure, the resonance cones launched by the source into the region of decreasing density are reflected when $K_{\parallel}(x) = 0$ and travel back into the high density region. Furthermore, Eq. (66) is just the solution for this case of the equation of the characteristics, Eq. (63). Consequently, the resonance cones propagate along the characteristics of Eq. (64), but they are confined to the region $K_{\parallel}(x) < 0$, where the characteristics are real.

The equations that describe the turning point where $K_{\perp}(x) = 0$ are much more difficult to solve. To avoid more mathematical complexity, I would like to build a model, which is motivated by the foregoing discussion, but which would be quite difficult to derive from it

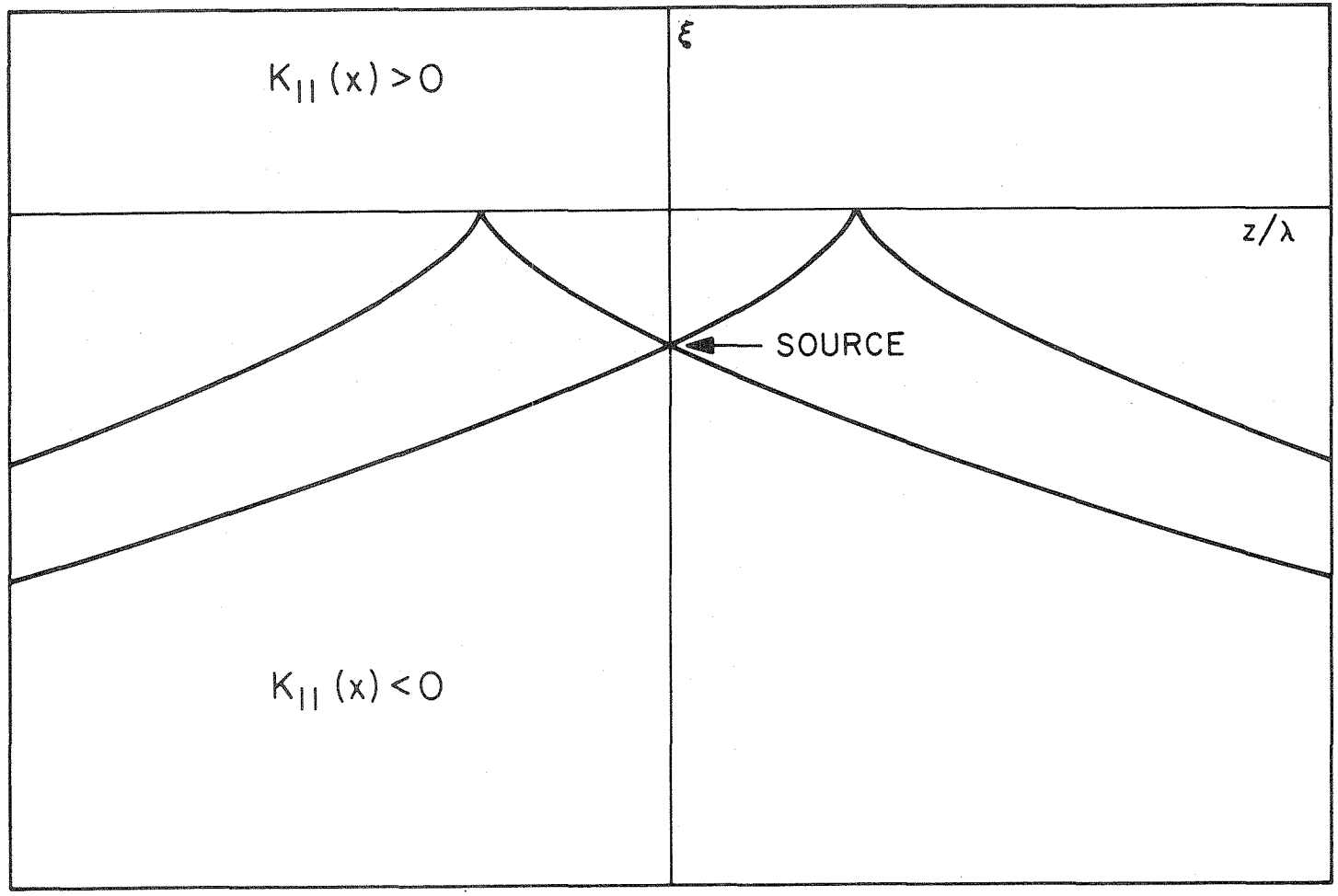

Fig. 8 The location of the resonance cones excited by a line source perpendicular to the magnetic field in a cold plasma whose density depends linearly on $\xi \propto x/\lambda$, where the x axis is perpendicular to both the antenna and $\underline{B}_0$.

rigorously. (Reflection from the layer where $K_\perp(x) = 0$ may require $T_e \neq 0$, as in the case of the Buchsbaum-Hasegawa resonances [58], or as discussed in Stix [11, Chapter 10].)

Assume that the resonance cones propagate everywhere along the characteristics of Eq. (61), which are given by the solution to Eq.(63). Assume further that the resonance cones are confined to the region $K_\perp(x)K_{||}(x) < 0$, and that they can reflect from these boundaries.

We would like to apply this model to a plasma that approximates the one used in the experiment. Consider a collisionless plasma whose density is an even function of x and which decreases as $|x|$ increases. Place an oscillating line source in the plasma at some point where $K_\perp(x)K_{||}(x) < 0$. Using the model, what do the resonance cone patterns look like in this plasma?

For the experiment, two cases need to be considered: either $K_{||}(x) < 0$ but $K_\perp(x) > 0$ in the region from $x = 0$ to the source (ω in the lower branch), or $K_\perp(x) < 0$ and $K_{||}(x) > 0$ in that region (ω in the upper branch). (The third case, where $K_{||}(x)K_\perp(x) < 0$ only in regions that do not contain $x = 0$, is neglected because the antenna configuration in the experiment precluded taking any data in this case.) We can indicate the general features of the solution without knowing $\omega_{pe}^2(x)$.

In the first case, since $K_{||}(x) < 0$ at the source, the turning points occur when $K_{||}(x) = 0$. (In this case, $K_\perp(x) < 0$ for all x.) This is very similar to the problem we just solved in Eq. (65), and the resonance cone patterns

can easily be sketched (see Fig. 9a). Near the lines $K_{\parallel}(x) = 0$, these patterns have the same qualitative features as Fig. 8; however, the maximum in the density at $x = 0$ has made multiple internal reflections possible.

In the second case, the turning points occur when $K_{\perp}(x) = 0$. (For this case, $K_{\parallel}(x) > 0$ for all x.) Consider Eq. (63) in the collisionless limit near the turning point $x = x_u > 0$, where $K_{\perp}(x_u) = 0$. Since the density gradient is monotonic, Eq. (63) can be rewritten as

$$\frac{dx}{dz} \simeq \left[\frac{K_{\perp}'(x_u)}{K_{\parallel}(x_u)}\,(x_u - x)\right]^{1/2}$$

If $z = z_u$ when $x = x_u$, then the solution near this point is

$$x_u - x = \frac{1}{4}\,\frac{K_{\perp}'(x_u)}{K_{\parallel}(x_u)}\,(z - z_u)^2$$

Thus, the resonance cone path turns around at $x = x_u$ and proceeds back into the plasma. This gives rise to the type of solution sketched in Fig. 9b. Again, multiple internal reflections occur.

It is these multiple internal reflections that give rise to experimentally observable effects. In the experiment, if the receiving antenna happens to go through any of the reflected resonance cones, the received signal will increase markedly. The increase will be particularly great at the points labeled A in Fig. 9. The location of point A in each half of Fig. 9 has a simple geometrical relationship to the location of the source.

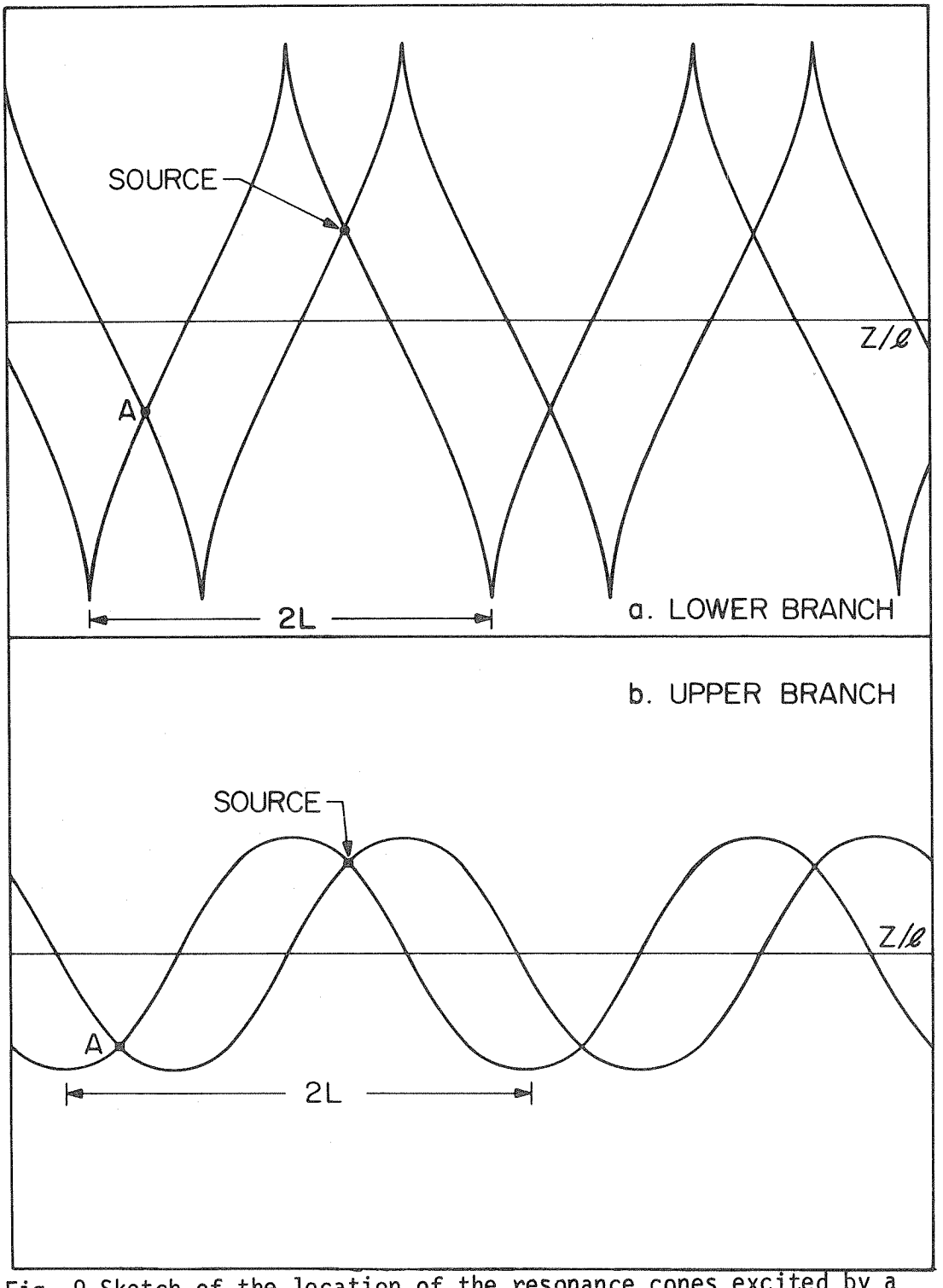

Fig. 9 Sketch of the location of the resonance cones excited by a line source perpendicular to the magnetic field and to the density gradient in a cold plasma with a symmetric density profile. a) $K_{\parallel}(x)<0$ and $K_{\perp}(x)>0$ in region from symmetry axis to the source. b) $K_{\parallel}(x)>0$ and $K_{\perp}(x)<0$ in that region.

Define L to be half the period of the patterns in Fig. 9. If the distance between the source and point A is r, and if the line between them makes an angle θ with the magnetic field, then the geometry of the patterns shows that

$$\cos \theta = L/r \tag{67}$$

This equation must hold, no matter what the density profile is.

To investigate these observable effects further, we can write down the formal solution to Eq. (63) and use it to obtain L. If we distinguish the upper and lower branch cases with subscripts,

$$L_{\ell,u} = 2 \int_0^{x_{\ell,u}} d\xi \left[- \frac{K_{\parallel}(\xi)}{K_{\perp}(\xi)} \right]^{1/2} \tag{68}$$

Here, $x_\ell > 0$ satisfies $K_{\parallel}(x_\ell) = 0$, while $x_u > 0$ satisfies $K_{\perp}(x_u) = 0$.

For any symmetric density profile, there are several qualitative features that can be obtained from Eq. (68), even without knowing the exact form of $\omega_{pe}^2(x)$.

First, as the resonance cone angle at $x = 0$ decreases, i.e., as $|K_{\parallel}(0)/K_{\perp}(0)|$ increases, L increases. Since the density decreases as x^2 increases, then as $|K_{\parallel}(0)/K_{\perp}(0)|$ increases, both x_ℓ and x_u increase. Further, the integrand in Eq. (68) is a monotonic function of ξ. Consequently, as $|K_{\parallel}(0)/K_{\perp}(0)|$ increases, the limits on the integral and the integrand itself both increase. Thus, L_u and L_ℓ increase.

Second, given a lower and an upper branch pattern that have the same value of $K_{\parallel}(0)/K_{\perp}(0)$, it is usually the case that $L_\ell < L_u$. To see this, consider two frequencies, one in the lower branch, ω_ℓ, and one in the upper branch ω_u, such that $K_{\parallel}(0)/K_{\perp}(0)$ is the same for both. If we assume that $\omega_{pe}^2(x)$ and ω_{ce} are the same throughout, then by considering the functional form of $K_{\parallel}$ and $K_{\perp}$, it is easy to show that

$$\omega_\ell^2 + \omega_u^2 = \omega_{pe}^2(0) + \omega_{ce}^2$$

Using this, one may show that x_ℓ and x_u are related by

$$\omega_{pe}^2(x_\ell) + \omega_{pe}^2(x_u) = \omega_{pe}^2(0)$$

The integrand in Eq. (68) is a monotonically increasing function of ξ for $\omega = \omega_u$, but it is monotonically decreasing for $\omega = \omega_\ell$. Accordingly, a sufficient condition for having $L_\ell < L_u$ is that $x_\ell \leq x_u$. Since $K_{\parallel}(x_\ell) = 0$ implies $\omega_\ell^2 = \omega_{pe}^2(x_\ell)$, if $\omega_{pe}^2(0)/\omega^2 \geq 0.5$, then the fact that the density is a monotonically decreasing function of x gives $x_\ell \leq x_u$. Consequently, $\omega_{pe}^2(0)/\omega_\ell^2 \geq 0.5$ is a sufficient condition to insure that $L_\ell < L_u$. In fact, this condition is much too strong; for any given case, more detailed analysis can find a better limit. However, it is good enough for our present purposes.

We now have all the theoretical results that we will need to make comparisons with the experimental data, and we can move on to discuss those data.

CHAPTER IV

EXPERIMENTAL EQUIPMENT

4.1 The Type of Plasma

The experiment was performed in the afterglow of a repetitively pulsed, argon plasma. The pulsed plasma has several advantages over a steady state plasma, even though the associated electronics are somewhat more complex. First, in the afterglow, the strong electric fields that are associated with plasma generation are absent, and cannot affect the wave propagation that we wish to study. Second, as the plasma decays in the afterglow, the velocity distribution function of the particles quickly becomes isotropic and nearly Maxwellian, thus facilitating comparison with the theory. Third, a whole range of plasma densities is easily available simply by taking data at different times in the afterglow. Fourth, such plasmas have low electron temperature, which makes the wavelength of the warm plasma waves very short, and makes it easier experimentally to attain the asymptotic limit for which the theory was developed in Chapters II and III.

The plasma used in this experiment had a density of the order of $5 \times 10^{8} cm^{-3}$. Its temperature, at the times in the afterglow where data were taken, was usually near $300^{o}K$. Using the measured argon collision cross section [34], the electron-neutral collision frequency was found to be near $1 \times 10^{6} sec^{-1}$. The electron Coulomb or self-collision frequency, as computed from the collision time given by Spitzer [35], was also of the same order.

4.2 Plasma Generation and Confinement

The plasma was produced in the apparatus shown in Fig. 10. It was contained in a glass vacuum vessel constructed with standard sections of Pyrex conical glass pipe (inside diameter ≃ 15 cm). One end of the vacuum vessel was connected to a vacuum station consisting of an oil diffusion pump and a mechanical forepump. It could produce an ultimate base pressure in the system of 5×10^{-7} torr.

Research grade argon gas was introduced into the system through a variable leak valve. Gas purity was insured by maintaining a small, continuous flow of gas through the system while the plasma discharge was in progress. The argon pressure, as measured by an ionization gauge just above the diffusion pump, was in the range 1.0×10^{-4} to 2×10^{-2} torr, with most work being done at 5×10^{-3} torr. The ionization gauge was a Veeco RG-75 gauge tube operated by a Varian gauge control unit (Model 971-0003); the accuracy of this combination is about 20%.

The external magnetic field was produced by a pair of water-cooled pancake coils in Helmholtz configuration (the glass pipe was aligned along the symmetry axis of the coils.) Driven by a voltage regulated power supply (Christie Electric Corp.), the coils were capable of producing a maximum field of 1.68 kG; however, the fields used in the experiment were usually about 100 G. The voltage across a current shunt in series with the coils was calibrated in terms of the electron cyclotron frequency by using an NMR unit (Alpha Scientific Laboratories, Model 675). By measuring the voltage with a digital voltmeter (Keithly Instruments Model 160), a calibration accuracy of 0.2%

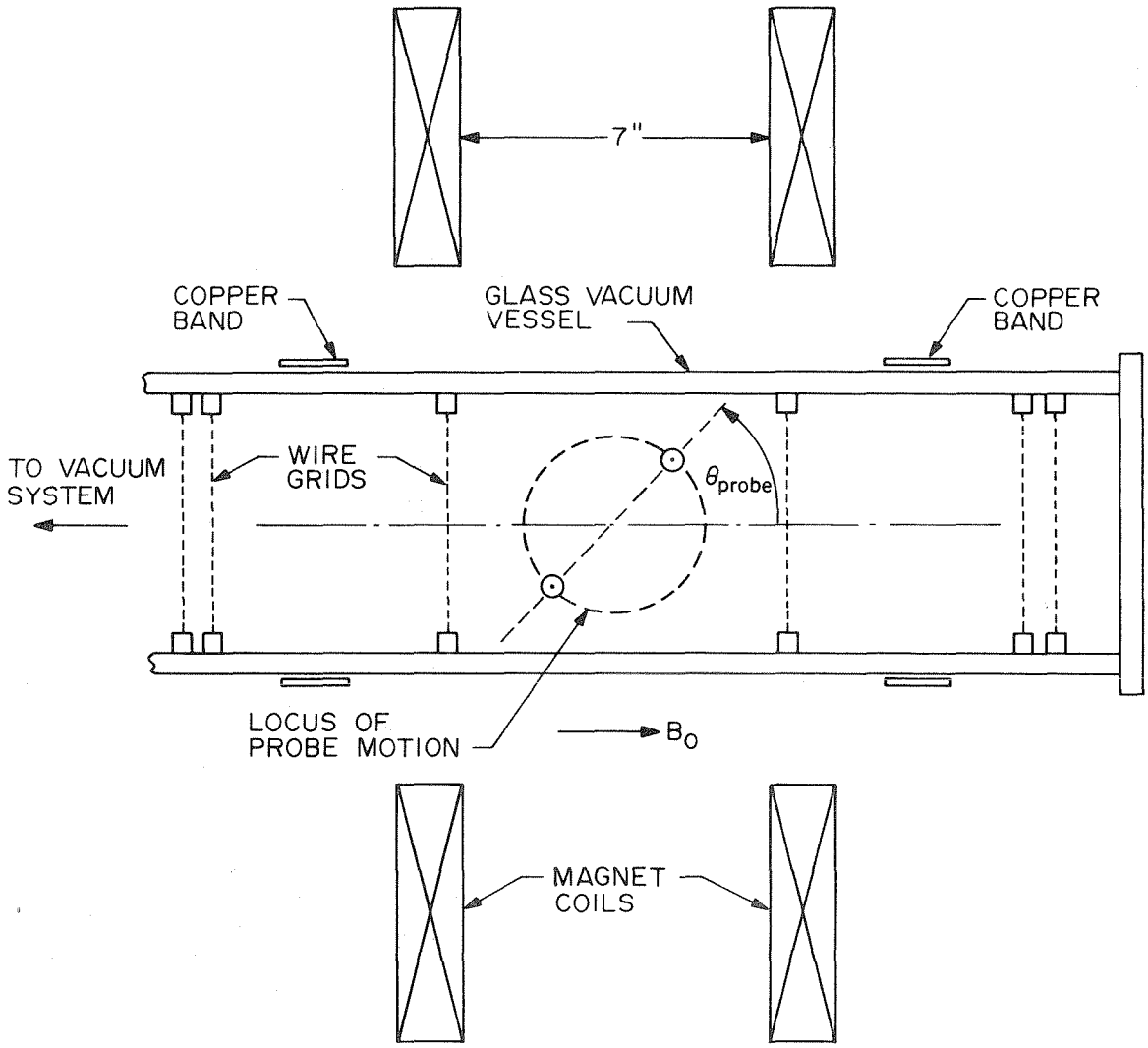

Fig. 10 Scale drawing of the experimental apparatus.

could be obtained.

The plasma was generated by gas discharge breakdown in an RF electric field. The field was produced by a two-tube, push-pull, power oscillator designed and built in our laboratory. In principle, the design is capable of producing a maximum output power of 400W, but since total power output was never a problem, this was never measured. When driving a resistive load, the oscillator frequency can be tuned continuously between 3 and 7 MHz. However, the coupling to the plasma is so strong that the oscillator usually works at about 30 MHz when the plasma is present. To generate the plasma, the oscillator is gated on once every 7 msec for about 100 μsec. No experimental measurements were made while the oscillator was on.

Originally, the output of the oscillator was coupled to the plasma by means of the two copper bands around the glass tube (see Fig. 10). In an attempt to obtain more plasma at lower argon gas pressures, the set of aluminum grids shown in Fig. 10 was inserted in the tube. This failed to produce more plasma, but it led to a much quieter, more reproducible one. The grids are usually connected in the following fashion: the grids closest to the probes are connected together, but are otherwise free to assume any potential; the grids farthest from the probes are tied to electrical ground; and the remaining grids and the copper bands are capacitatively connected to two symmetric taps on the coil in the resonant circuit in the power oscillator. Other configurations were also used, but any which involve the grids couple the oscillator so tightly to the plasma that its operation is seriously affected by the state of the plasma.

Each time the oscillator is gated on, the increasing plasma density between the grids causes the conductivity to increase markedly. It goes so high, in fact, that the oscillator can no longer maintain oscillation. If allowed to continue, this process would result in a relaxation oscillation. The density would rise, and this would shut the oscillator down; the plasma would then decay, allowing the oscillator to come back on, and the process would repeat itself. It was experimentally observed, however, that if the oscillator was gated off just after the plasma had stopped its oscillation for the first time, then a very reproducible discharge was obtained. Apparently, the density that is reached is determined by the fixed circuit elements in the oscillator, and thus is nearly the same every time. These elements do not control the density completely, for if several relaxation oscillations are allowed to occur before the oscillator is gated off, then the plasma is much noisier.

One could avoid this relaxation oscillation mode by changing the background gas pressure or the DC supply voltage to the oscillator. However, the mode with one relaxation oscillation is so quiet and so reproducible that almost all data were taken using it. The peculiar properties of this mode will not affect the experimental results, since, in the afterglow, the detailed characteristics of the plasma generation mechanism are quickly destroyed by the randomizing effects of collisions between the plasma particles and the background gas.

4.3 The Probe System

As indicated in Fig. 10, both the transmitting and receiving probes are mounted opposite each other on the same rotating structure, so that they each rotate about a common center at equal distances from it. In contrast to the probe configuration having one centrally located fixed probe with another probe rotating about it, this probe configuration allows the probes to be twice as far apart and still remain in the region of relatively uniform density near the center of a plasma whose density decreases near the walls.

The complete probe carriage is shown in Fig. 11. In addition to rotating through a full 360^{o}, the probe separation can be varied continuously from 1.5 to 11 cm by means of rack and pinion gears. The whole assembly is made of nonmagnetic materials, and all metal pieces near the probes are tied together by multiple ground paths, so that they will remain at the same electrical potential.

The electrical signals are brought in and out through 50 Ω semi-rigid coaxial cables (Phelps Dodge CT .020-50) which have solid copper outer conductors. The solid conductor cuts down on cross-talk between the cables. In areas where flexibility is needed, it is obtained by winding the cables into spirals and using the flexibility of these springs. This puts about 1.5m of cable between the probes inside the vacuum and the connectors outside it.

The whole probe carriage is mounted in the side arm of a Pyrex glass cross (15 cm inside diameter), as shown in Fig. 13. (The main stem of the cross is the cylinder shown in Fig. 10.) The side arm is long enough so that only the probes reach the main body of the plasma.

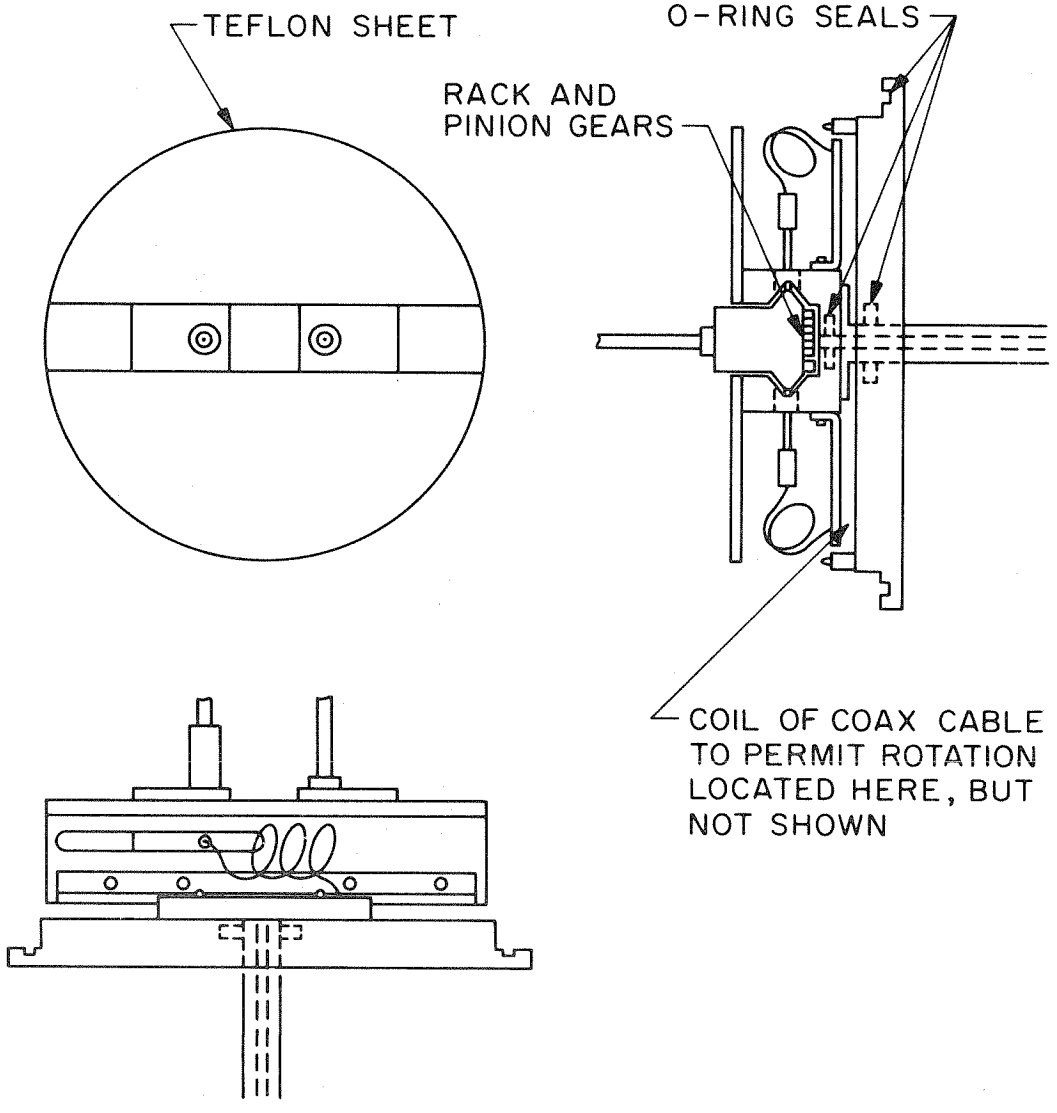

Fig. 11 Engineering drawing of the probe carriage (scale 0.25:1).

The probes themselves are shown in more detail in Fig. 12. Particular care was taken when building the transmitting probe to make the tip of the smallest wire that would not bend under its own weight. Stainless steel tubing of 250 μm outside diameter and 125 μm inner diameter was chosen and was inserted in place of the inner conductor of the semi-rigid coax. (The smaller the wire, the larger the electric field at the surface, and the better it will be able to affect the plasma particles near it.) The outer conductor of both probes was sheathed in Teflon tubing to prevent sputtering. SMC connectors were used on all cable inside the vacuum system.

Finally, potentiometers were attached to the gears which rotated the probe assembly and altered the probe separation; thus, a voltage proportional to these quantities could be obtained. The potentiometers are linear to within 0.25%. Since the probes are rotated continuously from stop to stop when data are taken, backlash in the gears is no problem; hence, the voltage is proportional to the angle to within 0.25%. Backlash is always a problem in the gears which drive the potentiometer that gives the probe separation; consequently, the separation can only be determined to within 0.1 cm.

4.4 The Experimental Electronics

A block diagram of the experimental electronics is given in Fig. 13. The master pulse generator (Data Pulse Type 101) controls the repetition rate of the experiment and the duration of plasma generation by gating the RF oscillator on and off. It also triggers the sample-hold module, which samples the received signal at a definite

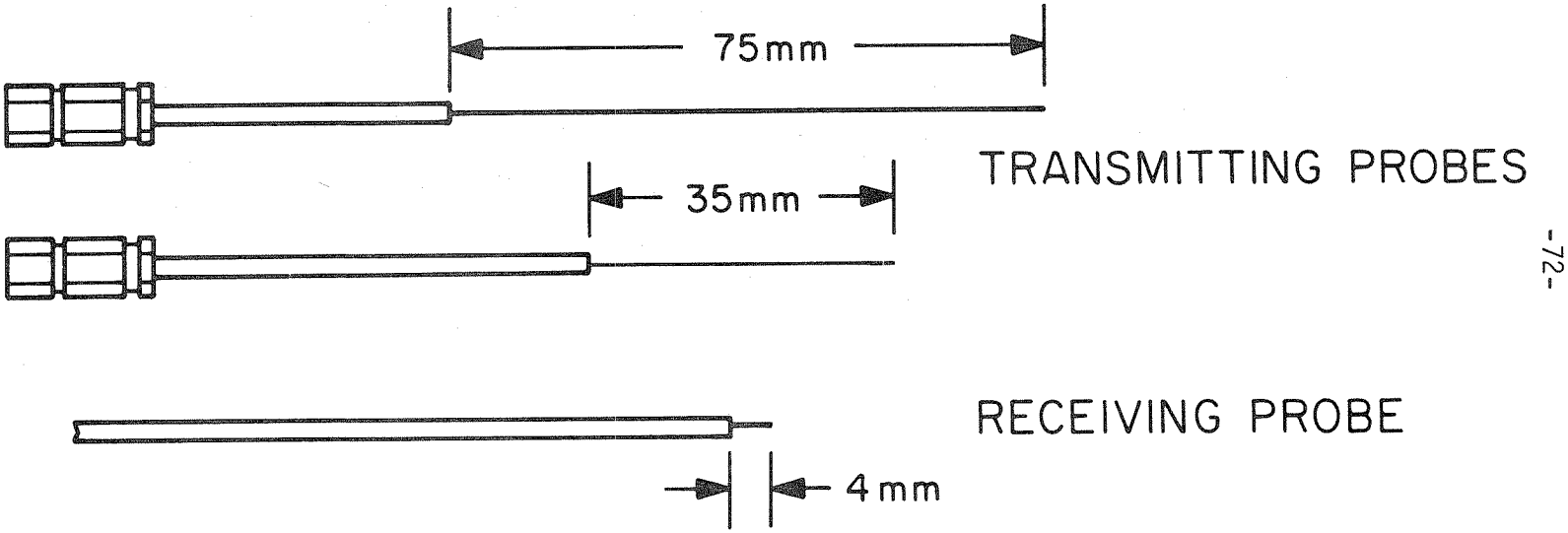

Fig. 12 RF probes used in the experiment. The outer diameter of the coaxial cable that forms the lower part of each probe is 2.2 mm, while that of the tips is 0.25 mm for the transmitting probes and 0.5 mm for the receiving probe.

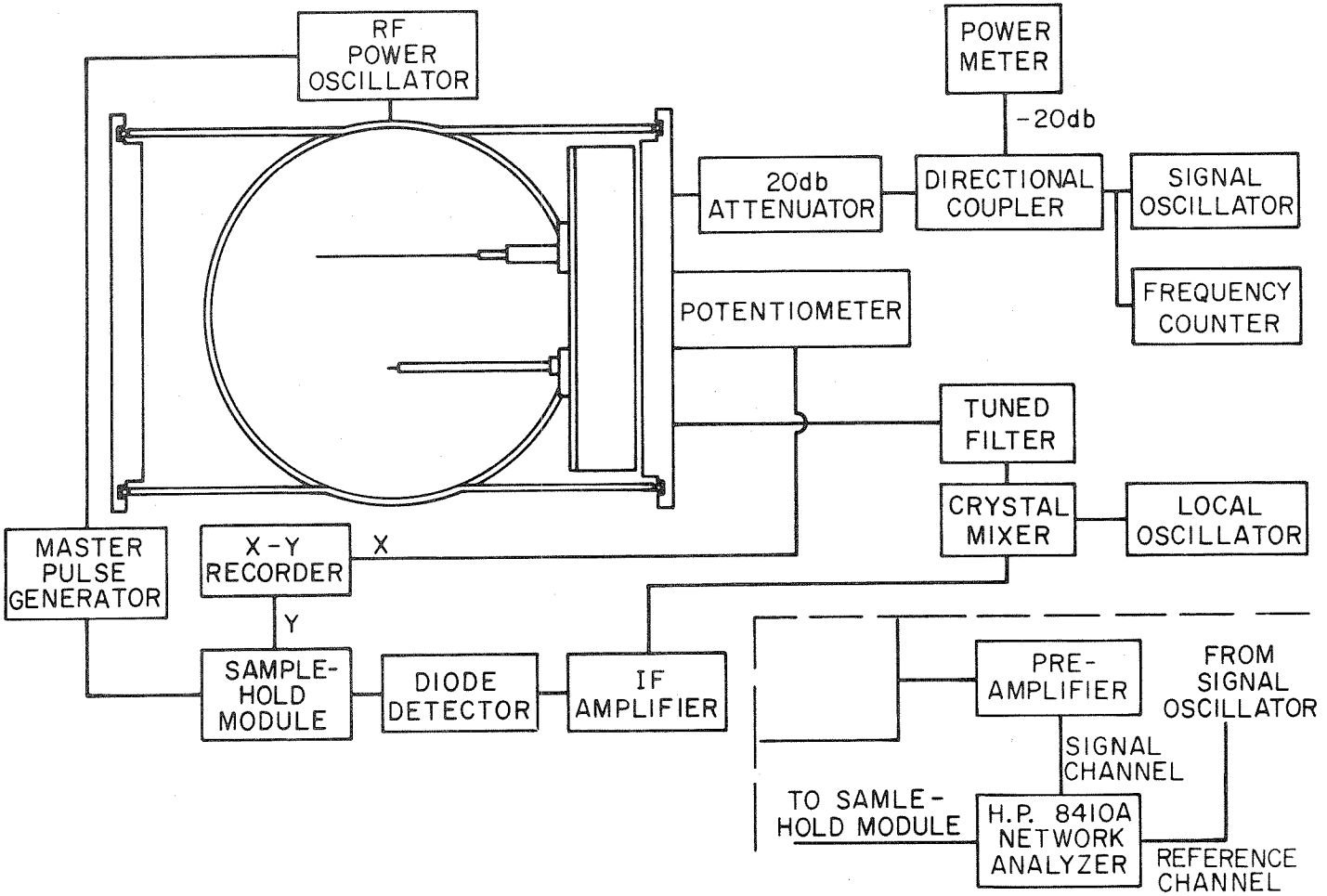

Fig. 13 Block diagram of the experimental electronics shown attached to a section of the experimental apparatus showing the probe carriage. The superheterodyne receiver is shown attached to the apparatus,while the receiver utilizing the Network Analyzer is shown in the inset.

time in the afterglow and maintains its output at that level until the next sample is taken. One may sample at any time in the afterglow.

The sample-hold unit is either a PAR Boxcar Integrator (Princeton Applied Research Model 160) or a unit, constructed by the author, with much the same characteristics, but without the nanosecond response time of the PAR boxcar. The second unit consists of a Datapulse 101 pulse generator, which accepts the trigger pulse and, after a variable delay, generates the sample command; a Burr-Brown sample-hold module (SHM-41); and a two-pole, low pass active filter with variable cutoff frequency, which integrates the output of the SHM-41. The 5 μsec sample time of the SHM-41 is more than adequate for this experiment, where the characteristic time for density variation is greater than 100 μsec.

The input signal for the transmitting probe is generated by a General Radio unit oscillator (GR 1208B) whose frequency is variable from 65 to 500 MHz . The frequency is measured by a 500 MHz frequency counter (a GR 1157B 100:1 scaler driving a Hewlett Packard 524D counter), which has 8-digit accuracy (many more than are necessary). The 20 db directional coupler (HP 778D) and the 20 db attenuator enable the power meter (HP 432A) to read the input power directly.

It was found empirically that an input power of more than 20 μW changed the appearance of the resonance cones; however, the appearance was independent of input power for any level below that. During data taking, the input power was held below 10 μW, and was usually 6 μW. (One should expect nonlinear effects to enter when the power level is too large, and this should bring with it a whole new class of phenomena.)

The received signal is detected either in the traditional superheterodyne receiver shown in the main body of Fig. 12, or with the HP Network Analyzer shown in the inset. The first detector uses a GR 874MRAL mixer, a GR 1208B as local oscillator, a GR 1236 IF amplifier, and an HP 421A crystal detector. The tuned filter helps with noise rejection, but serves primarily to keep the 30 MHz RF that generates the plasma from periodically saturating the 30 MHz IF amplifier. The preamplifier in the second detector is an Avantek UTA 68231 and two GR 1237B's in series. Both detectors are sensitive to the amplitude of the received signal.

Most of the data were taken with the superheterodyne receiver. The 500 kHz bandwidth of its IF amplifier insures more than enough frequency response. The 10 kHz bandwidth of the network analyzer is adequate, but some smoothing of rapidly varying features is noticeable. Also, until the Avantek preamplifier was acquired late in the experiment, we did not have enough low noise UHF preamplifiers to boost the received signal to a level that the network analyzer could use.

Without plasma in the glass tube, the signal passing between the probes is attenuated by about 60 db. Although the level with plasma is some 20 db higher, thermal noise in the receivers was always somewhat of a problem.

After the detector output is sampled by the sample-hold module, it is applied to the Y-axis of an X-Y recorder (HP Mosley 7004B). The X-axis is driven by the potentiometer voltage which is proportional to the angular location of the probes. One thus obtains a graph of received signal vs angle relative to the magnetic field.

Not shown in Fig. 13 is the oscilloscope that was used to monitor the experiment. By using a dual-beam oscilloscope (Tektronix type 555) and two multi-trace plug-in units, it is possible to continuously monitor six different signals as they vary with time in the afterglow. The oscilloscope was also used to measure the time intervals in the experiment (e.g, the time in the afterglow where the sample-hold unit takes its sample was determined from the oscilloscope display).

4.5 Langmuir Probes

In order to investigate the density profiles in the plasma, the current to a Langmuir probe was measured at various locations in the plasma. The probe itself was built as a double probe, but often one-half of it was used as a single probe. The double probe consisted of two pieces of semi-rigid coax (2.2 mm O.D.) located side by side with about 25 mm of the inner conductor (0.5 mm O.D.) exposed to the plasma. The two pieces of coaxial cable were soldered into a 0.25" brass tube which passed through a rotating vacuum feedthrough. The Langmuir probes entered the plasma through a plate in the arm of the glass cross opposite the probe carriage, and they could be moved radially into the plasma until they ran into the probe carriage.

The currents produced by the probes were of the order of 1 μA, and their time variation in the afterglow required a detector with bandwidth of 50 kHz. To monitor the current, commercial integrated circuit operational amplifiers were used to build a current to voltage converter that had a conversion ratio as high as 1 MΩ, but an input

impedance of only 20Ω . The output of the converter was sent to the sample-hold module so that the current at a specific time in the afterglow could be determined.

CHAPTER V

RESONANCE CONE LOCATION

5.1 The Most Useful Experimental Measurements

By far the most prominent feature in the experimental data is the resonance cone peak itself (see Figs. 14 and 15). The interference peaks are never as large as the theoretical development (see Figs. 3, 4, and 7) would suggest; in fact, as illustrated in Fig. 16, on many experimental graphs they are invisible. This mismatch is due to a defect in our model of the antenna.

Any material object in an actual plasma is surrounded by a plasma sheath, a boundary layer where static electric fields exist and where the electron and ion number densities fall from their value in the plasma to a much lower value (almost zero) right at the body. Since the sheath scale length is of the close order of the electron Debye length $\lambda_{de} = k_{de}^{-1}$, in a plasma with equal electron and ion temperatures, and since the hot plasma waves have wavelengths that can be as small as λ_{de}, the sheath affects these waves greatly.

Typically, the present plasma has $\lambda_{de} \simeq 40$ μm. Consequently, the near-field electromagnetic part of the fields radiated by the probe is not affected by the sheath. One would thus expect the relative amplitude of the main resonance cone peak and the interference peaks to be much different from that predicted by the theory developed in Chapters I-III.

A theoretical investigation of the RF properties of the sheath is far beyond the scope of this work. We will consequently confine

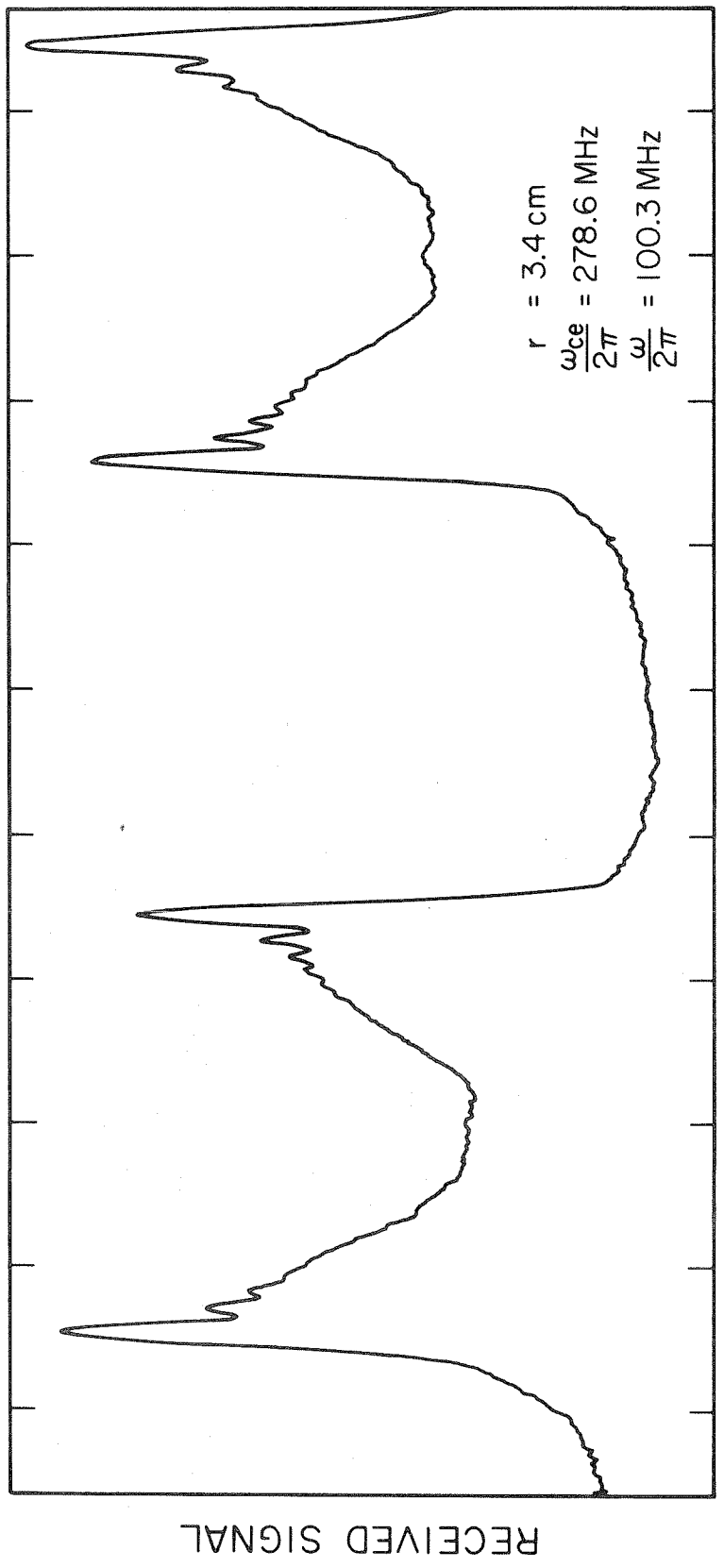

Fig. 14 An experimental graph of the received signal as a function of the angle of propagation relative to the magnetic field for a frequency in the lower branch. Both the resonance cone and the interference peaks are visible in this trace taken with the 75 mm transmitting antenna.

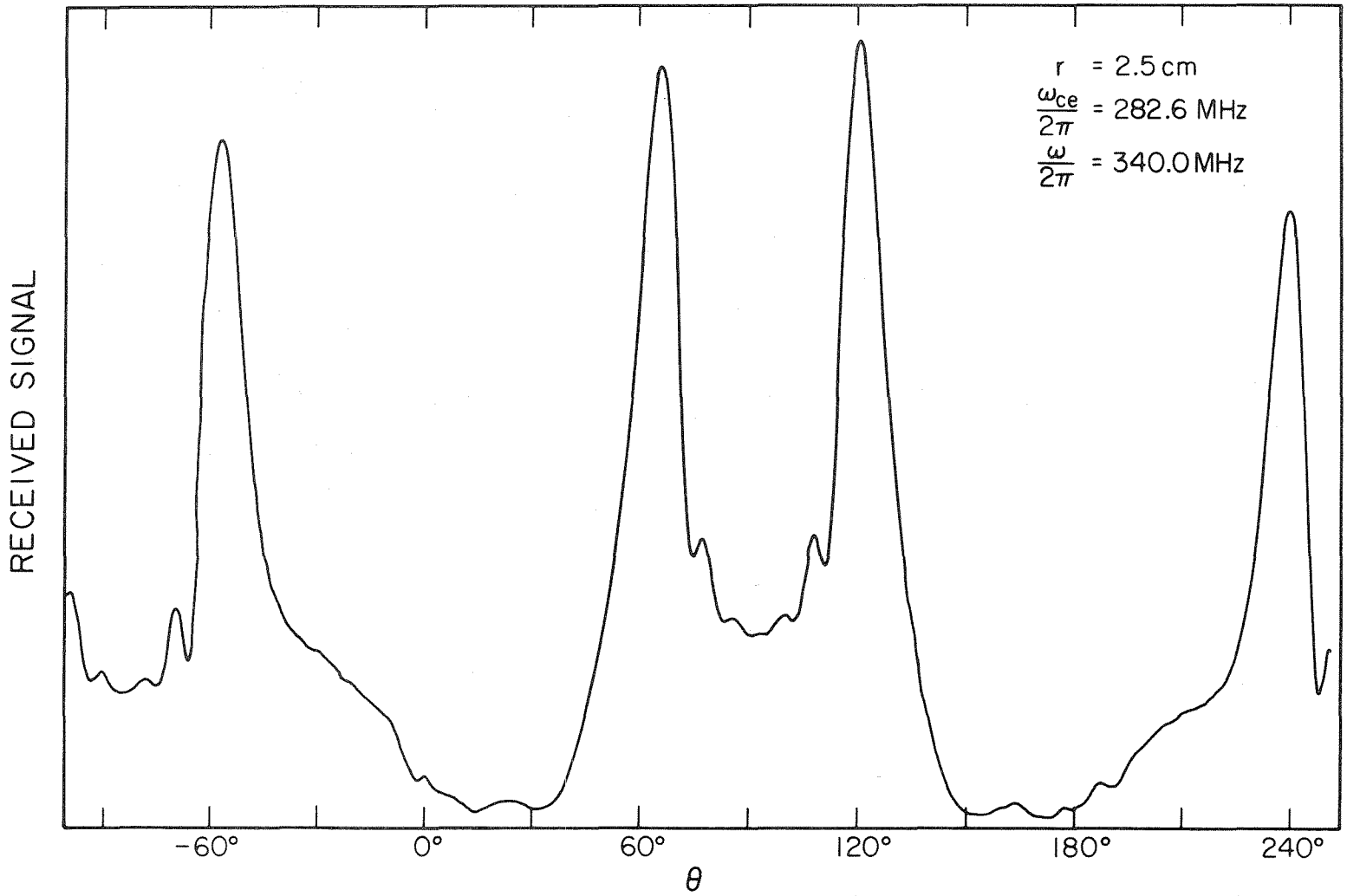

Fig. 15 An experimental trace showing the resonance cone and interference pattern for the frequency ω in the upper branch. The 35 mm transmitting antenna was used for this trace.

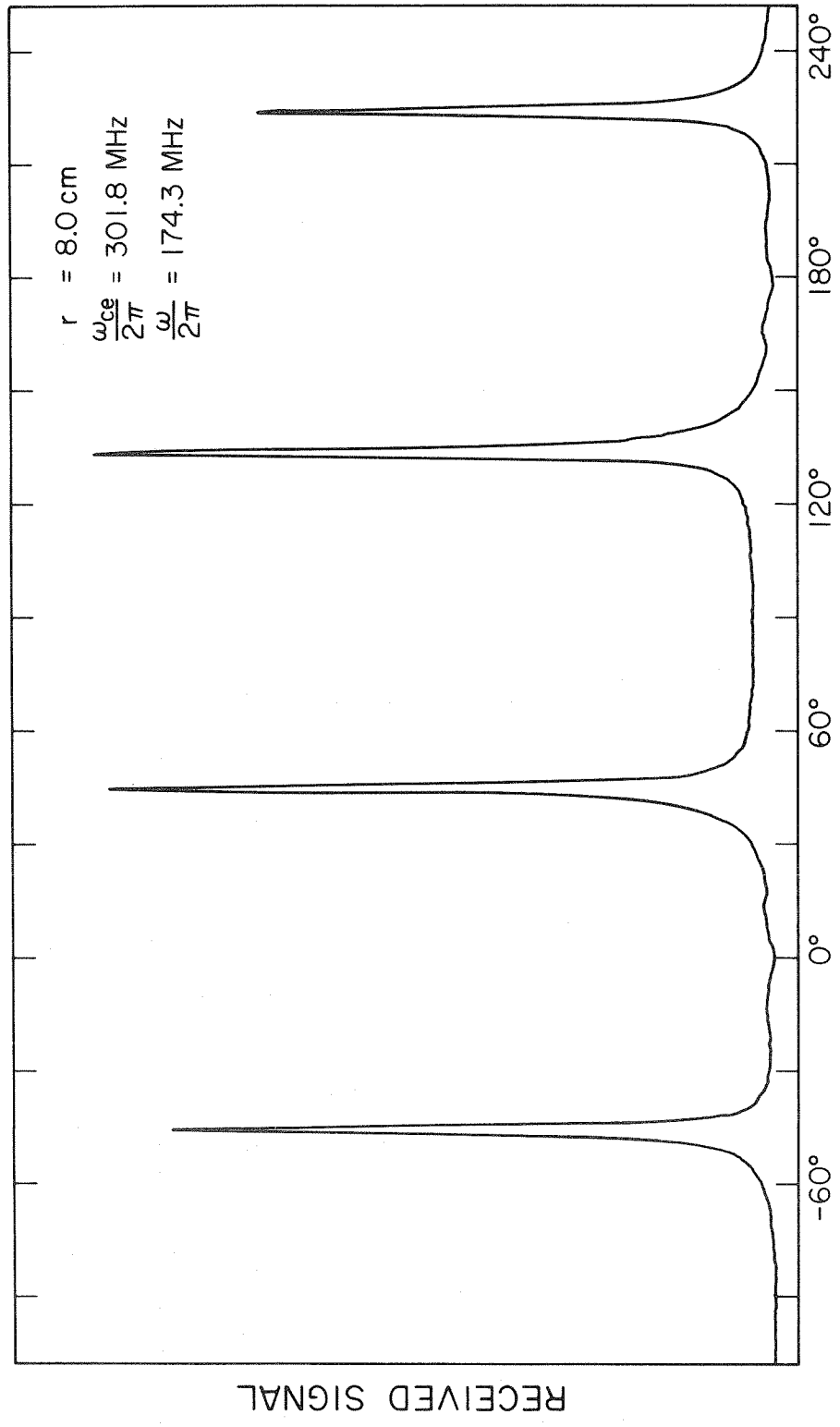

Fig. 16 An experimental trace taken with the frequency ω in the lower branch showing the resonance cone and demonstrating the absence of the interferences. The 35 mm transmitting antenna was used for this trace.

ourselves to investigating those aspects of the data which should be insensitive to the detailed antenna characteristics. These include the angular resonance cone location, the angular interference spacing, and the possibility of reflected resonance cones.

The raw data shown in Figs. 14, 15 and 16 exhibit four resonance cone peaks. Consequently, two independent determinations of the cone angle can be obtained from each original graph by measuring the distance between peaks. (By measuring from peak to peak, one avoids any possible errors that might occur due to shifts in the zero point.) Each data point considered in this chapter is thus the mean of two measurements. The errors quoted are simply the measurement errors in the particular quantities, combined by means of the usual mean square formula.

5.2 RF Probe Measurements

Since no general theory of antennas in plasmas exists, it is impossible to predict whether the small receiving probe is sensitive to the local value of the RF electric fields, or to the local value of the potential. Leuterer [36], by building on an equivalent circuit model of the antennas, has advanced theoretical reasons for believing that the receiver is sensitive to the potential difference between transmitter and receiver. The model's credibility is enhanced by how well its predictions match his measurements.

The equivalent circuit model is constructed by assuming that the coupling between the signal in the plasma and the receiving probe is through an equivalent, plasma-filled capacitor. To compute the

capacitance, the (unknown) free space value is multiplied by the plasma dielectric constant, which is computed using cold plasma theory. In Leuterer's work, the antenna is parallel to the magnetic field, which means that the dielectric constant chosen is $K_{\perp}$, the perpendicular component of the dielectric tensor. The dependence of $K_{\perp}$ on ω_{pe} then leads to some experimentally verifiable consequences.

Unfortunately, the antennas in the present work are perpendicular to the B-field, so what dielectric constant we might use becomes somewhat problematical. In the absence of any firm prediction, at points where there is a difference, both the theoretical results computed for the potential and for the electric fields will be compared with the experimental results.

5.3 Dependence of Main Peak Location on ω/ω_{ce} and ω_{pe}/ω_{ce}

As was first shown experimentally by Fisher and Gould [4], most of the dependence of the angular resonance cone position on ω/ω_{ce} and ω_{pe}/ω_{ce} can be accounted for by the collisionless cold plasma formula, Eq. (13). The results of the present work confirm that statement.

In Fig. 17, four sets of data are presented, showing the measured resonance cone angle as a function of ω/ω_{ce}. Within each set, the plasma conditions were kept constant, so that ω_{pe} should be constant. The solid lines in the figure are computed from Eq. (13), and it is clear that the theoretical curves and the experimental points correspond rather well. Fisher [1,4] has shown that the density obtained from plots like this one agrees with the density obtained from microwave interferometer measurements.

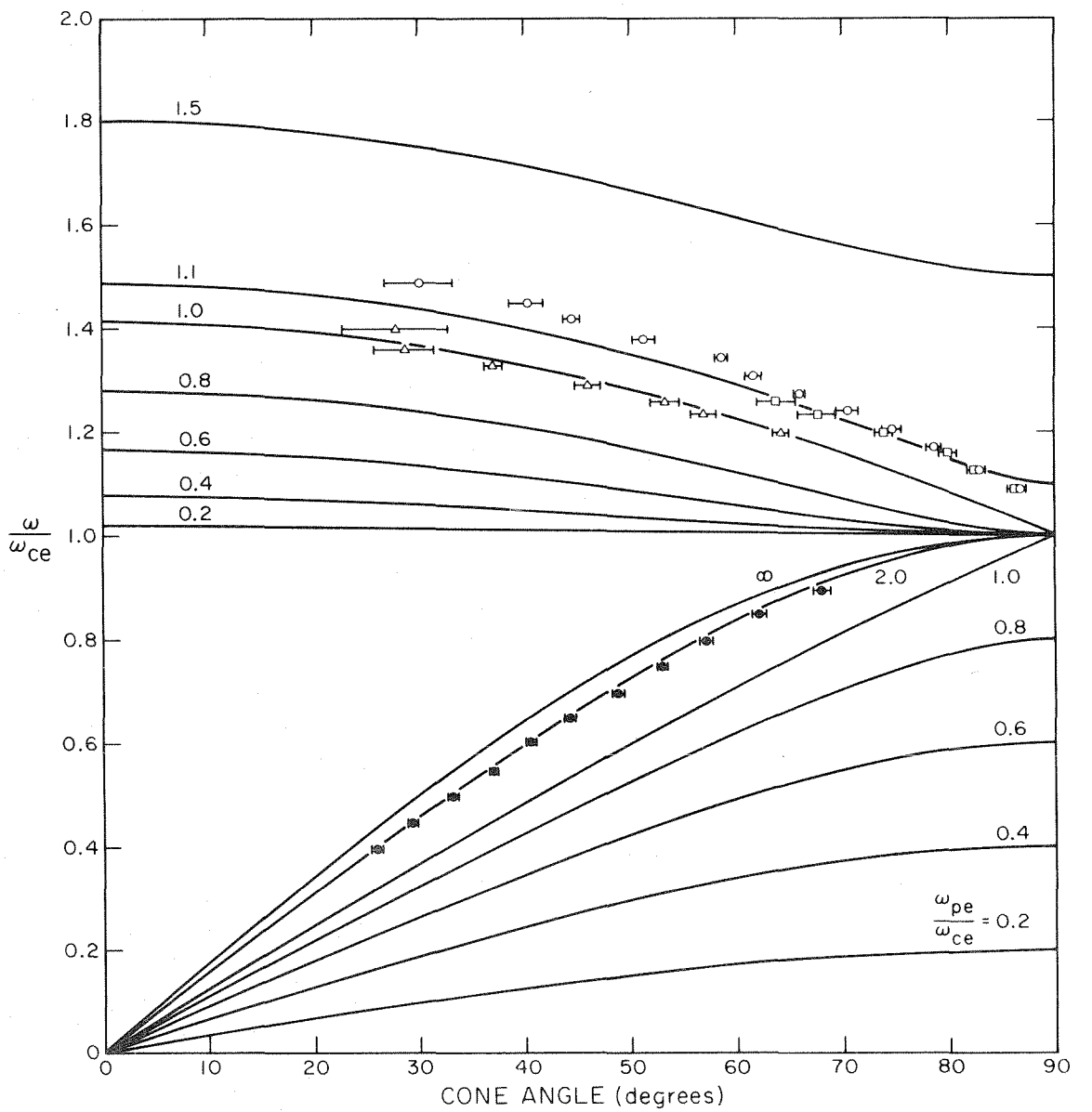

Fig. 17 A comparison of the experimentally measured values (points) of the resonance cone angle with the theoretical values (solid lines) for a cold plasma. The errors shown are the estimated measurement errors. All four sets of data were taken with the 35 mm transmitting antenna and with $r \geq 5$ cm.

We can use the density that is obtained by inserting the measured cone angle in the cold plasma cone formula as another check on the consistency of our theoretical interpretation of the data. By taking measurements at different times in the afterglow, different plasma densities can be obtained. In an afterglow plasma, simple diffusion theory predicts that the density should decay exponentially with time [37]. We can check to see that the density we infer from the measured cone angle has this behavior.

Two different plots of the inferred density vs time in the afterglow are given in Fig. 18, using a semi-logarithmic scale. If one considers only propagation of measurement errors, the error in the points is about the size of the symbols used in the plot. The density decays exponentially with time, as expected. The two sets of data have different slopes because the data were taken with different background pressures (which would change the diffusion coefficient), and with different electrical connections to the grids (which would change the loss processes). Gonfalone [38] has also reported similar density measurements using the resonance cones.

Figures 17 and 18 indicate that, as long as one knows ω and ω_{ce}, a measurement of the resonance cone angle is a useful way to determine the plasma density. This is the method used in the rest of the experiment to find the density.

One should, however, be aware of two sources of systematic error that can affect this method of density determination. First, if the density between the probes is not uniform, Fig. 9 shows that the measured angle from the transmitting to the receiving probe will

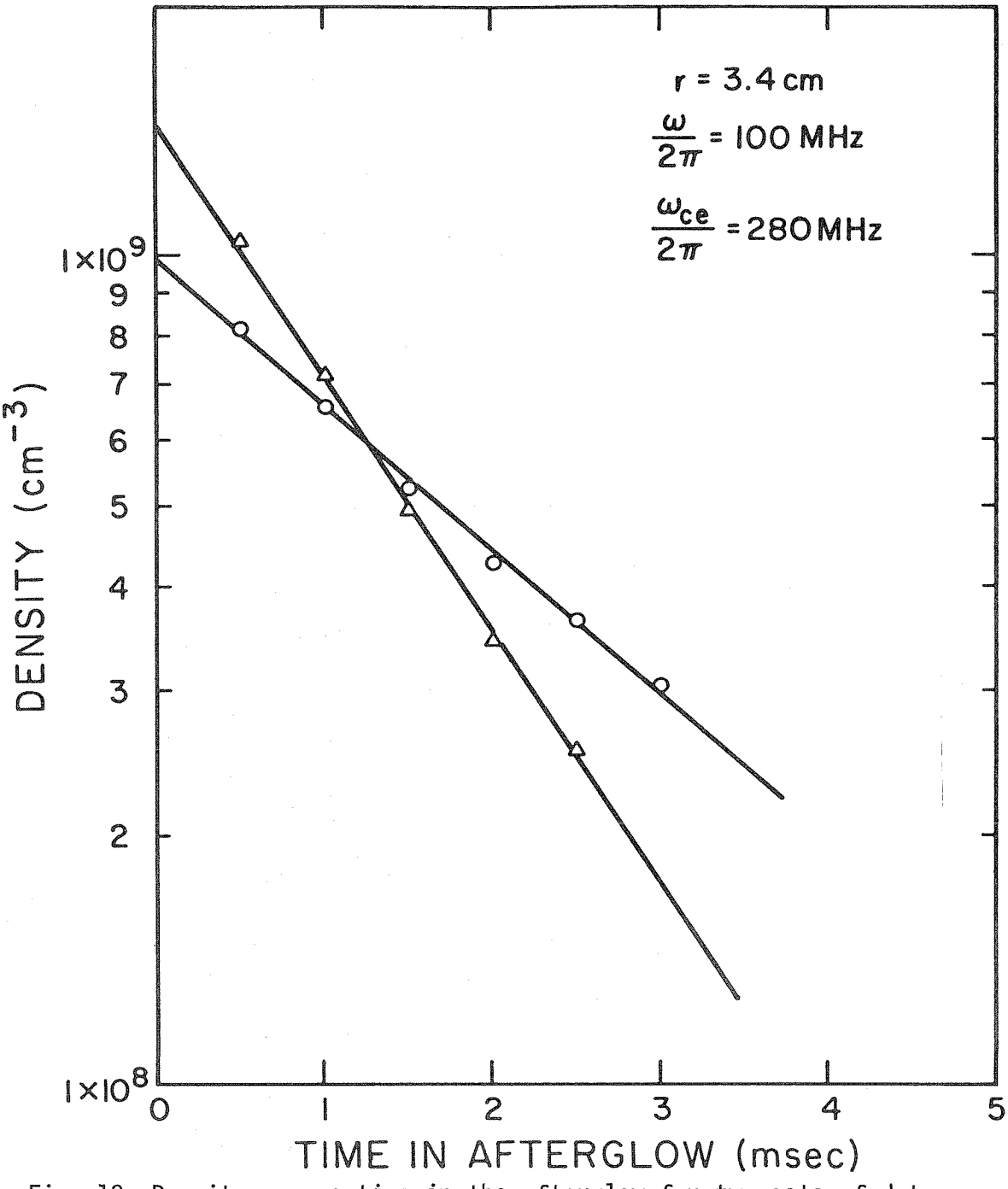

Fig. 18 Density versus time in the afterglow for two sets of data. The density was obtained from the resonance cone angle using the cold plasma formula. All data were taken with the 75 mm transmitting antenna.

underestimate the maximum density. Second, as the theory for a warm, uniform plasma shows, the actual cone angle depends on the separation r between the transmitting and receiving probes. (This will be dealt with more fully in the next section.) These systematic effects, and any random measurement errors as well, can have serious consequences if one is trying to find the density when $\omega_{pe}/\omega_{ce} > 1 > \omega/\omega_{ce}$. A glance at Fig. 17 shows that the cold plasma cone angle is very insensitive to the density in this parameter region. Consequently, any error in the measured cone angle can have a large effect on the inferred density in this region.

5.4 Dependence of Main Peak Location on Antenna Separation

In this section, we would like to make the first comparison between the data and the warm plasma theory developed in Chapters II and III. That theory is an asymptotic theory, valid in the limit where the probe separation is much larger than the scale lengths of the warm plasma waves. The characteristic lengths of the plasma waves are the Debye length λ_{de}, and the Larmor radius $r_{\ell e} = v_{th}/\omega_{ce}$. We will be in the region of validity of the asymptotic theory if $r/r_{\ell e} \gg 1$ and $r/\lambda_{de} \gg 1$. Since $r \geq 1.5$ cm and $T_e \sim 300^{\circ}K$, and since $\omega_{pe}/2\pi$ and $\omega_{ce}/2\pi$ are usually around 300 MHz

$$\frac{r}{r_{\ell e}} \gtrsim 290$$

$$\frac{r}{\lambda_{de}} \gtrsim 400$$

We are definitely working in the asymptotic limit.

From the work in Chapter III, we know that the main resonance cone peak occurs at an angle $\theta_1 = \theta_c - \Delta\theta_1$. In our work in the last section, we implicitly neglected $\Delta\theta_1$, but here we would like to consider its effect. From Eq. (57) or Eq. (59), we have $\Delta\theta_1 \propto r^{-2/3}$, while θ_c does not depend explicitly on r. If all other parameters are held constant as r varies, the predicted dependence on antenna separation would be easy to check.

In Fig. 19, we show a plot of the angular location of the main peak and the first interference peak as a function of $r^{-2/3}$. (Recall that the first interference peak should be located at $\theta_2 = \theta_c - \Delta\theta_2$ and that $\Delta\theta_2 \propto r^{-2/3}$.) The solid lines through the data points are lines of best fit as determined by a linear least-squares procedure. Since the data have errors in both the abscissa and ordinate, the procedure used is not the standard one; the details are given in Appendix E.

The linear fit is consistent with the data, thus confirming the prediction. Additional confirmation comes from the fact that, as predicted by theory, the intercepts of the two lines on the vertical axis agree within the experimental error. The least squares fit yields an intercept for the line through the main peak data of $30.4^{\circ} \pm 0.4^{\circ}$, while the intercept for the data for the first interference peak is $30.6^{\circ} \pm 0.7^{\circ}$. Further confirmation is given by the fact that the sign and relative magnitudes of the slopes agree with the theoretical predictions. Since $\omega/\omega_{ce} = 0.497$, Figs. 5 and 6 show that $\Lambda > 0$, and consequently the slopes should be negative, as they are. The ratio of the slopes should be given either by x_2/x_1, or

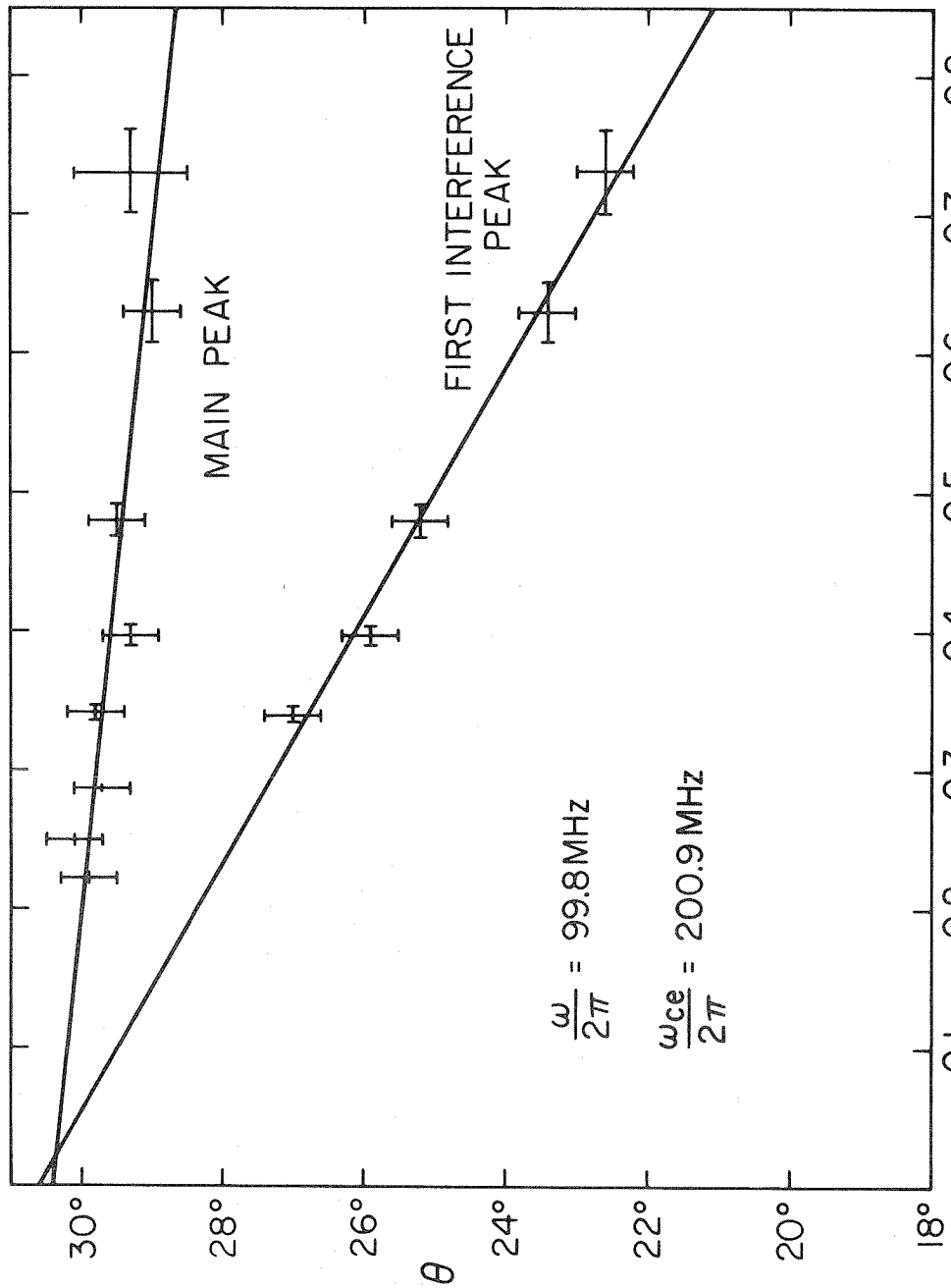

Fig. 19 Angular location of the main resonance cone and the first interference peak versus $r^{-2/3}$. Error bars represent the results of (instrumental) measurement errors. The data were taken with the 35 mm transmitting antenna.

x_2'/x_1' from Table 1, or y_2/y_1 from Table 2. The experimental value is 5.4 ± 2.8, while $x_2/x_1 = 4.10581$, $x_2'/x_1' = 2.23745$ and $y_2/y_1 = 2.93848$. (Unfortunately, without an independent knowledge of the temperature, we cannot check the absolute magnitude of the slopes.)

Notice that the data presented in Fig. 19 were taken under conditions such that it is difficult to determine the density with any accuracy. Mindlessly applying the cold plasma cone angle formula yields $\omega_{pe}/2\pi = 894$ MHz and $\omega_{pe}/\omega_{ce} = 4.47$, which is in the region where the cold plasma cone angle is very nearly density independent. The choice of this operating region was deliberate. It was found experimentally that the presence of the probes in the plasma affected the plasma density, and that the density in the region between the probes varied somewhat with the antenna separation. As Fig. 19 demonstrates, the variation in θ_1 due to $\Delta\theta_1$ is slight. If the data had been taken with $\omega_{pe}/\omega_{ce} \leq 1$, the density variation caused by the presence of the probes would have caused θ_c to vary so much that the change in θ_1 due to $\Delta\theta_1$ would have been undetectable.

A graphic illustration of what happens as the density drops is given in Fig. 20. Here we show the main peak angular location vs $r^{-2/3}$ with time in the afterglow as a parameter. Early in the afterglow, when the density is high and θ_c is nearly density independent, the slope of the data is negative, in agreement with the theoretical prediction. However, as the density falls, the slope gradually changes from negative to positive. Since the antennas act as sinks for the plasma, one would expect the density between the antennas to be smaller when the separation is smaller. As can be seen from Eq. (13), or

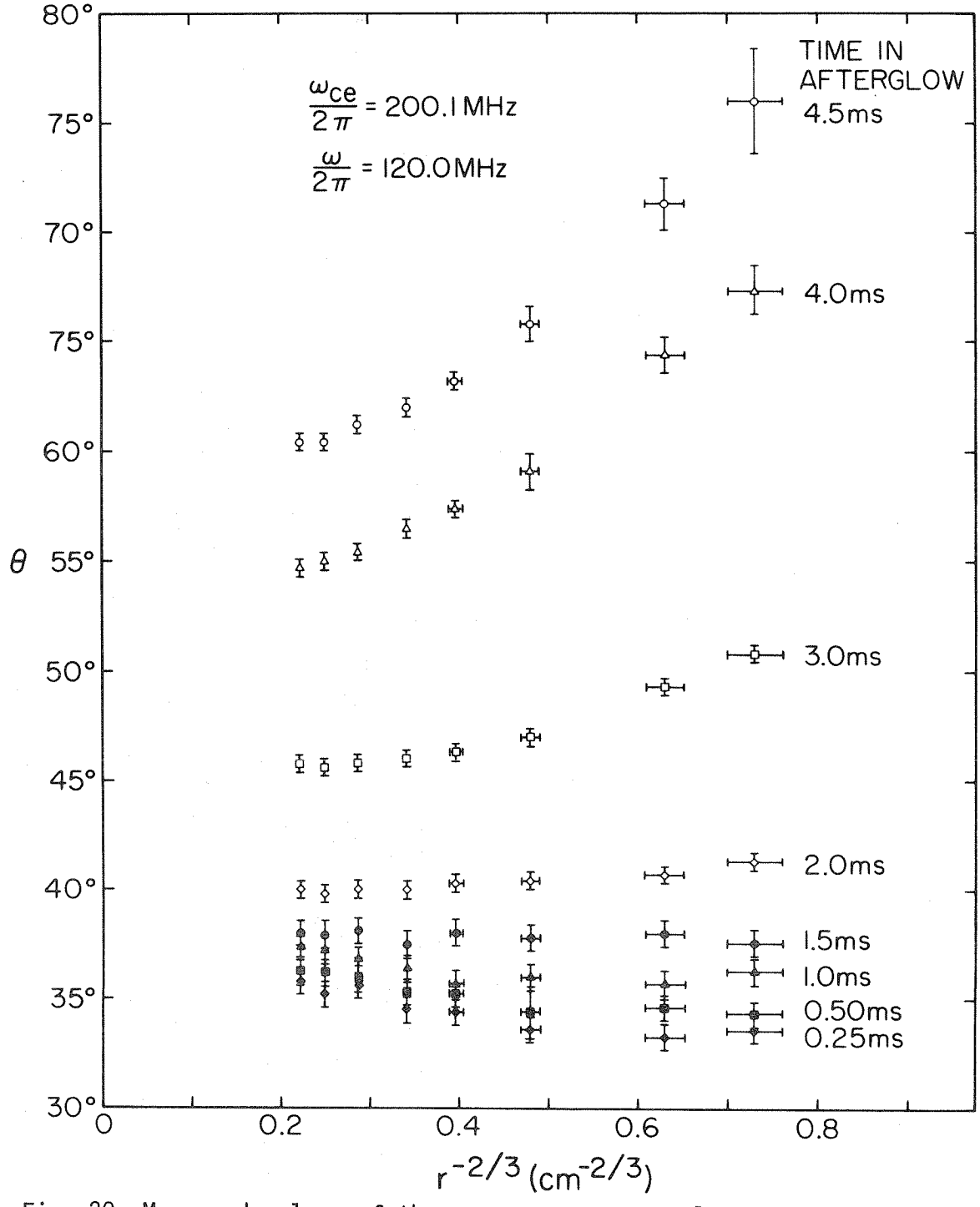

Fig. 20 Measured values of the resonance cone angle at various values of r and taken at different times in the afterglow. Note the change in slope as the time in the afterglow increases. The data were taken with the 35 mm transmitting antenna.

graphically from Fig. 17, this would produce a larger cone angle, in agreement with Fig. 20. The change in cold plasma cone angle with density is not linear; in the lower branch, the smaller the overall density is, the bigger the change in θ_c will be for a given fractional change in density.

In order to see whether the magnitude of the change in density necessary to produce the changes seen in Fig. 20 was reasonable, the relative density changes were measured with a Langmuir probe. The tip of the Langmuir probe was inserted into the region between the antennas, and, as shown in Fig. 21, the current was recorded as the antenna separation was varied. Since the density is directly proportional to the probe current, we see that the density changed by a factor of about 1.7. The change in density needed to account for the variation in cone angle for the $t = 4.0$ msec data in Fig. 20 is about 1.6 . This figure is arrived at by ascribing all variation in the measurement to changes in the density. If we try to be a bit more sophisticated and recall that the density changes will also have to overcome the changes due to the r dependence of $\Delta\theta_1$, we find the density must vary by a factor of 1.7 . (The close agreement of this last figure with the Langmuir probe results is fortuitous. The probe data are taken under somewhat different plasma conditions and at a different time in the afterglow.) Consequently, we see that density changes can account for the variations in the data.

In summary, we see that if the density were to remain constant as r varies, then Eq. (51) or Eq. (59) accounts rather well for the changes in cone angle. The changes due to $\Delta\theta_1$ are small, which

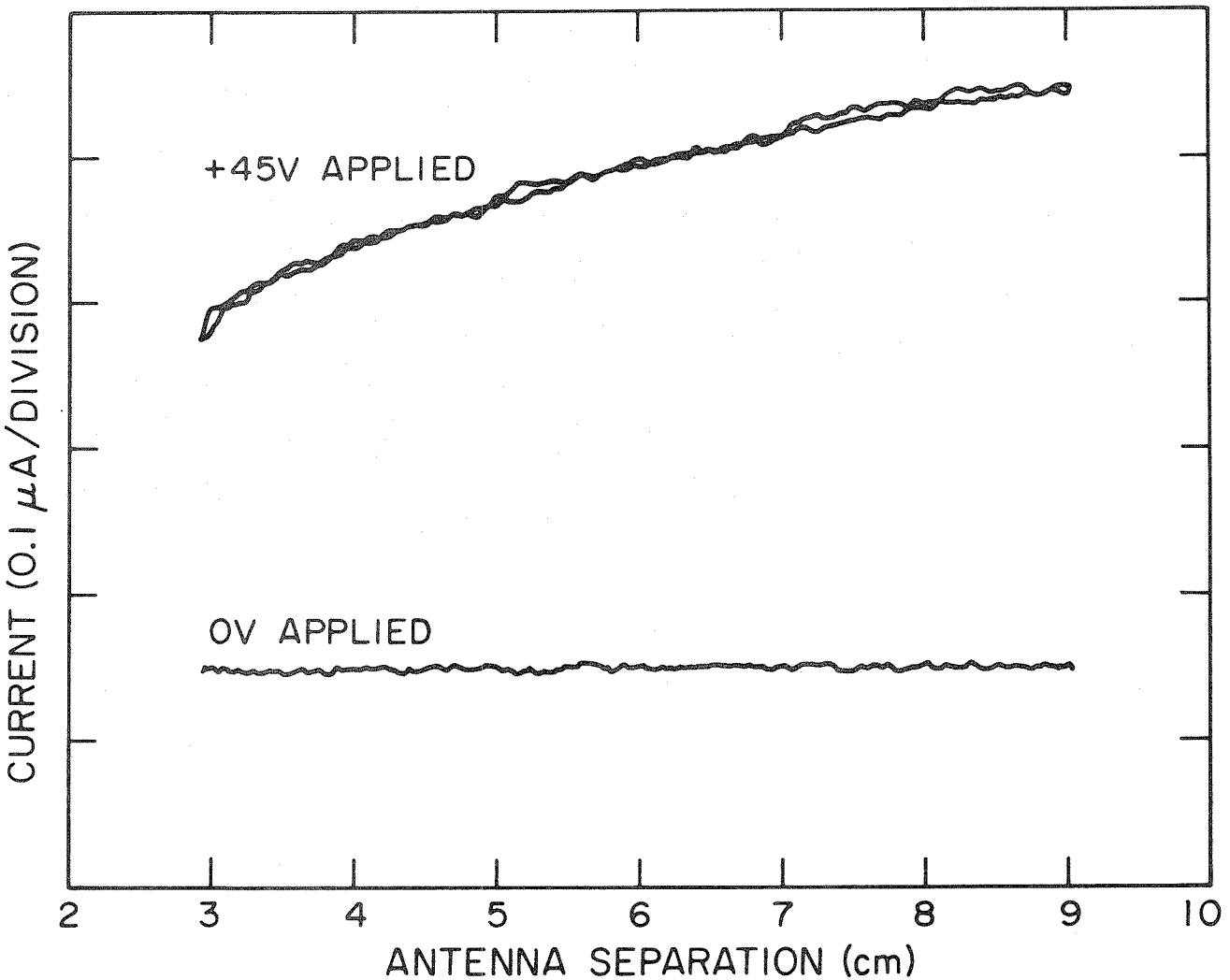

Fig. 21 Two traces of the current to a single Langmuir probe taken as a function of the separation of the transmitting and receiving antennas, which demonstrate the change in density. The data were taken at 2.2 msec in the afterglow with $\omega_{ce}/2\pi$ = 307.4 MHz.

explains why the cold plasma cone angle formula worked so well in the last section. The small hot plasma correction can easily be overshadowed by variations in the density that occur when the antenna separation changes.

5.5 The Reflected Resonance Cones

In Figs. 14 and 15 we see the normal appearance of the resonance cones and the associated interference structure. Being used to their appearance, it was somewhat startling when data like those in Fig. 22 were obtained. The peaks that look like interferences are much larger than any of the interference peaks caused by the warm plasma waves, and they have much different characteristics. As will be seen, they are actually due to the reflections that were investigated in Section 3.3.

Consider the sequence of graphs shown in Fig. 23. Six sets of data are shown, with the antenna separation as a parameter. Notice that for small values of r, the main resonance cone peaks alone can be seen, but as r increases, additional structure becomes apparent. Notice also that the new structure appears first near the axis of the plasma (i.e., near $\theta = 0^o$ or 180^o) and then spreads to other angles as r increases.

From other sets of data, we see that this structure is present, even for $r = 9.5$ cm, only when the main resonance cone angle is large (usually 70^o or greater).

If the structure seen in Fig. 23 for $r = 9.5$ cm were caused by a warm plasma wave, then that wave would also seriously affect the $r = 4.0$ cm data, for it would be even stronger there. The fact that

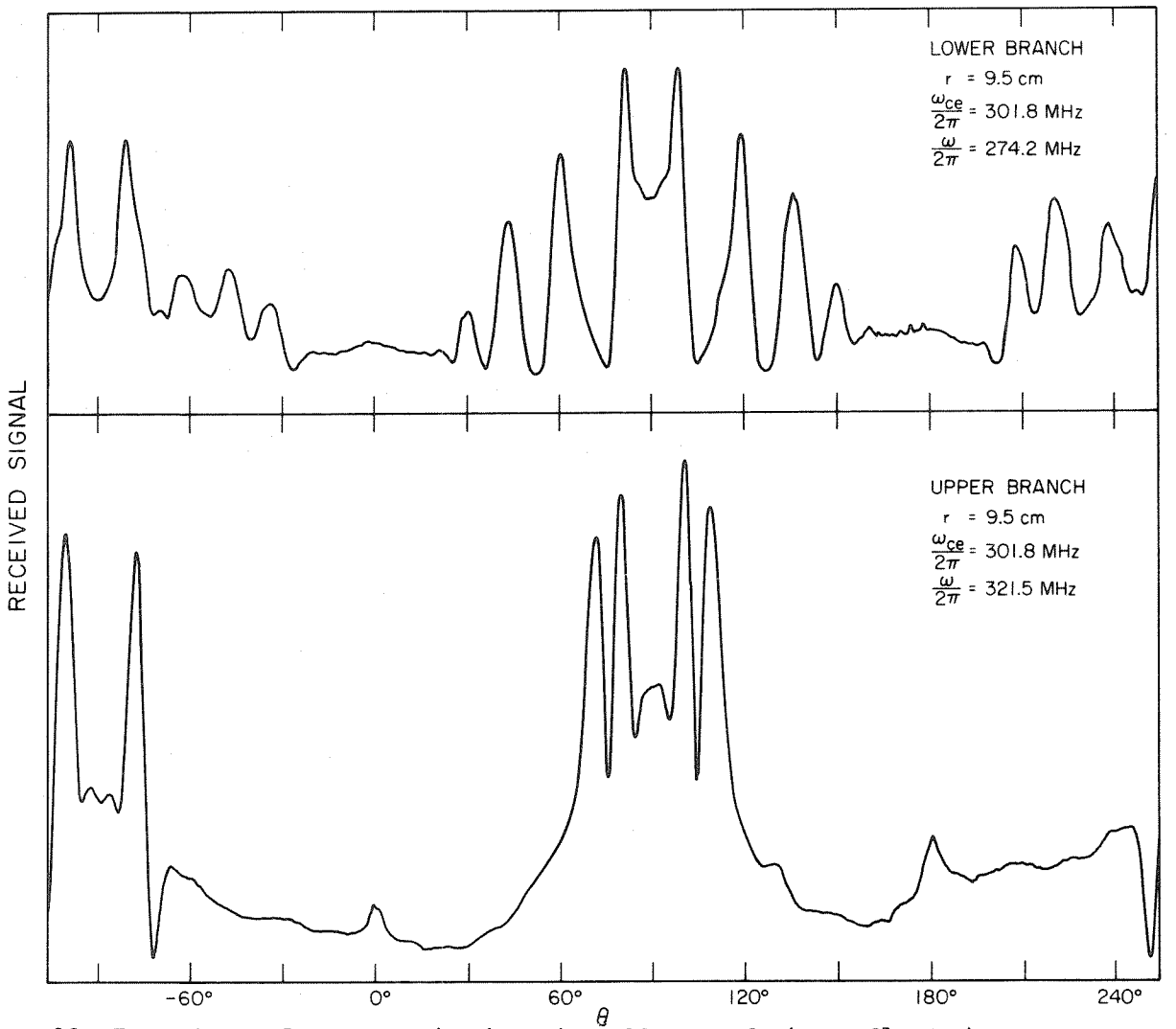

Fig. 22 Experimental traces showing the effects of the reflected resonance cones. The data were taken with the 35 mm transmitting antenna. From the cold plasma cone angle formula, one finds $\omega_{pe}/\omega_{ce} \simeq 1$.

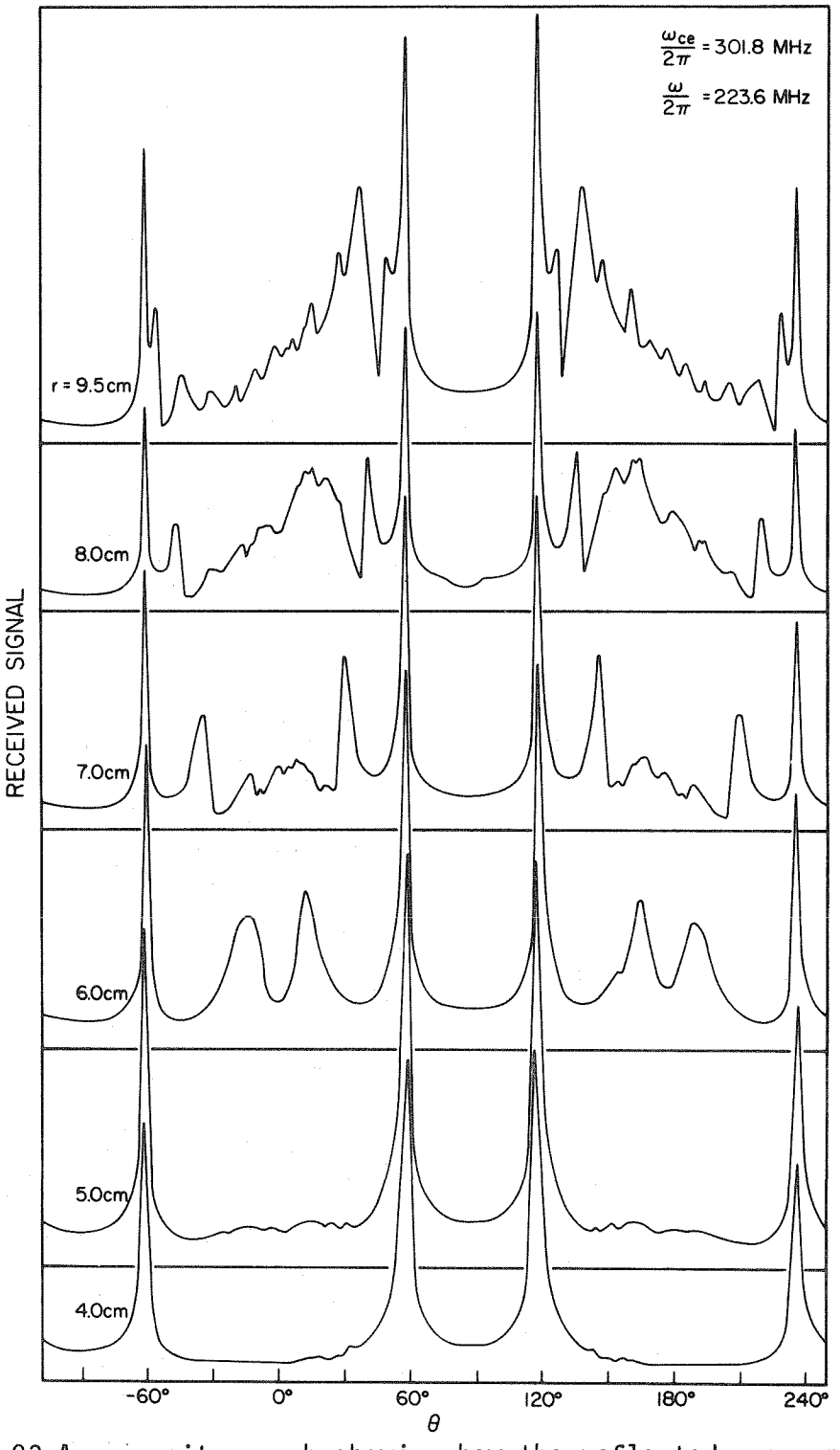

Fig. 23 A composite graph showing how the reflected resonance cones vary as r changes. All traces were taken with the 35 mm transmitting antenna.

the structure only appears for r sufficiently large shows that the signal which appears there must have arrived by a roundabout route.

The reflected resonance cone patterns sketched in Fig. 9 have the properties exhibited by the data in Figs. 22 and 23. The signal arrives by means of reflection off of the density gradient, and consequently can be seen only for r sufficiently large. How large r must be depends on the main cone angle at the center of the plasma; as it gets larger, the reflection pattern will be seen for smaller r. This is consistent with the experimental observation that the new structure is seen only when the main cone angle is large. Further, the shape of the patterns in Fig. 9 shows that, as r increases, the reflections will be observed first when the antennas are near the axis of the plasma. (In this context, please recall that the transmitting and receiving probes are mounted on the same structure and both rotate simultaneously.) Finally, the reflections should produce structure that is visible only at angles closer to the axis than the main resonance cone angle. The data in Fig. 22 exhibit this behavior for frequencies in both the lower and upper branches.

In Section 3.3, we showed that if the antenna separation and angular position are related by $r \cos \theta = L$, then the received signal would increase greatly. A bit more consideration of Fig. 9 will show that this is the condition which will give the peaks in Fig. 23 nearest to the main cone, if those peaks in the data are indeed due to reflections.

Figure 24 presents plots of $\cos \theta$ vs $1/r$ for the peaks in the data nearest the main resonance cone. Data from both the upper and

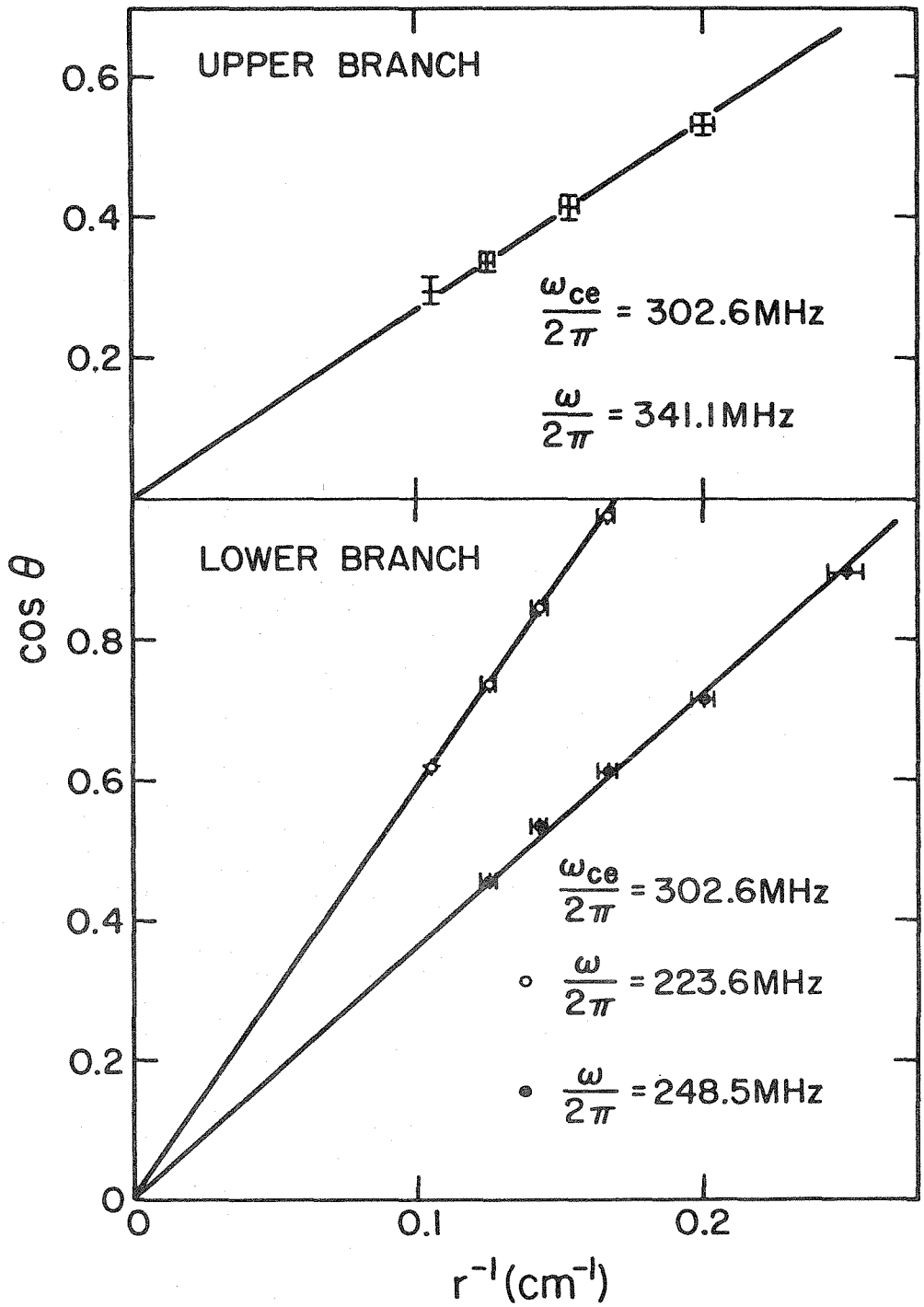

Fig. 24 Variation with antenna separation of the angle at which the reflected resonance cones occur for various frequencies in the upper and lower branch. All data were taken with the 35 mm transmitting antenna.

lower branches, including that shown in Fig. 23, are presented. Clearly, as predicted by the reflection idea, a straight line through the origin fits the data quite well.

We have verified that reflections of the resonance cones can account for the data, but one question remains. Is the turning point somewhere in the density gradient, or is the energy really reflecting off the glass vacuum vessel? Even if the latter were true, the natural density gradient of the bounded plasma is affecting the path that the energy takes. If the signal were almost unaffected in passing through the density gradient and if it then were reflected by the glass, reflection patterns for frequencies in the upper and lower branches would look the same when the resonance cone angles were the same. Figure 22 shows that this is not the case. In Section 3.3, we showed that a lower branch pattern has a smaller period L than one in the upper branch when the resonance cone angles of both are the same. This predicts that, for the same antenna separation, data taken in the lower branch will exhibit more peaks due to reflections than data taken in the upper branch. This is the behavior shown in Fig. 22.

It is Fig. 25 that really settles the question of possible reflections from the glass. This is a plot of received signal vs angular position with no plasma present. If reflections off the glass were important, the received signal graph would have a sinusoidal shape. In fact, the data are almost constant, with only a small sinusoidal component due to reflection. A reflection of this small an amplitude is not enough to account for peaks of the height seen in Figs. 22 and 23.

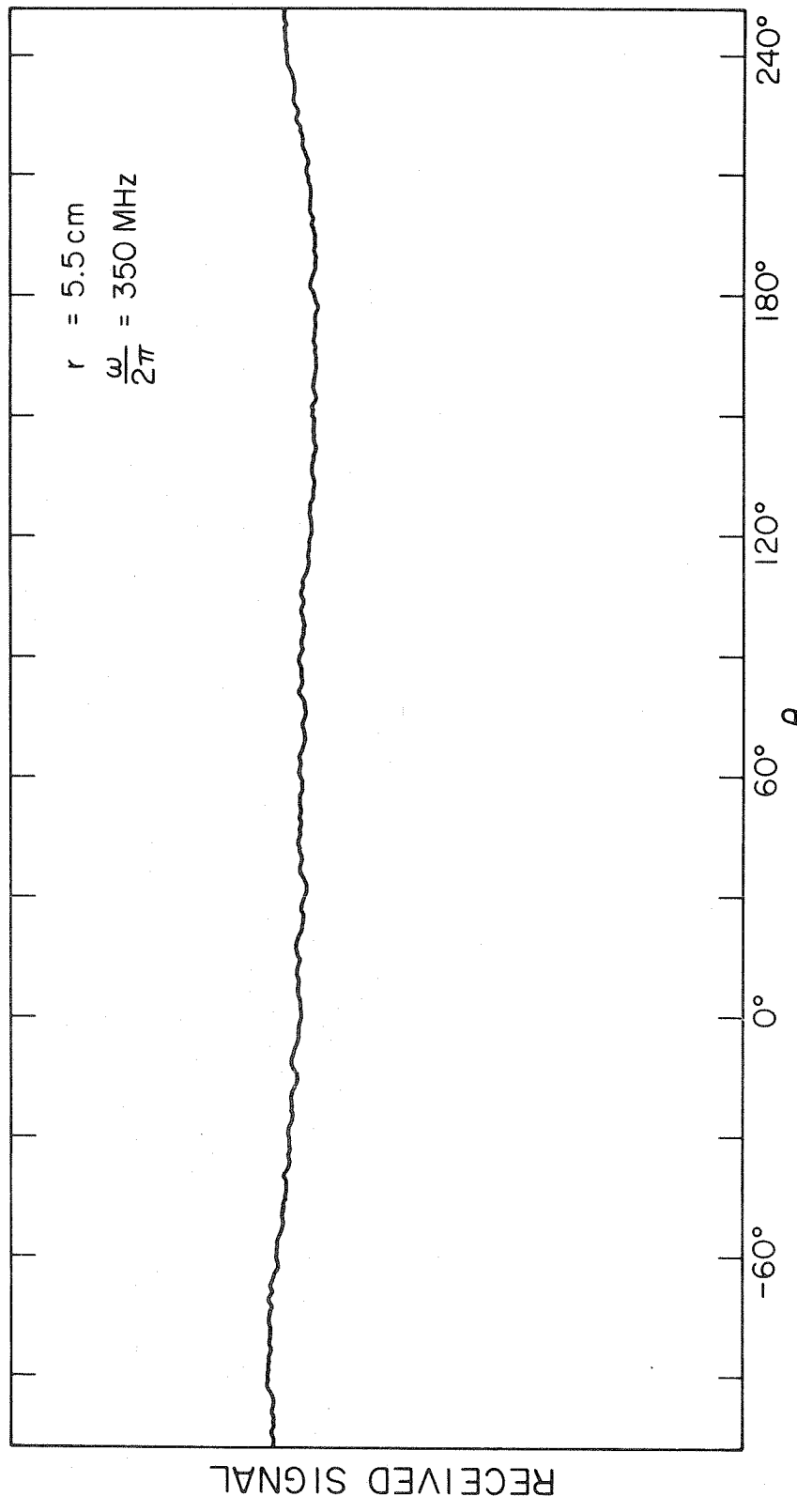

Fig. 25 Received signal with no plasma present. The 35 mm transmitting antenna was used.

Consequently, the model of the energy in the resonance cone reflecting off of the density gradient definitely accounts for the observed data.

CHAPTER VI

ANGULAR INTERFERENCE SPACING

6.1 Introduction

The presence of the interference structure near the resonance cone is the most striking difference between the simple cold plasma theory and the warm plasma theory developed in Chapters II and III. The aspect of the data that is most easily related to the nonzero plasma temperature is the angular spacing between the various interference peaks and the main resonance cone peak. The theory predicts that these should be governed by the $\Delta\theta_n$ defined in Eq. (51) or Eq. (59). In this chapter, we will present a series of parameter studies designed to verify the theoretical predictions.

6.2 Dependence of Angular Spacing on Antenna Separation

According to the work in Chapter III, the $\Delta\theta_n$ are proportional to $r^{-2/3}$ if all the other parameters are constant as r varies. However, we saw in Section 5.2 that the plasma density varies somewhat as the antenna separation changes. Fortunately, the resultant change in the plasma frequency is only about 30% and, as shown in Fig. 6, there is a large range of parameter values where a 30% variation in ω_{pe} will have a small effect on the theoretically predicted interference spacing. Consequently, if we have $\omega_{pe}/\omega_{ce} \geq 1$, a simple plot of the observed angular interference spacing vs. $r^{-2/3}$ can be used to check the theoretically predicted radial dependence.

In Fig. 26, we present a graph showing the angular spacing between the main peak and each of the first five interference peaks

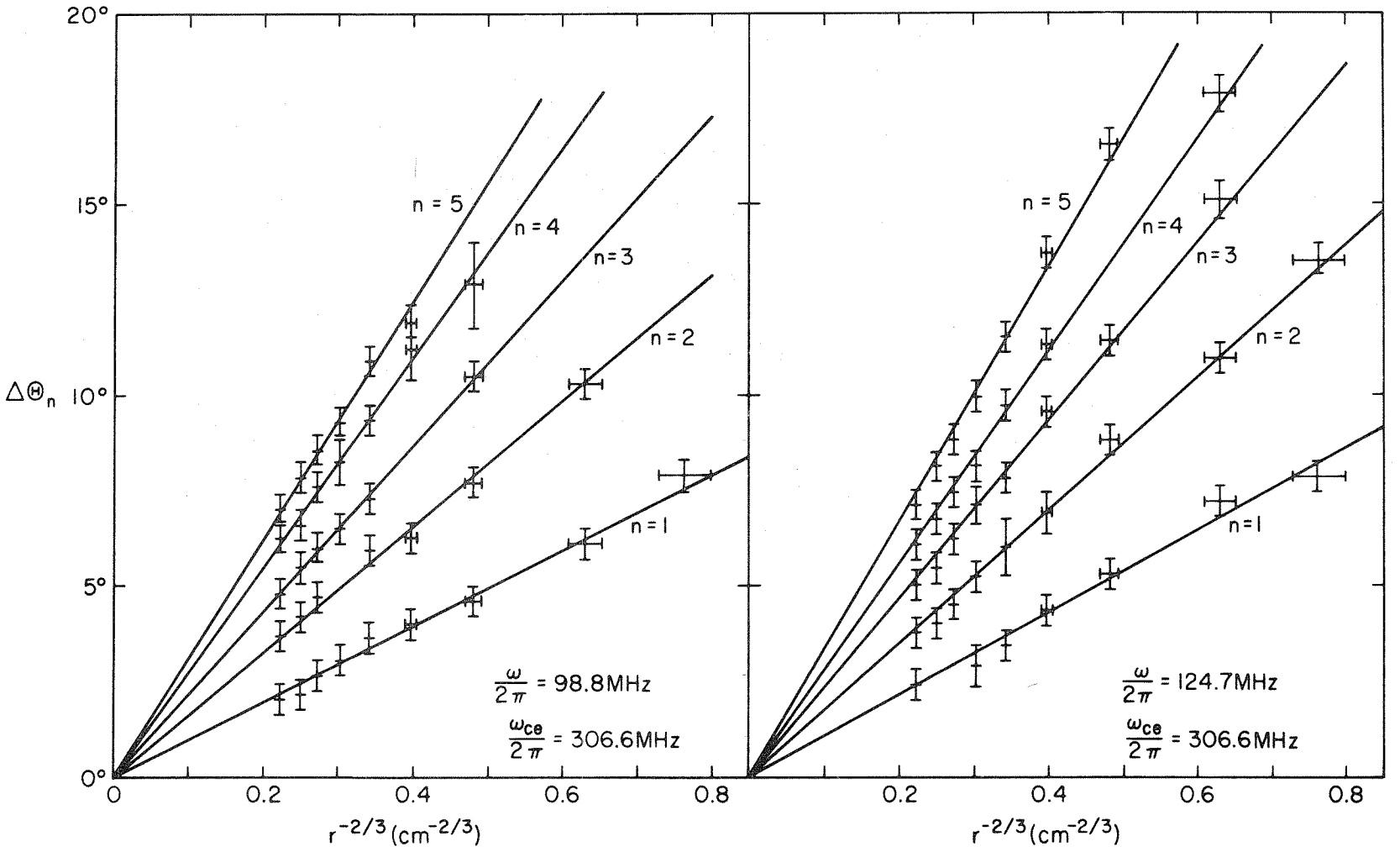

Fig. 26 Angular interference spacing $\Delta\Theta_n$ as a function of r for n =1(1)5. The data were taken with the 35 mm transmitting antenna. Each plotted point is the mean of four measurements.

plotted vs $r^{-2/3}$. The data were taken at two different frequencies but under the same plasma conditions, with $\omega_{pe}/\omega_{ce} \sim 1$. Each point plotted represents the mean of four measurements. The error is the standard deviation of the mean, or the basic measurement error, whichever is greater. The solid lines through the data points are the lines of best fit as determined by the least squares fit procedure given in Appendix E. This line is constrained to go through the origin.

Since the lines of best fit in Fig. 26 match the data so well, the assumed theoretical dependence of $r^{-2/3}$ is the correct one. The data for the first three interference peaks give an especially good test of the theory, since the error is smaller for these data. Whether the slopes of the lines of best fit have the proper magnitude will be dealt with in the next section.

6.3 Ratios of Interference Spacings

The interference spacings considered in the last section can be expressed in terms of the $\Delta\theta_n$ of Chapter III as

$$\Delta\theta_n = \Delta\theta_{n+1} - \Delta\theta_1 \qquad n \geq 1$$

The theory predicts that all the $\Delta\theta_n$ should be proportional to each other, i.e., that there should exist numbers $\alpha_{mn} = \Delta\theta_n/\Delta\theta_m$ which should be constant. We will examine the data to see whether this proportionality holds and whether the proportionality constants have the theoretically predicted values.

The theoretical values of the α_{mn} are easily obtained from the numbers in Table 1 (for a point source) or in Table 2 (for a line source) and they are given in Table 3 for $m,n \leq 5$. Since $\alpha_{mn} = 1/\alpha_{nm}$, only the upper, off-diagonal elements of the matrix are given. Since we also have $\alpha_{mn} = \alpha_{\ell n}/\alpha_{\ell m}$ for any ℓ, there are only four independent elements in each part of Table 3. The different predictions cover the alternatives: a transmitting antenna that acts either like a line source or a point source and a receiving antenna that is sensitive either to the potential or the electric fields. (One is missing, since the potential excited by a line source was analytically intractable.)

TABLE 3

THEORETICAL RATIOS OF INTERFERENCE SPACINGS

Point Source

(Potential)

1.6496	2.2019	2.6983	3.1564
	1.3348	1.6358	1.9134
		1.2254	1.4335
			1.1698

(Electric Field)

1.7472	2.3944	2.9808	3.5244
	1.3704	1.7060	2.0172
		1.2449	1.4720
			1.1824

Line Source

(Electric Field)

1.6901	2.2810	2.8136	3.3060
	1.3496	1.6647	1.9561
		1.2335	1.4494
			1.1750

Since the data in Fig. 26 can be fit with a set of straight lines, this shows that the $\Delta\theta_n$ with $n \leq 5$ remain proportional as r varies. From the slopes of the lines of best fit, experimental values for the α_{mn} can be found by taking ratios. These experimental values, along with their errors, are given in Table 4.

TABLE 4

EXPERIMENTAL RATIOS OF INTERFERENCE SPACINGS

(From Data in Fig. 26)

$\omega/2\pi$ = 98.8 MHz

Ratios				Errors in Ratios			
1.656	2.183	2.770	3.135	.071	.092	.114	.122
	1.318	1.672	1.893		.048	.059	.061
		1.269	1.436			.043	.045
			1.132				.034

$\omega/2\pi$ = 124.7 MHz

Ratios				Errors in Ratios			
1.619	2.169	2.586	3.107	.067	.086	.101	.117
	1.340	1.597	1.918		.040	.047	.053
		1.192	1.432			.031	.035
			1.201				.028

The experimental values of the α_{mn} agree reasonably well with both the theoretical predictions for the potential of a point source and the electric field of a line source. They do not agree nearly as well with the predictions based on a point source transmitter and a receiver sensitive to the electric field.

As identified in Fig. 26, these data were taken, as most were, with the short, 35 mm antenna. Some data were taken with the 75 mm antenna, which should be a better approximation to a line source. Since these data were taken with time in the afterglow as the variable, we can also use them to check whether the $\Delta\theta_n$ remain proportional as the density varies.

An example of the raw data taken with the 75 mm antenna is Fig. 14; these data also form the basis for Fig. 18 and 29. At most, four interferences are visible in them; hence, only three of the α_{mn} are independent.

In Fig. 27, we show plots of $\Delta\theta_n$ vs. $\Delta\theta_m$ for $m \leq n \leq 4$ and m=1,2,3 . The solid lines in the figure are the lines of best fit, which are constrained to go through the origin as theory demands. (Please note that the origin of the plot has been shifted for the m = 2 data). Clearly, the various $\Delta\theta_n$ are proportional. The experimentally determined α_{nm} , which are the proportionality constants, are given in Table 5.

The sets of data that went into Fig. 27 were taken with r and ω/ω_{ce} constant; the change in the $\Delta\theta_n$ is caused by the variation in the plasma frequency, $0.56 \leq \omega_{pe}/\omega_{ce} \leq 1.12$. As theory predicts, the $\Delta\theta_n$ vary proportionally as the density varies. Furthermore, the α_{nm} calculated for a line source fit the data best.

Finally, to verify that the $\Delta\theta_n$ remain proportional as ω/ω_{ce} varies, we make the plot in Fig. 28 of $\Delta\theta_1$ vs. $\Delta\theta_2$. Since these two are proportional as r and ω_{pe}/ω_{ce} vary, no attempt was made to restrict the data to sets with constant values of these

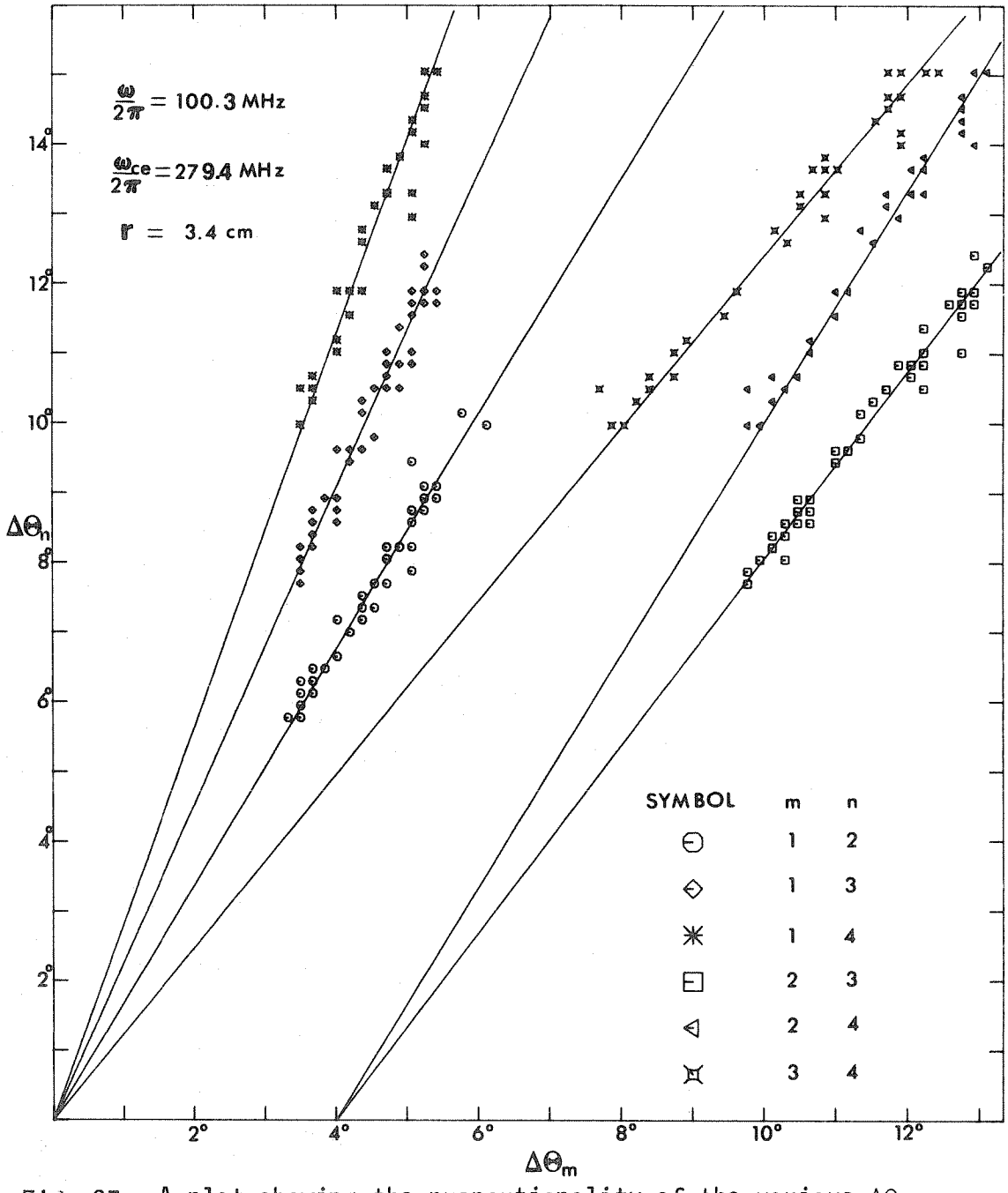

Fig. 27 A plot showing the proportionality of the various $\Delta\Theta_n$. For clarity, the set of data with m = 2 has been displaced 4° to the right, and all error bars have been suppressed Errors ranged from 0.4° to 1.1°. All data were taken with the 75 mm transmitting antenna.

TABLE 5

EXPERIMENTAL RATIOS OF INTERFERENCE SPACINGS

(From Data in Fig. 27)

Ratios			Errors in Ratios		
1.689	2.263	2.815	.025	.035	.051
	1.343	1.667		.019	.027
		1.240			.021

parameters. The frequency varies in the range $0.32 \leq \omega/\omega_{ce} \leq 1.24$ in this plot, and most of the points in the third quadrant come from upper branch measurements.

Figure 28 confirms that $\Delta\theta_1$ and $\Delta\theta_2$ are proportional. The slope of the line of best fit that passes through the origin gives a value $\alpha_{12} = 1.692 \pm 0.013$, which compares quite well with the line source prediction. Indeed, it is somewhat startling that the agreement is so good, for all these data were obtained with the 35 mm antenna.

In summary, we have verified that the $\Delta\theta_n$ are proportional to each other when r, ω_{pe}/ω_{ce}, and ω/ω_{ce} are varied, as predicted by theory, and that the proportionality constants agree with the theoretical predictions.

6.4 Interference Spacings as a Function of ω_{pe}/ω_{ce} and ω/ω_{ce}

Since the interference spacings are proportional, they all have the same dependence on the physical parameters. It will thus only be necessary to investigate that dependence for $\Delta\theta_1$, which is the easiest of these quantities to measure in the data. As Sections

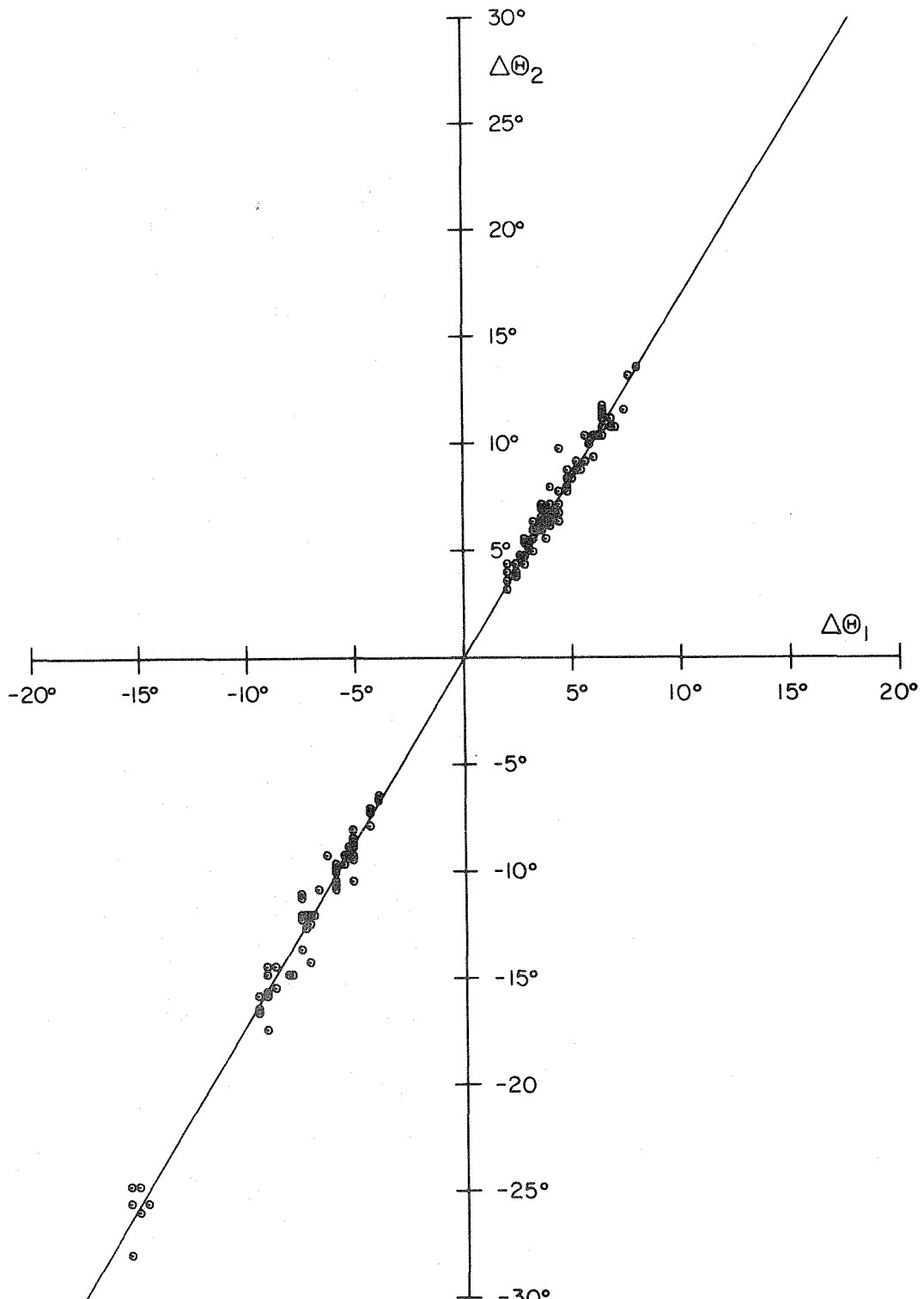

Fig. 28 Demonstration of the proportionality of $\Delta\theta_1$ and $\Delta\theta_2$. The data were taken with the 35 mm transmitting antenna. For clarity, the error bars, which ranged from 0.4° to 1.2°, have been suppressed.

3.1 and 3.2 show, the dependence of $\Delta\Theta_1$ on ω_{pe}/ω_{ce} and ω/ω_{ce} is embodied in the function Λ .

The data used to investigate the dependence on ω_{pe}/ω_{ce} were originally taken in an attempt to see how the plasma temperature decayed with time in the afterglow. By assuming the theory to be correct, one can invert Eq. (51) or Eq. (59) and find the temperature. However, the derived temperature always came out near 300^{o}K. (The raw data in Fig. 14 and the data used to form Figs. 18 and 27 are all part of this data.) If we assume that the temperature is constant, we can attempt to verify the dependence of $\Delta\Theta_1$ on ω_{pe}/ω_{ce}.

In Fig. 29, $\Delta\Theta_1$ is shown as a function of ω_{pe}/ω_{ce} . The solid line through the data is the theoretical function, with the temperature adjusted to give the best fit. Recall that the temperature enters only as a multiplicative scale factor. The shape of the curve (see Fig. 6) is independent of T_e .

As we saw in the last section, the constants from the line source work are appropriate for the long antenna. Using this, the temperature that gives the best fit is 330 ± 31^{o}K. It is quite believable that a temperature this close to room temperature can persist for the interval of 4 msec in the afterglow during which the data were taken.

Several different methods were tried in an attempt to obtain an independent measure of the temperature. All failed. They involved determining the temperature from the dispersion curves for various types of electrostatic warm plasma waves whose behavior has been studied previously. The waves included Bernstein, or cyclotron

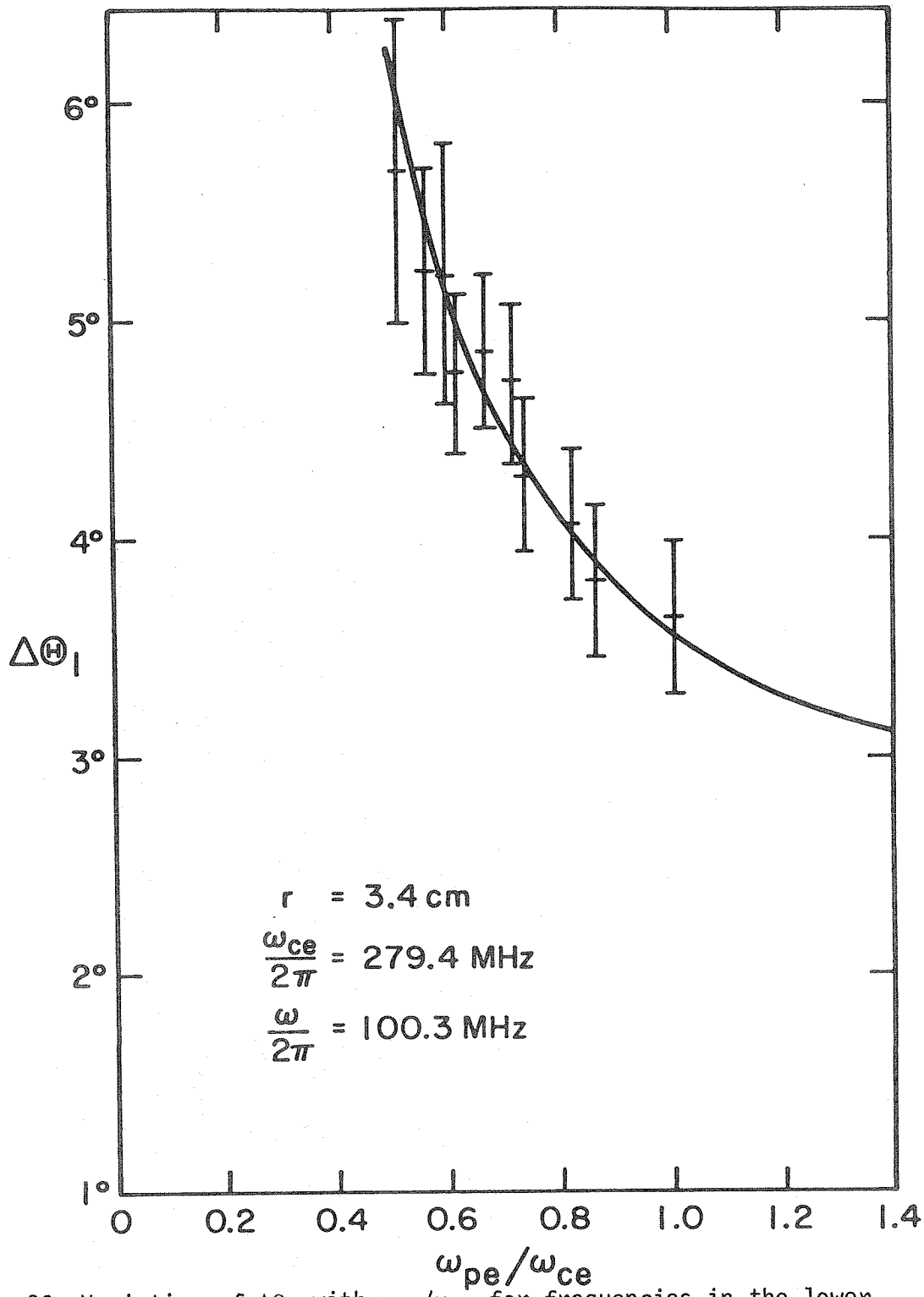

Fig. 29 Variation of $\Delta\Theta_1$ with ω_{pe}/ω_{ce} for frequencies in the lower branch. The 75 mm transmitting antenna was used for these data.

harmonic waves, which propagate perpendicular to the magnetic field, and Landau waves and ion acoustic waves, which propagate parallel to the field. All proved to be undetectable. The failure is, at least, consistent with the low temperature inferred from the interference spacing. If $T_e = 300^oK$, the wavelength of the Bernstein and Landau waves when $\omega/2\pi$, $\omega_{pe}/2\pi$, $\omega_{ce}/2\pi \sim 300MHz$ would be so short (≤ 1 mm) that detection would be difficult, while ion acoustic waves should be very strongly damped in a plasma with equal electron and ion temperatures. Even in the absence of an independent determination, the fact that a temperature which is constant in time is also found to be quite near room temperature tends to confirm the accuracy of the measurement.

Other sets of data were taken to see how $\Delta\Theta_1$ varied with ω/ω_{ce}. Figure 5 shows how the theoretical predictions behave for this case. One interesting prediction is that, even in the lower branch, the interference structure can appear outside the resonance cone ($\Delta\Theta$, $\Lambda < 0$) for certain values of ω/ω_{ce} if ω_{pe}/ω_{ce} is large enough. The plot in Fig. 30 demonstrates that this is indeed the case.

The data presented in Fig. 30 were taken with fixed antenna separation and fixed plasma frequency. A nonlinear least squares fit [39] was used to obtain the temperature and ω_{pe}/ω_{ce}. The best fit values were $T_e = 800 \pm 100^oK$ and $\omega_{pe}/\omega_{ce} \sim 10^{15}$. The absurdly large value of the plasma frequency occurs because the density is sufficiently high that the interference spacing is quite insensitive to its value. The resonance cone angle itself yields $\omega_{pe}/\omega_{ce} \sim 2$, which is in the region where the cone angle, too, is very insensitive to ω_{pe}. All that can be said with certainty is that $\omega_{pe}/\omega_{ce} > 2$.

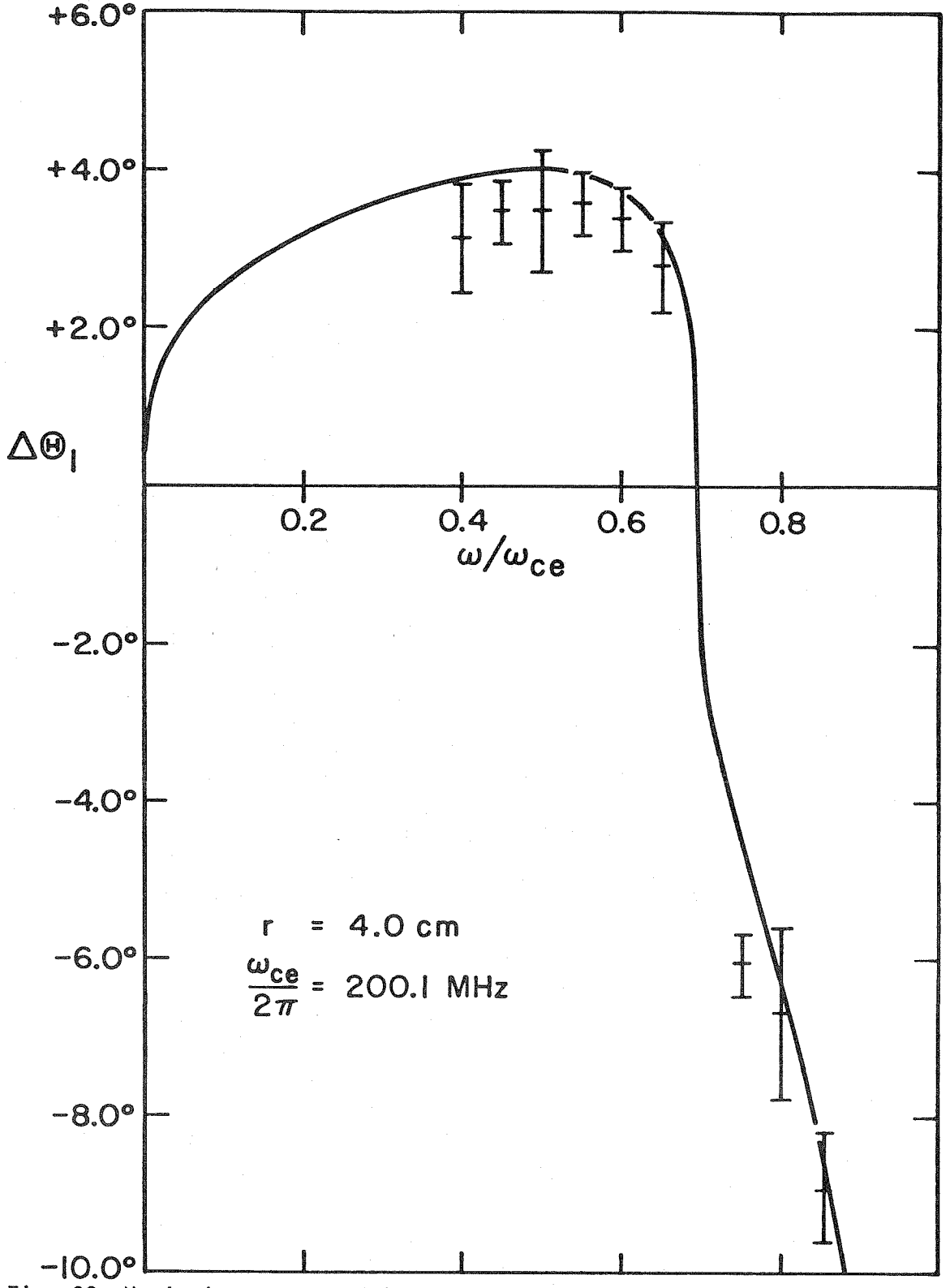

Fig. 30 Variation of $\Delta\Theta_1$ with ω/ω_{ce} for ω in the lower branch. The 35 mm transmitting antenna was used for these data.

The temperature is found by using the constant computed for a line source. If the point source results were used, the computation for the potential would result in a temperature smaller by a factor of 1.2696, while that for the electric field would give one larger by 1.3867. These different factors, of course, do not affect the fit to the data, since the theoretical function just contains the product of $T_e^{1/3}$ and an appropriate numerical factor.

The upper branch is much more challenging experimentally, since $\Delta\theta_1$ changes much more rapidly with ω/ω_{ce} and ω_{pe}/ω_{ce}. As shown in Fig. 31, reasonably good data were obtained here also. The three sets of data shown were taken at several frequencies and radii, but the plasma conditions were kept constant. The theoretical lines fitted to the data yield the parameter values given in Table 6. The temperature was again computed using the constant appropriate for a line source. The internal agreement of the best fit parameters provides a check of the self-consistency of our theoretical interpretation of the data.

TABLE 6

BEST FIT PARAMETERS FROM Fig. 31

Antenna Separation (cm)	ω_{pe}/ω_{ce}	$T_e(^oK)$
5.0	0.931 ± .053	868 ± 82
6.5	0.948 ± .067	771 ± 91
8.0	0.962 ± .095	796 ± 138

Another check of internal consistency can be made by comparing the values of ω_{pe}/ω_{ce} in Table 6 with that derived from the main

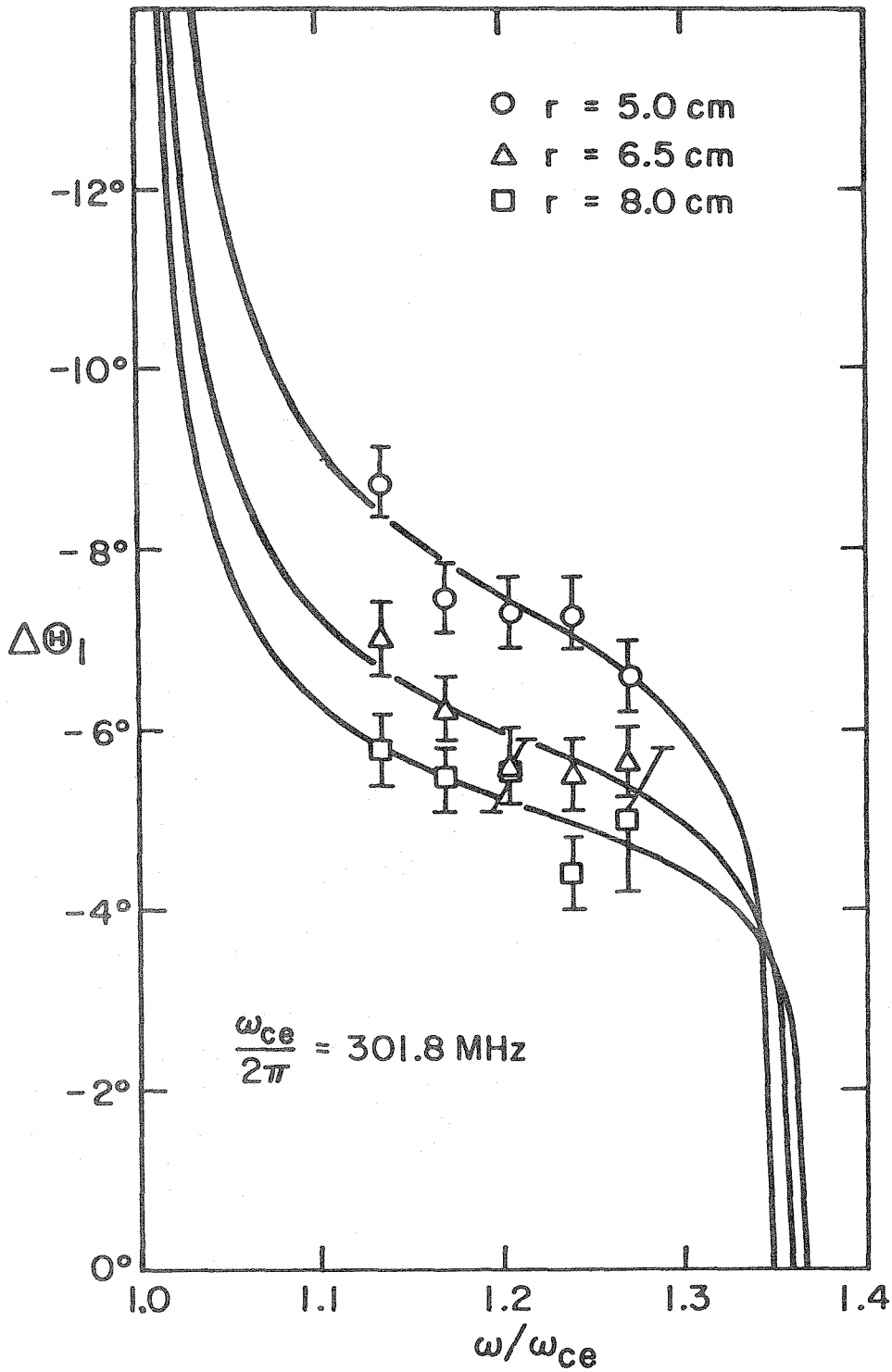

Fig. 31 Variation of $\Delta\Theta_1$ with ω/ω_{ce} for ω in the upper branch The 35 mm transmitting antenna was used for these data.

resonance cone angle, using the cold plasma cone angle formula. Since ω is in the upper branch, the cone angle should give a good measure of ω_{pe}/ω_{ce}. A least squares fit to the data giving the cone angle as a function of frequency yields $\omega_{pe}/\omega_{ce} = 0.989 \pm .008$. These two methods of measuring the plasma frequency are independent; their agreement confirms that the theoretical development is correct.

In conclusion, in this chapter we have verified that the interference spacing depends on the antenna separation as $r^{-2/3}$, as predicted by theory; that all the spacings remain proportional as r, ω_{pe}/ω_{ce} and ω/ω_{ce} vary, with proportionality constants that agree with theoretical predictions; and that the spacing changes with ω/ω_{ce} and ω_{pe}/ω_{ce} in a manner consistent with the theory.

CHAPTER VII

CONCLUSION

7.1 Summary and Evaluation

In this thesis, we have presented a detailed theoretical and experimental investigation of the resonance cone pattern excited by a small antenna in a warm, magnetized plasma.

The warm plasma theory, valid for arbitrary $\omega < \omega_{UH}$ has been developed for a uniform plasma in the limit that $r/\lambda_{de} >> 1$ and $r/r_{\ell e} >> 1$. This led to predictions about the functional dependence of the angular position of the main resonance cone peak and the angular interference spacing on the physical parameters r, ω, ω_{pe}, ω_{ce} and T_e. The theory for plasmas of nonuniform density was also developed, but in the cold plasma limit, leading to predictions that the resonance cones could reflect off of density gradients.

The experimental work verified the theoretical picture. The main resonance cone angle was shown to depend on ω, ω_{pe}, ω_{ce} and r in a manner consistent with the theory, as did the angular interference spacing. In addition, the idea of resonance cones reflecting from density gradients was able to explain features of the data that were otherwise incomprehensible.

From the data, values of plasma frequency could be derived in more than one way, and the results were consistent. The temperature obtained from the data was appropriate for the afterglow plasma employed in the experiment. Since both ω_{pe} and T_e can be obtained from one experimental trace, resonance cone measurements are an

important diagnostic technique for any plasma in which one dares to put antennas.

7.2 Suggestions for Further Work

The theory developed in this work is incomplete in two respects. First, it proved to be extremely difficult to evaluate the electrostatic potential excited by a line source, so we could not check whether the receiving probe was sensitive to the potential or the electric field. Perhaps a calculation for an antenna of finite length could remedy this. Second, the effects of the sheath around the antenna were neglected. If theoretical calculations could be done including it, they could probably be checked by comparing their predictions of the relative height of the main peaks and the interference peaks to the actual measurements.

The work done here on the propagation of the resonance cones in a plasma with nonuniform density was somewhat unsophisticated. How energy travels in a nonuniform plasma is a vast subject, but one of particular interest for fusion applications. Further investigations in this area would be most useful.

The present investigation was confined to frequencies sufficiently high that the motion of the ions in the plasma could be neglected. Some theoretical work [40] has been done for frequencies where ion motion is important, but a more complete study would be useful. I made an attempt to see the cones that exist at these low frequencies, but it was inconclusive. Since these cones are sensitive to ion temperature, if they could be seen they would provide

another useful diagnostic technique.

Finally, especially for ionospheric applications, a warm plasma theory should be developed for antennas in a flowing plasma separated by only a few wavelengths of the warm plasma waves. This would enhance the usefulness of resonance cone measurements made in the ionosphere by spacecraft.

APPENDIX A

DETAILS OF THE GREEN'S FUNCTION SOLUTION

In this appendix we will carry out the solution to Eqs. (5)-(7), which describe the Green's function. In order to keep our notation consistent with those who obtain the electrostatic approximation as the $c \to \infty$ limit of the electromagnetic solution, we will take a roundabout route, and use the continuity equation to modify Eq. (6). Conservation of charge demands

$$\frac{\partial \rho_p}{\partial t} + \underline{\nabla} \cdot \underline{J} = 0$$

where ρ_p is the charge density and $\underline{J}$ is the current density. Since the charge density in the plasma is $\rho_p = -n_1 e$, and since n_1 varies as $e^{-i\omega t}$, Eq. (6) becomes

$$\underline{\nabla} \cdot (\underline{\nabla}\phi + \frac{\underline{J}}{i\omega\varepsilon_o}) = -\frac{q}{\varepsilon_o}\delta(\underline{x})\, e^{-i\omega t} \tag{A.1}$$

To close the system, we replace Eq. (7) with

$$\underline{J} = -e \int d\underline{v}\, \underline{v}\, f^{(1)}(\underline{x},\underline{v},t) \tag{A.2}$$

Equation (5) remains unchanged, but we will drop the superscript on $f^{(1)}(\underline{x},\underline{v},t)$ from now on for ease of notation. Also, we will replace $f^{(o)}$ by f_o.

It is easiest to solve Eq. (5) for $f(\underline{x},\underline{v},t)$ in terms of ϕ by using the method of characteristics. Since

$$\frac{e}{m}\,\underline{v}\times\underline{B}_o\cdot\frac{\partial f}{\partial \underline{v}} = -\,\omega_{ce}\,\frac{\partial f}{\partial \lambda}$$

where λ is the azimuthal angle in velocity space, the equations for the characteristics are

$$\frac{dX}{dt'} = v_\rho \cos\lambda$$

$$\frac{dY}{dt'} = v_\rho \sin\lambda$$

$$\frac{dZ}{dt'} = v_z$$

$$\frac{d\lambda}{dt'} = \omega_{ce}$$

where $v_\rho = \sqrt{v_x^2 + v_y^2}$ and v_z are constants of the motion, and where t' is a coordinate along the characteristic. If the characteristic is to pass through the phase space location (x,y,z,v_x,v_y,v_z) when $t = t'$, then the phase space coordinates of the characteristics (X, Y, Z, V_x, V_y, V_z) are given by

$$\underline{V} = \underline{\underline{N}}(t-t')\cdot\underline{v}$$

$$\underline{X} = -\underline{\underline{M}}(t-t')\cdot\underline{v} + \underline{x}$$

where $\underline{V}$ and $\underline{v}$ are velocity vectors, $\underline{X}$ and $\underline{x}$ are position vectors, and

$$\underline{\underline{N}}(\tau) = \begin{pmatrix} \cos\omega_{ce}\tau & \sin\omega_{ce}\tau & 0 \\ -\sin\omega_{ce}\tau & \cos\omega_{ce}\tau & 0 \\ 0 & 0 & 1 \end{pmatrix} \qquad (A.3)$$

$$\underline{\underline{M}}(\tau) = \frac{1}{\omega_{ce}} \begin{pmatrix} \sin \omega_{ce}\tau & 1 - \cos \omega_{ce}\tau & 0 \\ -1 + \cos \omega_{ce}\tau & \sin \omega_{ce}\tau & 0 \\ 0 & 0 & \omega_{ce}\tau \end{pmatrix} \tag{A.4}$$

Since $f(\underline{x},\underline{v},t)$ varies as $e^{-i\omega t}$, in characteristic coordinates Eq. (5) becomes

$$\frac{df}{dt'} - i(\omega+i\nu)f = -\frac{e}{m}\frac{\partial\phi}{\partial\underline{x}} \cdot \frac{\partial f_o}{\partial\underline{v}} \tag{A.5}$$

where all variables are evaluated on the characteristic. Using the fact that $e^{-i(\omega+i\nu)t}$ vanishes as $t \to -\infty$, the solution to Eq. (A.5) is

$$f(\underline{x},\underline{v},t) = -\frac{e}{m}\int_{-\infty}^{t} dt' \, \frac{\partial\phi}{\partial\underline{x}} \cdot \frac{\partial f_o}{\partial\underline{v}} \exp[-i(\omega+i\nu)(t'-t)]$$

If we let $\tau = t-t'$,

$$f(\underline{x},\underline{v},t) = -\frac{e}{m}\int_{0}^{\infty} d\tau \, \frac{\partial\phi}{\partial\underline{x}} \cdot \left.\frac{\partial f_o}{\partial\underline{v}}\right| \exp[-i(\omega+i\nu)\tau] \tag{A.6}$$

The vertical bar has been inserted in the integrand to remind us that all functions are evaluated on the characteristic.

By Fourier transforming in space, Eqs. (A.1), (A.2) and (A.6) can be solved for the potential. We will denote the Fourier transform of a function $h(\underline{x})$ by

$$h(\underline{k}) = \int d\underline{x} \, h(\underline{x}) \, e^{-i\underline{k}\cdot\underline{x}}$$

Using this,

$$f(\underline{k},\underline{v},t) = -\frac{e}{m}\int_0^\infty d\tau\, \exp[i(\omega+i\nu)\tau]\left.\frac{\partial f_o}{\partial \underline{v}}\right| \cdot \int d\underline{x}\, e^{-i\underline{k}\cdot\underline{x}}\left[\left.\frac{\partial\phi}{\partial \underline{x}}\right|_{\underline{x}=\underline{X}}\right]$$

$$= i\frac{e}{m}\phi(\underline{k},t)\int_0^\infty d\tau\, \underline{k}\cdot\left.\frac{\partial f_o}{\partial \underline{v}}\right| \exp[i(\omega+i\nu)\tau - i\underline{k}\cdot\underline{\underline{M}}\cdot\underline{v}] \qquad (A.7)$$

Combining this with the transforms of Eq. (A.1) and (A.2) yields

$$\underline{k}\cdot\underline{\underline{K}}\cdot\underline{k}\;\phi(\underline{k},t) = \frac{q}{\varepsilon_o}e^{-i\omega t}$$

where $\underline{\underline{K}}$ is the k-space dielectric tensor

$$\underline{\underline{K}} = \underline{\underline{I}} - \frac{ie^2}{m\omega\varepsilon_o}\int d\underline{v}\,\underline{v}\int_0^\infty d\tau\left.\frac{\partial f_o}{\partial \underline{v}}\right| \exp[i(\omega+i\nu)\tau - i\underline{k}\cdot\underline{\underline{M}}\cdot\underline{v}] \qquad (A.8)$$

The dispersion function for the problem is $D(\underline{k}) = \underline{k}\cdot\underline{\underline{K}}\cdot\underline{k}$. The expression for $D(\underline{k})$ can be greatly simplified if we define the normalized velocity space Fourier transform of $f_o(\underline{v})$

$$F(\underline{\beta}) = \frac{1}{n_o}\int d\underline{v}\, e^{-i\underline{\beta}\cdot\underline{v}} f_o(\underline{v})$$

Using this, we find

$$D(\underline{k}) = \underline{k}^2 + \omega_{pe}^2(1+i\nu/\omega)\int_0^\infty d\tau\, \underline{k}\cdot\underline{\underline{M}}\cdot\underline{k}\, e^{i(\omega+i\nu)\tau}\, F(\underline{\underline{M}}\cdot\underline{k}) \qquad (A.9)$$

Consequently,

$$\phi(\underline{k},t) = \frac{q}{\varepsilon_o}e^{-i\omega t}\,\frac{1}{D(\underline{k})} \qquad (A.10)$$

If we now specialize to an isotropic Maxwellian, then

$$f_o(\underline{v}) = \frac{n_o}{\pi^{3/2}v_{th}^3}\exp\left(-\frac{\underline{v}^2}{v_{th}^2}\right)$$

where $v_{th}^2 = 2\kappa T_e/m$. This produces

$$F(\underline{\beta}) = \exp(-\tfrac{1}{4}\,\underline{\beta}^2 v_{th}^2)$$

Using this, and the identity

$$\frac{d}{d\tau}\,(\underline{\underline{M}}\cdot\underline{k})^2 = 2\underline{k}\cdot\underline{\underline{M}}\cdot\underline{k}$$

we can write $D(\underline{k}) \equiv D(k_\perp, k_\parallel)$ as

$$D(k_\perp, k_\parallel) = k_\perp^2 + k_\parallel^2 + k_{de}^2(1+i\nu/\omega)(1 + i(\omega+i\nu)\int_0^\infty d\tau\, \exp\{i(\omega+i\nu)\tau$$

$$- \frac{k_\perp^2 v_{th}^2}{\omega_{ce}^2}\sin^2\tfrac{1}{2}\omega_{ce}t - \tfrac{1}{4}k_\parallel^2 v_{th}^2 t^2\}) \qquad \text{(A.11)}$$

where $k_\perp^2 = k_x^2 + k_y^2$ and $k_\parallel = k_z$.

Equations (A.10) and (A.11) complete the solution for the Fourier transform of the potential. The inverse transform is dealt with in the main text.

APPENDIX B

NUMERICAL RESONANCE CONE CALCULATIONS

A variety of numerical procedures are referred to in the text. Some are standard, and some were developed specifically for this work. Those that deal with theoretical predictions of resonance cone structure and location are the subject of this section. Others may be found in Appendix E. The procedures presented here are the numerical evaluation of the integral in Eq. (16) and evaluation of the various Airy functions needed in Chapter III.

To perform the integration in Eq. (16), we need both an integration procedure and a method of evaluating the special functions in the integrand. The evaluation of $K_o(z)$ for complex z has been published elsewhere [16], so only the calculation for $Z'(z)$ needs to be discussed here.

The plasma dispersion function $Z(z)$ is related to the complex error function [41] by

$$Z(z) = i\sqrt{\pi}\, w(z) = i\sqrt{\pi}\, e^{-z^2}\, \mathrm{erfc}(-iz)$$

Gautschi [42,43] has written an algorithm to calculate $w(z)$. Since $Z'(z) = -2(1 + zZ(z))$, in principle one could use his algorithm to find $Z'(z)$. Unfortunately, this approach loses accuracy due to round off error when $|z| > 4$. One must either carry more significant digits in the calculation, which leads to a slow routine, or write another procedure.

The complex error function and $w(z)$ are special cases of the

confluent hypergeometric function. Using this fact, a number of authors [44,45,46] have developed continued fraction representations for them. Although somewhat of a mathematical curiosity, continued fractions [47] can be the basis for extremely rapid numerical methods of function evaluation. Adapting these fractions to the present case, we have

$$Z'(z) = \frac{2}{2z^2 - 3} \; \frac{2\cdot 3}{-2z^2 - 7} \; \frac{4\cdot 5}{-2z^2 - 11} \cdots$$

$$\cdots \frac{2n(2n+1)}{-2z^2 - (4n+3)} \cdots \qquad \text{Im } z > 0 \tag{B.1}$$

and

$$Z'(z) = -2i\sqrt{\pi}\, z e^{-z^2} - \frac{2}{z^2}\left[\frac{1}{z^{-2} + 2} + \frac{8/3}{z^{-2} - 6/5} + \frac{16/525}{z^{-2} - 2/39}\right.$$

$$\left. \cdots + \frac{8n(2n-3)/[(4n-1)(4n-3)^2(4n-5)]}{z^{-2} - 6/[(4n+1)(4n-3)]} \cdots \right] \tag{B.2}$$

The continued fraction in Eq. (B.1) is an adaptation of the Laplace continued fraction. Even though it is not convergent when z is real, Gautschi [43] has shown that it is an asymptotic approximation to Re $Z'(z)$ when z is large enough (e.g., $z \gtrsim 5$). (For z real, Im $Z(z) = -2i\sqrt{\pi}\, z \exp(-z^2)$, of course.) Due to its rapid convergence for large $|z|$, Eq. (B.1) is useful there, while Eq. (B.2) is good for small z.

Equations (B.1) and (B.2) were used to develop the Fortran subroutine presented in Fig. 32. Some preliminary computer runs were

```
      COMPLEX FUNCTION ZPRIME(Z)
C
C       THIS FUNCTION SUBPROGRAM EVALUATES THE DERIVATIVE OF THE
C       PLASMA DISPERSION FUNCTION FOR COMPLEX VALUES OF THE ARGUMENT.
C       THE COMPUTATION IS PERFORMED BY USING TWO CONTINUED
C       FRACTIONS, ONE FOR SMALL ARGUMENT AND THE OTHER FOR LARGE.
C       THE FRACTION USED FOR SMALL ARGUMENT WAS DEVELOPED FROM THE
C       POWER SERIES EXPANSION OF THE FUNCTION BY USING THE GD
C       ALGORITHM.  ITS COEFFICIENTS ARE STORED IN THE ARRAYS A AND B.
C       THE FRACTION FOR LARGE ARGUMENT IS THE TRADITIONAL LAPLACE
C       CONTINUED FRACTION.  THE NUMBER OF CONVERGENTS OF EACH
C       FRACTION THAT IS USED IS CHOSEN BY EMPIRICAL FORMULAS THAT
C       WERE DEVELOPED DURING SOME INITIAL TRIAL RUNS. THE ABSOLUTE VALUE
C       OF THE RELATIVE ERROR IN THE RESULT IS LESS THAN 6.0E-6
C
      INTEGER I,M
      COMPLEX Z,ZPRIME
      REAL X,Y,X2,Y2,RE,IM,RZ2,IZ2,D,T,A(20),B(20),R
      DATA A/-1.772454D 00, 2.198389D-01,-1.929780D-01,-1.945556D-01,
     &-1.825269D-01,-1.703509D-01,-1.596796D-01,-1.505391D-01,
     &-1.424836D-01,-1.416862D-01, 7.879816D-03, 3.586354D-01,
     &-1.431593D-01, 4.567910D-01,-2.035771D-01, 5.235408D-01,
     &-3.600042D-01, 3.520949D-01,-2.531981D-01,-8.186648D-02/
      DATA B/1.14159D 00,7.469541D-02,
     & 4.508787D-02, 3.110716D-02, 2.362925D-02, 1.901996D-02,
     & 1.590448D-02, 1.366566D-02, 1.185415D-02, 1.405589D-02,
     &-4.824088D-02, 5.540440D-02,-1.728404D-02, 1.182689D-01,
     &-8.085029D-03, 1.921583D-01,-5.804203D-03, 1.221379D-01,
     &-1.942373D-02, 1.742264D-01/
      X=REAL(Z)
      Y=AIMAG(Z)
      R=CABS(Z)
      IF(Y.GE.(4.75-X)*(0.112*X+0.369)) GO TO 50
      IF(R.NE.0.0) GO TO 10
      ZPRIME=(-2.0,0.0)
      RETURN
   10 D=1.C/(R*R)
      X2=-Y*D
      Y2=-X*D
      M=3.C5*R+4.79
      RE=X2+A(M)
      IM=Y2
   30 M=M-1
      D=B(M)/(RE*RE+IM*IM)
      RE=X2+A(M)+D*RE
      IM=Y2-D*IM
      IF(M.GT.1) GO TO 30
      D=-2.C/(RE*RE+IM*IM)
      T=D*(RE*X2+IM*Y2)
      IM=D*(RE*Y2-IM*X2)
      RE=T
      ZPRIME=CMPLX(RE,IM)
      RETURN
   50 RZ2=(X-Y)*(X+Y)
      IZ2=2.0*X*Y
      X2=2.0*RZ2-3.0
      Y2=2.C*IZ2
      I=18.45/R+2.12
      M=4*I
      I=2*I+2
      RE=X2-M
      IM=Y2
   70 M=M-4
      I=I-2
      D=I*(I+1)/(RE*RE+IM*IM)
      RE=X2-M-D*RE
      IM=Y2+D*IM
      IF(M.GT.0) GO TO 70
      D=2.C/(RE*RE+IM*IM)
      RE=RE*D
      IM=-D*IM
      IF(Y.EQ.0.0 .AND.ABS(RZ2).LT.160.0)IM=-3.5449077D*X*EXP(-RZ2)
      ZPRIME=CMPLX(RE,IM)
      RETURN
      END
```

Fig. 32 Algorithm to calculate the derivative of the plasma dispersion function $Z'(z)$ for z with $0 \leq \arg z \leq \pi/2$.

used to decide how many convergents of each fraction to use and in what region of the complex plane each fraction should be used. As presently written, the subroutine is valid only for z in the first quadrant of the complex plane. The accuracy of the procedure was checked against the tabulated values of $Z(z)$ [15] and against the value obtained from a double precision evaluation of Gautschi's algorithm [42]. All numerical work was performed on an IBM 370-158.

Once the special functions in the integrand were known, Eq. (16) was evaluated using Filon's quadrature method [48,49].

We now turn to the evaluation of the Airy functions needed for the work in Chapter III: $Ai(x)$, $Bi(x)$, $Gi(x)$ and their derivatives. Gordon [50] has developed an algorithm for $Ai(x)$, $Bi(x)$, $Ai'(x)$ and $Bi'(x)$ valid for all real x. The remaining functions, $Gi(x)$ and $Gi'(x)$, are computed in two different ways, one for positive x and the other for negative.

For $x < 0$, we employ the auxiliary function $Hi(x)$ [29], which satisfies

$$Gi(x) + Hi(x) = Bi(x) \tag{B.3}$$

and which is defined by

$$Hi(x) = \frac{1}{\pi} \int_0^\infty dt \exp(-\frac{1}{3} t^3 + xt) \tag{B.4}$$

The integrand in Eq. (B.3) is a positive function of t, and is thus ideally suited for numerical integration using Simpson's rule [51]. Once $Hi(x)$ is known and $Bi(x)$ is obtained from Gordon's algorithm, $Gi(x)$ is easy to find using Eq. (B.3). By using the derivatives of

Eqs. (B.3) and (B.4), $Gi'(x)$ can be found in an analogous manner.

Unfortunately as $x \to +\infty$, $Bi(x)$ and $Hi(x)$ both grow without bound. Consequently, round off error precludes use of Eqs. (B.3) and (B.4) to find $Gi(x)$ for $x > 0$. Instead, we start with the identity [31]

$$Ai(x) + iGi(x) = \frac{1}{\pi} \int_0^\infty dt \exp[\tfrac{i}{3} t^3 + ixt]$$

and then, for $x > 0$, deform the path of integration in the complex t plane to yield the representation

$$Gi(x) = \frac{1}{\pi} \int_0^\infty dt \exp[f(x,t)] \tag{B.5}$$

where

$$f(x,t) = \begin{cases} -xt + \frac{1}{3} t^3 & t \leq x^{1/2} \\ 2xt - \frac{8}{3} t^3 & t \geq x^{1/2} \end{cases}$$

The path of integration is now the path of steepest descent, and $\exp[f(x,t)]$ is a positive monotonically decreasing function of t. Again, the integrand is easily evaluated using Simpson's rule. Evaluation of the derivative of Eq. (B.5) would yield $Gi'(x)$, but it was never needed for $x > 0$.

The derivatives of the Airy functions, in addition to the functions themselves, were required so that the maxima of the functions used in Chapter III could be found from the zeros of the derivatives of those functions.

APPENDIX C

MODIFICATIONS TO THE ASYMPTOTIC EXPANSION

In Chapter II we found that the form of the asymptotic expansion would change if either $R_n(k_{nj}) = 0$ or $P_n''(k_{nj}) = 0$ for $n > 0$. Since the contribution to that expansion is strongly damped if $\text{Im } k_{nj}$ is appreciable, these changes will be important only if $\text{Im } k_{nj}$ is very small when $R_n(k_{nj}) = 0$ or when $P_n''(k_{nj}) = 0$. It is the goal of this appendix to show that there do exist points where the expansion contained in Eq. (23) or Eq. (40) must be modified if one wishes to have a complete, uniform asymptotic expansion.

A word should be said about why the heavily damped terms in Eq. (23) do not contribute, when it appears that the denominators of some of them vanish. In actuality, the denominators of several terms vanish simultaneously, and an accurate asymptotic expansion shows that the final result still remains finite. To see that several vanish at once, consider the dispersion relation and the stationary phase condition, which can be written

$$D(k_\perp, k_\parallel) = 0 \tag{C.1}$$

$$\frac{\partial D}{\partial k_\parallel} - \cot\theta \frac{\partial D}{\partial k_\perp} = 0 \tag{C.2}$$

The theory of implicit functions [52] shows that there is a unique solution to these two equations whenever

$$\left|\frac{\partial D}{\partial k_\perp}\right|^2 \left|\cot^2\theta \frac{\partial^2 D}{\partial k_\perp^2} - 2\cot\theta \frac{\partial^2 D}{\partial k_\perp \partial k_\parallel} + \frac{\partial^2 D}{\partial k_\parallel^2}\right|^2 \neq 0 \tag{C.3}$$

By differentiating the dispersion relation, Eq. (C.1), and using the stationary point condition, Eq. (C.2), one can easily show that the denominators in Eq. (23) can be written

$$R_n(k_{nj})[\cos^2\theta + \mathscr{D}_n'(k_{nj})\sin^2\theta]^{1/2} = [\tfrac{1}{2} R_n(k_{nj})]^{1/2} \{\cos^2\theta \frac{\partial^2 D}{\partial k_\perp^2} - 2 \sin\theta\cos\theta \frac{\partial^2 D}{\partial k_\perp \partial k_\parallel} + \sin^2\theta \frac{\partial^2 D}{\partial k_\parallel^2}\}^{1/2} \Bigg|_{\substack{k_\parallel = k_{nj} \\ k_\perp = iP_n(k_{nj})}} \qquad (C.4)$$

Since $P_n''(k_{nj}) = 0$ implies $\cos^2\theta + \mathscr{D}'(k_{nj})\sin^2\theta = 0$ and since $R_n(k_{nj}) = 0$ implies $\partial D/\partial k_\perp = 0$, we see that if the denominators in Eq. (23) vanish at a point in $(k_\perp, k_\parallel)$ space, the solution to Eqs. (C.1) and (C.2) is not unique in the neighborhood of that point. This indicates that at least two otherwise distinct solutions meet at this point, and that the asymptotic expansion has a place where stationary points coalesce. Near any such points, the method of Chester, Friedman and Ursell [28] can be used to do the asymptotic expansion. The result will be finite, and of $O(r^{-5/6})$ at most [19]. However, any damping will make these terms of much higher order, so we only need to consider lightly damped solutions to Eqs. (C.1) and (C.2).

First, we will consider whether it is possible to have $R_n(k_{nj}) = 0$. We will be able to prove that $R_n(k_{nj}) \neq 0$ for all important cases simply by showing that $R_n(k_\parallel) \neq 0$, without having to consider that k_{nj} satisfies Eq. (24).

For $\mathrm{Re}\ k_{\|}^2 \geq 0$, the dispersion function $D(k_\perp, k_\|)$ defined in Eq. (9) is an entire function of the complex variable $k_\perp^2$ of order one. According to Hadamard's factorization theorem [53], it can thus be expressed as

$$D(k_\perp, k_\|) = \exp(Q(k_\perp^2, k_\|))\, \mathscr{P}(k_\perp^2) \tag{C.5}$$

where Q is a polynomial in $k_\perp^2$ of degree one or less, and $\mathscr{P}$ is the canonical product of the zeros of $D(k_\perp, k_\|)$, defined in the following manner. Let $E(u,0) = 1-u$ and $E(u,M) = (1-u)\exp(u + u^2/2 + \cdots u^M/M)$ where M is an integer. We then have

$$\mathscr{P}(k_\perp^2) = \prod_{m=0}^{\infty} E\left(-\frac{k_\perp^2}{P_m^2(k_\|)}, M\right) \tag{C.6}$$

where $M \leq 1$. This decomposition of $D(k_\perp, k_\|)$ is valid as long as $P_m^2(k_\|) \neq 0$ for all m, i.e., as long as there are no solutions to $D(k_\perp, k_\|) = 0$ that also have $k_\perp = 0$.

Using Eqs. (C.5) and (C.6), we can write

$$R_n(k_\|) \equiv \left.\frac{\partial D}{\partial(k_\perp^2)}\right|_{k_\perp^2 = -P_n^2(k_\|)}$$

$$= e^Q \prod_{\substack{m=0 \\ m\neq n}}^{\infty} E\left(\frac{P_n^2(k_\|)}{P_m^2(k_\|)}, M\right) \tag{C.7}$$

Thus, $R_n(k_\|) = 0$ if and only if $P_n^2(k_\|) = P_m^2(k_\|)$ for some m. However, we can also write

$$\left.\frac{\partial D}{\partial k_{\parallel}}\right|_{k_\perp^2 = -P_n^2(k_\parallel)} = -2\,\frac{P_n'(k_\parallel)}{P_n(k_\parallel)}\,e^{Q}\prod_{\substack{m=0\\ m\neq n}}^{\infty} E\left(\frac{P_n^2(k_\parallel)}{P_m^2(k_\parallel)}, M\right) \qquad (C.8)$$

This shows that any solutions to the dispersion relation that yield $R_n = 0$ when $P_n(k_\parallel) \neq 0$ also must have $\partial D/\partial k_\parallel | = 0$.

This particular conclusion may seem esoteric, but it has an important physical consequence. If $R_n(k_\parallel) = 0$, then the component of the group velocity perpendicular to the magnetic field is zero. We have shown that the component parallel to the magnetic field is also zero as long as $P_n(k_\parallel) \neq 0$. Since a $k_\parallel$ that gives $P_n(k_\parallel) = 0$ is a root of the Landau dispersion relation, Eq. (20), we have shown that, except for the Landau modes, the group velocity vanishes if its perpendicular component is zero.

We will now show that in the frequency range of interest, $\omega < \omega_{UH}$, the assumption $R_n = 0$ leads to a contradiction for all lightly damped modes.

From Eq. (9), R_n and $\partial D/\partial k_\parallel$ can be explicitly evaluated.

$$R_n(k_\parallel) = 1 - \frac{2i\,\omega_{pe}^2(\omega+i\nu)^2}{\omega\,\omega_{ce}^2}\int_0^\infty dt\,\sin^2\tfrac{1}{2}\omega_{ce}t\,e^{h(t)} \qquad (C.9)$$

$$\left.\frac{\partial D}{\partial k_{\parallel}}\right|_{k_\perp^2 = -P_n^2(k_\parallel)} = 2k_\parallel\left[1 - \frac{i\omega_{pe}^2(\omega+i\nu)^2}{\omega\,\omega_{ce}^2}\int_0^\infty dt\,\tfrac{1}{2}\omega_{ce}^2 t^2\,e^{h(t)}\right] \qquad (C.10)$$

where $h(t) = i(\omega+i\nu)t + (P_n^2(k_\parallel)v_{th}^2/\omega_{ce}^2)\sin^2\tfrac{1}{2}\omega_{ce}t - \tfrac{1}{4}k_\parallel^2 v_{th}^2 t^2$

If $R_n(k_\parallel) = 0$, we have seen that $\partial D/\partial k_\parallel | = 0$ as well. If the latter is zero because the factor in brackets in Eq. (C.10)

vanishes, then it is necessary that

$$\int_0^\infty dt\left(\frac{1}{4}\omega_{ce}^2 t^2 - \sin^2\frac{1}{2}\omega_{ce}^2 t^2\right) e^{h(t)} = 0 \qquad (C.11)$$

However, there is no $k_{||}$ with $\mathrm{Re}\, k_{||}^2 \geq 0$ such that Eq. (C.11) is true. If it were true, then we would have

$$\int_0^\infty dt\left(\frac{1}{4}\omega_{ce}^2 t^2 - \sin^2\frac{1}{2}\omega_{ce} t\right) \cos[\mathrm{Im}\, h(t)] \exp[\mathrm{Re}\, h(t)] = 0$$

$$\int_0^\infty dt\left(\frac{1}{4}\omega_{ce}^2 t^2 - \sin^2\frac{1}{2}\omega_{ce} t\right) \sin[\mathrm{Im}\, h(t)] \exp[\mathrm{Re}\, h(t)] = 0 \qquad (C.12)$$

Except for the trigonometric functions, the integrands in Eq. (C.12) are positive definite. Consequently, if either integral is to vanish, it must do so by cancellation due to the trigonometric function. However, sin and cos are 90^o out of phase, and it is thus impossible to have both integrals vanish simultaneously. (This proof requires $\mathrm{Re}\, k_{||}^2 \geq 0$; however, waves with $k_{||}$'s that violate this are too strongly damped to be important.

If we are to have $\partial D/\partial k_{||} | = 0$, Eq. (C.10) requires that $k_{||} = 0$. With this assumption, the dispersion relation becomes identical to that for Bernstein waves, Eq. (21). For $\omega < \omega_{UH}$, there are no solutions to this dispersion relation with $\partial D/\partial k_{\perp} = 0$ [24]. Hence we have $R_n \neq 0$, and we have reached a contradiction. Consequently, the original assumption is invalid, and $R_n(k_{||}) \neq 0$ for all $k_{||}$ for which $P_n(k_{||}) \neq 0$.

If $P_n(k_{\parallel}) = 0$ for $n > 0$, then $k_{\parallel}$ is one of the higher order Landau roots [54]. All of these are strongly damped. Accordingly, all terms which could contribute significantly to the asymptotic expansion have $R_n(k_{\parallel}) \neq 0$.

We now must turn to the question of whether we can satisfy $P_n''(k_{nj}) = 0$. We will show that the answer is affirmative. The easiest place to see this is when $\cot\theta = 0$, which yields propagation of energy perpendicular to the magnetic field.

Since $\cot\theta = 0$, Eq. (C.2) can be satisfied by requiring $k_{\parallel} = 0$, which means that Eq. (C.1) reduces to the Bernstein wave dispersion relation, Eq. (21). Since solutions to this for $\omega < \omega_{UH}$ and $\omega \neq m\,\omega_{ce}$ have $R_n \neq 0$ and $P_n \neq 0$ for $n \geq 1$, if we are to violate the uniqueness condition, Eq. (C.3), by having $P_n''(0) = 0$, we must have

$$\Xi \equiv \left.\frac{\partial^2 D}{\partial k_{\parallel}^2}\right|_{\substack{k_{\parallel}=0 \\ k_{\perp}=iP_n(0)}} = 0 \qquad (C.13)$$

To find a point where $\Xi = 0$ requires that one take the collisionless limit, $\nu = 0$. As defined in Eq. (9), it is difficult to evaluate derivatives of the dispersion function $D(k_{\perp}, k_{\parallel})$ with respect to $k_{\parallel}$ when $k_{\parallel} = 0$. We will consequently employ the series representation, obtained from Eq. (9) by using the following identities

$$\exp[-z\sin^2(\theta/2)] = e^{-z}\sum_{n=-\infty}^{+\infty} I_n(z)\, e^{in\theta}$$

and

$$Z(z) = 2i\, e^{-z^2} \int_{-\infty}^{iz} dt\, e^{-t^2}$$

where I_n are the modified Bessel functions, and Z is the plasma dispersion function. Using this, Eq. (9) can be restated as

$$D(k_\perp, k_\parallel) = k_\perp^2 + k_\parallel^2 + k_{de}^2 \left\{1 + \frac{\omega}{k_\parallel v_{th}} e^{-\lambda} \sum_{n=-\infty}^{+\infty} I_n(\lambda)\, Z\left(\frac{\omega + n\omega_{ce}}{k_\parallel v_{th}}\right)\right\} \tag{C.14}$$

where $\lambda = k_\perp^2 v_{th}^2 / 2\omega_{ce}^2$

From Eq. (C.14), we obtain the usual series expression for the Bernstein wave dispersion function

$$D(k_\perp, 0) = k_\perp^2 + k_{de}^2 \left\{1 - \omega e^{-\lambda} \sum_{n=-\infty}^{+\infty} \frac{I_n(\lambda)}{\omega + n\omega_{ce}}\right\} \tag{C.15}$$

The expression for Ξ is also easily developed

$$\Xi = 2\left[1 - \omega_{pe}^2 \omega\, e^{-\lambda} \sum_{n=-\infty}^{+\infty} \frac{I_n(\lambda)}{(\omega + n\omega_{ce})^3}\right] \tag{C.16}$$

The values of λ to be used in Eq. (C.16) are the ones that make $D(k_\perp, 0) = 0$ true. There are real λ that satisfy this dispersion relation. Hence, except for poles at $\omega = m\omega_{ce}$, Ξ is a continuous function of the parameters ω, ω_{pe}, and ω_{ce}.

We will now show that it is possible for Ξ to change sign for some $m\omega_{ce} \leq \omega \leq (m+1)\omega_{ce}$. First, consider the case $\omega \to \omega_{UH}$. For this we have $\lambda \to 0$; hence

$$\Xi \to 1 - \frac{\omega_{pe}^2}{\omega_{UH}^2} > 0 \qquad \text{(C.17)}$$

Second, consider $\omega \to m\omega_{ce}^+$. As is well known [24], $k_\perp$ and λ become infinite as $\omega \to m\omega_{ce}^+$. Accordingly, an approximate solution to $D(k_\perp,0) = 0$ can be obtained by using the asymptotic form

$$e^{-\lambda} I_n(\lambda) \sim (2\pi\lambda)^{-1/2} \qquad \lambda \to \infty$$

in Eq. (C.15), and keeping only the largest terms. The result is

$$k_\perp^3 \simeq \sqrt{\frac{\pi}{2}}\, k_{de}^3 \frac{\omega}{\omega_{pe}} \cot(\pi\omega/\omega_{ce}) \qquad \text{(C.18)}$$

In obtaining this result, we have used the identity [55]

$$\cot \pi x = \frac{1}{\pi x} + \frac{2x}{\pi} \sum_{n=1}^{\infty} \frac{1}{x^2 - n^2}$$

Substituting Eq. (C.18) in Eq. (C.16), we find

$$\Xi \simeq 2 \left\{1 - \frac{\pi^3 \omega_{pe}^2}{\omega_{ce}^2 \sin^2 \pi\omega/\omega_{ce}} \left[\frac{\omega \cot \pi\omega/\omega_{ce}}{\omega_{pe}}\right]^{2/3}\right\}$$

It is clear that $\Xi \to -\infty$ as $\omega \to m\omega_{ce}^+$.

Since Ξ is continuous for $m\omega_{ce} \leq \omega \leq (m+1)\omega_{ce}$ for all m, then we must have $\Xi = 0$ somewhere in the range $M\omega_{ce} < \omega < \omega_{UH}$, where M is such that $\omega_{UH} < (M+1)\omega_{ce}$. Consequently, it is possible to have $P_n''(k_{nj}) = 0$. If one wishes to obtain a complete, uniform asymptotic expansion, some of the terms in the sums in Eqs. (23) and

(40) must be modified in parameter ranges where $P_n''(k_{nj}) = 0$.

Kuehl [8] has presented graphs of numerical solutions of the full dispersion relation $D(k_\perp, k_\parallel) = 0$ that change their curvature from positive to negative as $k_\parallel$ varies. Since $P_n''(k_\parallel)$ is related to the curvature, his numerical calculation confirms what we have obtained here by analytic methods. He finds such behavior only for ω near ω_{UH} , and it appears to be connected with the multi-wave interference patterns that he presents in this frequency range. No experimental evidence of such patterns was seen, perhaps because they depend so strongly on ω_{pe} for ω near ω_{UH} that density fluctuations could broaden them until they are unrecognizable.

In conclusion, we have seen that there are parameter values for $\omega > \omega_{ce}$ for which $P_n''(k_{nj}) = 0$. This would require modification of the asymptotic expansion if we needed the $n \geq 1$ terms in Eq. (18). All of the experimentally observed features seem to be connected with the $n = 0$ term; we will leave the complete asymptotic expansion for later work.

APPENDIX D

ASYMPTOTIC EXPANSION WITH $\sin\theta = 0$

In Chapter II, the asymptotic expansion of the electrostatic Green's function was obtained under the assumption that $\sin\theta \neq 0$. As was noted there, the expansion was still finite when $\sin\theta = 0$ and we will now demonstrate that the $\sin\theta \to 0$ limit of that expansion is indeed correct.

Returning to Eq. (8), for $\sin\theta = 0$, the electrostatic Green's function can be written as

$$\phi(0,z,t) = \frac{qe^{-i\omega t}}{4\pi^2\varepsilon_o}\int_0^{\infty} dk_\perp k_\perp \int_{-\infty}^{+\infty} dk_\parallel \frac{e^{ik_\parallel z}}{D(k_\perp,k_\parallel)}$$

$$= \frac{iqe^{-i\omega t}}{4\pi^2\varepsilon_o}\sum_{n=0}^{\infty}\int_0^{\infty} dk_\perp \frac{\exp[ik_n(k_\perp)z]}{\left.\frac{\partial D}{\partial k_\parallel}\right|_{k_\parallel = k_n(k_\perp)}} \qquad (D.1)$$

The last step in Eq. (D.1) follows from the first by use of the residue theorem. Here $k_\parallel = k_n(k_\perp)$ is a solution of the dispersion relation $D(k_\perp, k_\parallel) = 0$ with $\mathrm{Im}\, k_n(k_\perp) \geq 0$.

As $z \to \infty$, there are three possible contributions to the asymptotic expansion of the integrals in Eq. (D.1): the endpoint contribution, contributions from stationary points of the integrand, and contributions from any integrable singularities of the integrand. We will show that the first is $O(z^{-1})$, while the latter two are $O(z^{-2})$ at best, so that the first dominates as $z \to \infty$.

A stationary point exists if

$$\frac{\partial k_n}{\partial k_\perp} = 0 \tag{D.2}$$

By differentiating the dispersion relation, we get

$$\frac{\partial D}{\partial k_\parallel}\bigg| \frac{\partial k_n}{\partial k_\perp} + \frac{\partial D}{\partial k_\perp}\bigg| = 0 \tag{D.3}$$

where the vertical bar is to remind us that the derivatives are evaluated at one of the solutions $k_\parallel = k_n(k_\perp)$. As long as $k_n(k_\perp) \neq 0$, $\partial D/\partial k_\parallel |$ is an analytic function of $k_\perp$; hence, for all finite $k_\perp$ such that $k_n(k_\perp) \neq 0$, $\partial D/\partial k_\parallel |$ is finite. If $k_n(k_\perp) = 0$, then we have $\partial D/\partial k_\parallel | = 0$. Accordingly, for all $k_\perp$, the stationary point condition, Eq. (D.2), is equivalent to requiring

$$\frac{\partial D}{\partial k_\perp}\bigg| = 0 \tag{D.4}$$

In Appendix C we showed that when $\omega < \omega_{UH}$, it is impossible to have a solution to the dispersion relation with $\partial D/\partial k_\perp| = 0$ when $k_\perp \neq 0$. Thus, the only possible stationary point is at $k_\perp = 0$. However, as long as $\partial D/\partial k_\parallel| \neq 0$ at $k_\perp = 0$, the integrand in Eq. (D.1) vanishes at $k_\perp = 0$. Thus, any contribution to the asymptotic expansion is at most $O(z^{-2})$. The case $\partial D/\partial k_\parallel| = 0$ at $k_\perp = 0$ will be dealt with as part of the endpoint contribution.

In the frequency range $\omega_{ce} < \omega < \omega_{UH}$, it is possible to have $k_n(k_\perp) = 0$ for $k_\perp \neq 0$. This is, of course, the Bernstein mode solution. Such a solution would lead to a singularity in the integrand in Eq. (D.1), since $\partial D/\partial k_\parallel = 0$ for $k_\parallel = 0$.

Since $\partial^m D/\partial k_{\parallel}^m = 0$ at $k_{\parallel} = 0$ for all odd m, near the Bernstein mode solution, the dispersion relation must have a solution of the form

$$k_{\perp}(k_{\parallel}) \tilde{=} k_{\perp}(0) + \alpha k_{\parallel}^{2m} \qquad m \geq 1 \tag{D.5}$$

with $m \geq 1$, we have allowed for the possibility that some of the higher order even derivatives of $k_{\perp}$ may vanish at $k_{\parallel} = 0$.

For the moment, consider $m = 1$ in Eq. (D.5). Inverting that equation, for one definite n we get

$$k_n(k_{\perp}) = \left|\frac{k_{\perp} - k_{\perp}(0)}{\alpha}\right|^{1/2} \exp\{ - \frac{i\pi}{2} [\mathrm{sign}(\frac{k_{\perp} - k_{\perp}(0)}{\alpha}) - 1]\} \tag{D.6}$$

(Implicitly, Eq. (D.6) has been specialized to the collisionless case $\nu = 0$; hence α is real. The calculation with $\nu = 0$ is the most difficult; $\nu \neq 0$ is easily done.)

The contributions to the asymptotic expansion come from the neighborhood of the singularity, so they are given by

$$\int_{k_{\perp}(0)-\varepsilon}^{k_{\perp}(0)+\varepsilon} dk_{\perp} \frac{k_{\perp} \exp[ik_n(k_{\perp})z]}{\partial D/\partial k_{\parallel}|}$$

$$= -i \int_{k_{\perp}(0)-\varepsilon}^{k_{\perp}(0)} dk_{\perp} \frac{k_{\perp} \exp\{-z[(k_{\perp}(0) - k_{\perp})/|\alpha|]^{1/2}\}}{\beta(k_{\perp}(0) - k_{\perp})^{1/2}}$$

$$+ \int_{k_{\perp}(0)}^{k_{\perp}(0)+\varepsilon} dk_{\perp} \frac{k_{\perp} \exp\{iz[(k_{\perp} - k_{\perp}(0))/|\alpha|]^{1/2}\}}{\beta(k_{\perp} - k_{\perp}(0))^{1/2}} \tag{D.7}$$

where $\beta = \lim_{k_\perp \to k_\perp(0)} \frac{1}{|\alpha|^{1/2}} \frac{1}{k_{\parallel}} \frac{\partial D}{\partial k_{\parallel}} \Big|_{k_{\parallel} = k_n(k_\perp)}$

If we let $\lambda^2 = k_\perp(0) - k_\perp$ in the first integral in Eq. (D.7) and $\lambda^2 = k_\perp - k_\perp(0)$ in the second, the right hand side of that equation becomes

$$- \frac{2i|\alpha|^{1/2}}{\beta} \int_0^{\sqrt{\epsilon}} d\lambda (k_\perp(0) - \lambda^2) \exp(-z|\alpha|^{-1/2}\lambda)$$

$$+ \frac{2|\alpha|^{1/2}}{\beta} \int_0^{\sqrt{\epsilon}} d\lambda (k_\perp(0) + \lambda^2) \exp(iz|\alpha|^{-1/2}\lambda)$$

As $z \to \infty$, using the asymptotic forms given in Copson [22], this becomes

$$- \frac{2i|\alpha|^{1/2} k_\perp(0)}{\beta} \frac{1}{z|\alpha|^{1/2}} + \frac{2i|\alpha|^{1/2} k_\perp(0)}{\beta} \frac{1}{z|\alpha|^{1/2}} = 0$$

Consequently, any contribution to the asymptotic expansion must be $O(z^{-2})$ at most.

If $m > 1$ in Eq. (D.5), one can go through an analogous derivation. The change of variable would then be $\lambda^{2m} = k_\perp - k_\perp(0)$, which would produce an integrand proportional to $\lambda^{2(m-1)}$. Since this vanishes at $\lambda = 0$, the contribution to the asymptotic expansion is still $O(z^{-2})$.

Finally, we come to the endpoint contribution. It, too, would be $O(z^{-2})$, except for the fact that there is one $k_n(k_\perp)$ (the inverse of $P_0(k_{\parallel})$ in the main text) that approaches zero as $k_\perp \to 0$. If we call this $k_0(k_\perp)$, the work in the main text shows

$$k_o \cong k_\perp \left(-\frac{K_\perp}{K_\parallel}\right)^{1/2}$$

where $\mathrm{Im}(-K_\perp/K_\parallel)^{1/2} \geq 0$. Using this, we find that the endpoint contribution yields

$$\phi(0,z,t) \sim \frac{qe^{-i\omega t}}{4\pi\varepsilon_o K_\perp z} \tag{D.8}$$

If one takes the $\sin\theta \to 0$ limit of Eq. (40), it is identical with Eq. (D.8). Accordingly, Eq. (40) is valid for all $0 \leq \theta \leq \pi$.

APPENDIX E

LEAST SQUARES FIT WITH ERROR IN BOTH VARIABLES

The conventional method of fitting an assumed theoretical equation $y = a + bx$ to a set of N data points (x_i, y_i) with errors σ_i in the y_i involves minimizing the likelihood function

$$L = \sum_{i=1}^{N} \frac{(y_i - a - bx_i)^2}{\sigma_i^2}$$

with respect to a and b. However, Lindley[56] has shown that if (x_i, y_i) have errors $(\sigma_{xi}, \sigma_{yi})$, the appropriate likelihood function is

$$L = \sum_{i=1}^{N} \frac{(y_i - a - bx_i)^2}{\sigma_{yi}^2 + b^2\sigma_{xi}^2} \qquad \text{(E.1)}$$

In order to find the a and b that minimize this new L, one must usually resort to iterative solutions on a computer; the extremum conditions

$$\frac{\partial L}{\partial a} = 0 = \frac{\partial L}{\partial b} \qquad \text{(E.2)}$$

are polynomials in b of order 2(N+1). By using the a and b from the conventional fit as a starting point, the iterative solution converges quite rapidly, so that the lack of an analytical solution presents no practical difficulty.

The error in the fitted parameters is determined from the usual error propagation formula [57]

$$\sigma_z^2 = \sum_{i=1}^{N} \left[\left(\frac{\partial z}{\partial y_i}\right)^2 \sigma_{yi}^2 + \left(\frac{\partial z}{\partial x_i}\right)^2 \sigma_{xi}^2 \right] \qquad \text{(E.3)}$$

where z stands for either a or b. (This holds as long as the errors in x and y are independent.) The partial derivatives needed can be found by differentiating the extremun conditions Eq. (E.2) and then solving the pairs of linear equations that result.

Consequently, using this procedure, one can obtain a and b and their errors when fitting a straight line to experimental data which have errors in both the independent and dependent variables.

Occasionally, a one parameter least squares fit was needed for a case where the theory predicted a relationship of the form $y = bx$. The likelihood function in Eq. (E.1) is still valid for this case if we set $a = 0$. The extremum conditions Eq. (E.2) and the error calculations Eq. (E.3) are then executed with b as the only variable.

APPENDIX F

Presented here is a bibliography of the work done before 1970 on small antennas in magnetized plasmas. This work provides a background for the present study, but few of the detailed calculations in these works were used.

1. Arbel, E. and Felsen, L. B., "Theory of Radiation from Sources in Anisotropic Media, Part I: General Sources in Stratified Media", Jordan, E. C., Editor, Proc. Symp. on Electromagnetic Theory and Antennas, Pergamon Press, Inc., New York (1963), pp. 391-420.

2. Arbel, E., and Felsen, L. B., "Theory of Radiation from Sources in Anisotropic Media, Part II: Point Sources in Infinite, Homogeneous Medium", Jordan, E. C., Editor, Proc. Symp. on Electromagnetic Theory and Antennas, Pergamon Press, Inc., New York (1963), pp. 421-459.

3. Balmain, K., "The Impedance of a Short Dipole Antenna in a Magnetoplasma", IEEE Trans. Ant. Prop. AP-12, 605 (1964).

4. Bunkin, F. V., "On Radiation in Anisotropic Media", Soviet Phys. JETP 5, 277 (1957).

5. Clemmow, P. C., "The Theory of Electromagnetic Waves in a Simple Anisotropic Medium", Proc. IEE 110, 101 (1963).

6. Clemmow, P. C., "On the Theory of Radiation from a Source in a Magneto-Ionic Medium", Jordan, E. C., Editor, Proc. Symp. on Electromagnetic Theory and Antennas, Pergamon Press, Inc., New York (1963), pp. 461-475.

7. Chen, H. C., "Radiation Characteristics of an Electric Dipole in a Warm, Anisotropic Plasma", J. Appl. Phys. 40, 4068 (1969).

8. Deschamps, G. A. and Kesler, A. B., "Radiation on an Antenna in a Compressible Magnetoplasma", Radio Science 2 (new series), 757 (1967).

9. Kaiser, T. R., "The Admittance of an Electric Dipole in a Magneto-Ionic Environment", Planet. Space Sci. 9, 639 (1962).

10. Kenney, J., "Electric Dipole Radiation in Isotropic and Uniaxial Plasmas", Antenna Laboratory Report No. 44, California Institute of Technology, Pasadena, California (1968).

11. Kogelnik, H. and Motz, H., "Electromagnetic Radiation from Sources Embedded in an Infinite Anisotropic Medium and the Significance of the Poynting Vector", Jordan, E. C., Editor, Proc. Symp. on Electromagnetic Theory and Antennas, Pergamon Press, Inc., New York (1963), pp. 477-493.

12. Kogelnik, H., "The Radiation Resistance of an Elementary Dipole in Anisotropic Plasmas", Fourth Int. Conf. on Ioniz. Phenomena in Gases, Uppsala, IIIC, North Holland Publishing Company (1960), pp. 721-725.

13. Kogelnik, H., "On Electromagnetic Radiation in Magneto-Ionic Media", J. Res. Natl. Bur. Stds. (U.S.) 64D, 515 (1960).

14. Kononov, B., Rukhadze, A. A., and Solodukhov, G. V., "Electric Field of a Radiator in a Plasma in an External Magnetic Field", Zh. Tekh. Fiz. 31, 565 (1961) [Translation: Soviet Phys. Tech. Phys. 6, 405 (1961).

15. Kuehl, H. H., "Radiation from an Electric Dipole in an Anisotropic Cold Plasma", Antenna Laboratory Report No. 24, California Institute of Technology, Pasadena, California (1960).

16. Kuehl, H. H., "Electromagnetic Radiation from an Electric Dipole in a Cold Anisotropic Plasma", Phys. Fluids 5, 1094 (1962).

17. Kuehl, H. H., "Resistance of a Short Antenna in a Warm Plasma", Radio Science 1 (new series), 218 (1966).

18. Lee, S. W. and Mittra, R., "Transient Radiation of an Electric Dipole in a Uniaxially Anisotropic Plasma", Radio Science 2, 813 (1967).

19. Lee, K.S.H., and Papas, C.H., "Irreversible Power and Radiation Resistances of Antenna in Anisotropic Ionized Gases", J. Research NBS/USNC-URSI 69D, 1313 (1965).

20. Lee, K.S.H., and Papas, C. H., "A Further Explanation of the New Theory of Antenna Radiation with Particular Reference to Uniaxial Media", Radio Science 1, 1020 (1966).

21. Lee, K.S.H., and Papas, C. H., "On Walsh and Weil's Defense of the Conventional Method", Radio Science 1, 1027 (1966).

22. Mittra, R. and Deschamps, G. A., "Field Solutions for a Dipole in an Anisotropic Medium", Jordan, E. C., Editor, Proc. Symp. on Electromagnetic Theory and Antennas, Pergamon Press, Inc., New York (1963), pp. 495-512.

23. Seshadri, S. R., "Radiation Resistance of a Linear Current Filament in a Simple Anisotropic Medium", IEEE Trans. on Antennas and Propagation, Sept. 1965, p. 819.

24. Seshadri, S. R., "Radiation Resistance of Elementary Electric-Current Sources in a Magneto-Ionic Medium", Proc. IEE 112, 1856 (1965).

25. Staras, H., "The Impedance of an Electric Dipole in a Magneto-Ionic Medium", IEEE Trans. AP-12, 695 (1964).

26. Staras, H., "The Infinity Catastrophe Associated with Radiation in Magneto-Ionic Media", Radio Science 1 (new series), 1013 (1960).

27. Tunaley, J. K. E., and Grard, R. J. L., "The Impedance of a Probe in a Warm Plasma", Ann. Geophys. 25, 55 (1969).

28. Wait, James R., "Radiation from Sources Immersed in Compressible Plasma Media", Canadian J. Phys. 42, 1760 (1964).

29. Walsh, D., and Weil, H., "Irreversible Power and Radiation Resistance of Antennas in Magneto-Ionic Media", Radio Science 1, 1025 (1966).

30. Wang, T. C. N., and Bell, T. F., "Radiation Resistance of a Short Dipole Immersed in a Cold Magneto-Ionic Medium", Radio Science 4, 167 (1969).

REFERENCES

[1] R.K. Fisher, "Resonance Cones in the Field Pattern of a Short Radio Frequency Probe in a Warm Anisotropic Plasma", Ph.D. Thesis, California Institute of Technology, April, 1970.

[2] R.K. Fisher and R.W. Gould, "Resonance Cones in the Field Pattern of a Short Antenna in an Anisotropic Plasma", Phys. Rev. Letters 22, 1093 (1969).

[3] R.K. Fisher and R.W. Gould, "Resonance Cone Structure in Warm Anisotropic Plasma", Physics Letters 31A, 235 (1971).

[4] R.K. Fisher and R.W. Gould, "Resonance Cones in the Field Pattern of a Radio Frequency Probe in a Warm Anisotropic Plasma", Phys. Fluids 14, 857 (1971).

[5] N. Singh, "Radiation from a Short Electric Dipole Antenna in a Hot Uniaxial Plasma", Ph.D. Thesis, California Institute of Technology, July, 1970.

[6] N. Singh and R.W. Gould, "Radiation from a Short Electric Dipole in a Hot Uniaxial Plasma", Radio Science 6, 1151 (1971).

[7] N. Singh and R.W. Gould, "Waves in a Hot Uniaxial Plasma Excited by a Current Source", Phys. Fluids 16, 75 (1973).

[8] H.H. Kuehl, "Interference Structure near the Resonance Cone", Phys Fluids 16, 1311 (1973).

[9] H.H. Kuehl, "Electric Field and Potential near the Plasma Resonance Cone", Phys. Fluids to be published.

[10] I.B. Bernstein, "Waves in a Plasma in a Magnetic Field", Phys. Rev. 109, 10 (1958).

[11] T.H. Stix, The Theory of Plasma Waves (McGraw-Hill Book Company, Inc., New York, 1962).

[12] P.J. Catto and D.E. Baldwin, "Single-Integral Form of the Dispersion Relation for Waves in a Magnetized Plasma", Phys. Fluids 13, 214 (1970).

[13] I.S. Gradshteyn and I.M. Rhyzik, Tables of Integrals, Series and Products (Academic Press, New York, 1965), Eqs. 6.532.4 and 6.671.14.

[14] ibid. Eq. 6.532.4.

[15] B.D. Fried and S.D. Conte, The Plasma Dispersion Function (Academic Press, New York, 1961).

[16] K.H. Burrell, "Evaluation of the Modified Bessel Functions $K_0(z)$ and $K_1(z)$ for Complex Arguments", Comm. ACM to be published.

[17] J.A. Tataronis and F.W. Crawford, "Cyclotron Harmonic Wave Propagation and Instabilities II. Oblique Propagation", J. Plasma Physics 4, 249 (1970).

[18] D.S. Jones and M. Klein, "Asymptotic Expansion of Multiple Integrals and the Method of Stationary Phase", J. Math. Phys. 37, 1 (1958).

[19] M.J. Lighthill, "Studies on Magneto-Hydrodynamic Waves and Other Anisotropic Wave Motions", Phil. Trans. Roy. Soc. A 252, 397, (1960).

[20] N. Chako, "Asymptotic Expansions of Double and Multiple Integrals Occurring in Diffraction Theory", J. Inst. Maths. Applics. 1, 372 (1965).

[21] M. Abramowitz and I.A. Stegun, Handbook of Mathematical Functions (National Bureau of Standards, Applied Mathematics Series 55, Washington, D.C., 1964), Chapter 9.

[22] E.T. Copson, Asymptotic Expansions (Cambridge University Press, Cambridge, 1965).

[23] L. Landau, "On the Vibrations of the Electronic Plasma", J. Physics USSR 10, 25 (1946).

[24] J.A. Tataronis and F.W. Crawford, "Cyclotron Harmonic Wave Propagation and Instabilities I. Perpendicular Propagation", J. Plasma Physics 4, 231 (1970).

[25] I.P. Shkarofsky and T.W. Johnston, "Cyclotron Harmonic Resonances Observed by Satellites", Phys. Rev. Letters 15, 51 (1965).

[26] M.J. Lighthill, "Group Velocity", J. Inst. Maths. Applics. 1, 1 (1965).

[27] Copson, p. 30.

[28] C. Chester, B. Friedman, and F. Ursell, "An Extension of the Method of Steepest Descents", Proc. Cambridge Phil Soc. 53, 599 (1957).

[29] Abramowitz and Stegun, Chapter 10.

[30] R. Buckley, "RF Characteristics of a Plane-Grid Capacitor immersed in a Hot Collision-free Plasma with Uniform Magnetic Field paralled to the Grid Plates", Plasma Waves in Space and in the Laboratory, J.O. Thomas and B.J. Landmark (Editors), (American Elsevier, New York, 1970), Vol. II, pp. 129-158.

[31] R. S. Scorer, "Numerical Evaluation of Integrals of the Form $I = \int_{x_1}^{x_2} f(x)\, e^{i\phi(x)} dx$ and the tabulation of the function

$$Gi(z) = \frac{1}{\pi} \int_0^\infty \sin(uz + \frac{1}{3} u^3) du$$ ",

Quart. J. Mech. Appl. Math. 3, 107 (1950).

[32] Abramowitz and Stegun, Eq. 10.4.108.

[33] P. R. Garabedian, Partial Differential Equations (John Wiley and Sons, Inc., New York, 1964), p. 107.

[34] L. S. Frost and A. V. Phelps, "Momentum-Transfer Cross Sections for Slow Electrons in He, Ar, Kr and Xe from Transport Coefficients", Phys. Rev. 136, A1538 (1964).

[35] Lyman Spitzer, Physics of Fully Ionized Gases (Interscience Publishers, New York, 1967), Eq. (5-26).

[36] F. Leuterer, "Cyclotron Harmonic Waves in an Inhomogeneous Plasma --II. Experiment", Plasma Physics 14, 499 (1972).

[37] E. W. McDaniel, Collision Phenomena in Ionized Gases (John Wiley and Sons, Inc., New York, 1964), Chapter 10.

[38] A. Gonfalone, "Densité et Température Electroniques Déduites de L'Observation du Cône de Résonance d'une Antenne dans un Magnéto-plasma", Le Journal de Physique 33, 521 (1972).

[39] D. W. Marquardt, "An Algorithm for Least-Squares Estimation of Nonlinear Parameters", SIAM Journal 11, 431 (1963). See also IBM Share Library, Distribution No. 309401.

[40] K. H. Burrell, "Low Frequency Resonance Cone Structure in a Warm Anisotropic Plasma", submitted for publication to Phys. Fluids.

[41] Abramowitz and Stegun, Chapter 7.

[42] W. Gautschi, "Algorithm 363 Complex Error Function", Comm. ACM 12, 635 (1969).

[43] W. Gautschi, "Efficient Computation of the Complex Error Function", SIAM J. Numer. Anal. 7, 187 (1970).

[44] H. C. Thacher, "Computation of the Complex Error Function by Continued Fractions", Blanch Anniversary Volume, B. Mond (Editor), (Aerospace Research Laboratories, Washington, D. C., 1967), pp. 315-337.

[45] P. Henrici, "Some Application of the Quotient-Difference Algorithm", Proc. Symp. Appl. Math. 15, 159 (1963).

[46] T. C. Simonen, Landau Waves, SUIPR Report No. 100, Stanford University (1966), Appendix B.

[47] A. N. Khovanskii, The Application of Continued Fractions and Their Generalizations to Problems in Approximation Theory (P. Noordhoff N.V., Groningen, The Netherlands, 1963).

[48] L.N.G. Filon, "On a Quadrature Formula for Trigonometric Integrals", Proc. Roy. Soc. Edin. XLIX, 38 (1928-29).

[49] C. J. Tranter, Integral Transforms in Mathematical Physics (John Wiley and Sons, Inc., New York, 1951), Chapter V.

[50] R. G. Gordon, "New Method for Constructing Wavefunctions for Bound States and Scattering", J. Chem. Physics 51, 14 (1969), Appendix A.

[51] D. D. McCracken and W. S. Dorn, Numerical Methods and Fortran Programing (John Wiley and Sons, Inc., New York, 1964), p. 172.

[52] A. E. Taylor, Advanced Calculus (Blaisdell Publishing Co., New York, 1965), Chapter VIII.

[53] Fred Gross, Factorization of Meromorphic Functions (Mathematics Research Center, Naval Research Laboratory, Washington, D. C., 1972), Theorem 2.6.

[54] H. Derfler and T. C. Simonen, "Higher Order Landau Modes", Phys. Fluids 12, 269 (1969).

[55] Gradshteyn and Ryzhik, Eq. 1.421.3.

[56] D. V. Lindley, "Regression Lines and the Linear Functional Relationship", J. Royal Statistical Society (Supplement) IX, 218 (1947).

[57] P. R. Bevington, Data Reduction and Error Analysis for the Physical Sciences (McGraw-Hill, Inc., New York, 1969), Chapter 4.

[58] H. Derfler and F. Leuterer, "Cyclotron Harmonic Waves in an Inhomogeneous Plasma--I. Theory", Plasma Physics 14, 473 (1972).

Better is the end of a thing than the beginning thereof

ECCLESIASTES 7:8